



**Politecnico  
di Torino**

**POLITECNICO DI TORINO**

Department of Control and Computer Engineering

Master's Course in Mechatronic Engineering

Master's Degree Thesis

**Study of control strategies  
for lower-limb rehabilitation exoskeletons**

Thesis advisor:

**Prof. Maurizio Morisio**

Thesis supervisor:

**Giuseppe Menga**

Candidate:

**Niccolò Mondin**

Academic Year 2021/2022

Graduation session July 2022



# Abstract

*A robotic exoskeleton is a mechatronic system designed to interact extensively with the human wearer. Generally, the system aims to enhance the user's strength or agility, resulting in either in power augmentation, allowing the human to bear and support heavy loads or increasing their walking speed, or in applications within the medical field, in particular, in rehabilitation therapy, to help patients affected by motor dysfunctions whose muscles are not able to exert the forces required to perform the training exercise, and which need the assistance of an external element, traditionally the physiotherapist, nowadays also robotic exoskeletons, that intervene by providing the complementary torques required to complete the task, keeping the patients actively involved, hence maintain all the benefits of the neuroplasticity-based recovery.*

*This Thesis analyzes control strategies implemented in exoskeletons for lower-limb rehabilitation with emphasis on patient compliance and the ability to intervene whether dangerous conditions arise, such as falling risk, or when the patient's movements overly deviate from the pre-generated trajectories ensuring the correct execution of the training exercise. Then, the main aspect is the interaction between the exoskeleton and its environment. Different from the classic manipulator, for which the environment is treated as a source of disturbances to be minimized, the environment for an exoskeleton is the human wearer. Hence, to control the dynamic behavior of the interaction, it is paramount to ensure that both systems are passive and stable in isolation, and that, once coupled, the obtained coupled system is stable, consequently, the interaction behavior is stable. Classical control techniques require the characterization of both systems to regulate the interaction. However, circular reasoning arises: it is impossible to interact in a stable way without acquiring the knowledge of the dynamic characteristics of the environment and those can be obtained only by interacting stably with it. Another strategy relies on port functions, i.e., dynamic operators able to describe the dynamic behavior of the robot at the port of interaction with the environment. There are two port functions: the mechanical impedance (at a port), mapping the input mechanical motion (velocity) to the output mechanical effort (torques or forces) at the same port, and the mechanical admittance, its causal dual. The control techniques determine the coupled stability and the interaction behavior based solely on the robot's port's characteristics. In addition, they define the robot's interactive behavior, manifested at the interaction port, in terms of stiffness, damping, and inertial behaviors perceived as haptic sensations by the human. To operate, these ports need non-human data at the port interaction, employing IMUs, encoders, force or torque sensors, or biological signals such as EEG and EMG.*

*To assist patients, rehabilitative exoskeletons must be able to compensate for their passive dynamics and provide ulterior torques, namely the interaction torques, to aid the users. Although both control methods are able to compensate adequately for damping, stiffness, and gravitational effects, impedance control is unable to mask the robot's inertial behavior at low-frequency range, which is the bandwidth in which human movements happen, being the apparent inertia value lower bounded by a positive constant. Practically, the patients would be forced to move their limbs plus the inertia of the mechanical structure they are coupled to. On the other side, in addition to a higher implementation simplicity, admittance control is characterized by passivity and coupled stability conditions which allows apparent inertia lower bounded by a negative constant, allowing, therefore, the possibility not only of compensating the robot's inertia, but also compensating partially the inertia of the coupled human limb.*

*The main tasks of a lower-limb rehabilitation exoskeleton are regulating postural balance and being patient-compliant. Therefore, two control strategies are presented and applied, as an example, to the postural exercise of sit-to-stand. The first one focuses on postural balance maintenance and recovery. The internal control loop focuses on aiding the human wearer in performing sit-to-stand exercises, while the external control loop acts on the projection to the ground of the system's center of mass with the objective of the center of pressure under the feet, i.e., the zero-moment point (ZMP). In fact, when the ZMP falls outside the support polygon of the feet the balance is lost. The second control strategy focuses on patient compliance based on the estimation of the user's intention of motion and measurements of the interaction forces and the joints' kinematic trajectories. The external control loop derives the estimation of the user's muscle torques, which are used to generate the deviations from the pre-generated trajectories through the virtual admittance model. The internal control loop consists of a velocity tracking control loop, using the sum between the pre-computed trajectories and the deviations as the reference signal and comparing it with the observed trajectories to compute the actuators' torques. An extension of these techniques makes it possible to impose the exoskeleton to manifest a transparent behavior, i.e., make the coupled robot imperceptible to the human while they perform some movements, and making the robot intervene only to assist in solving unwanted situations, such as falling risk, or deviation from the pre-generated trajectory. This control strategy is based on the zeroing of the interaction torques by making the exoskeleton follow the human movements without delay. Two strategies are presented, one based on the measurement of the interaction forces, and one based on the measurement of the exoskeleton and human' accelerations. Mixed control techniques leave the transparent parameter, representing the patient's control authority over the whole coupled system, to be tuned by the physiotherapist according to the patient's progress in therapy.*

*Ai miei genitori per il costante supporto,  
ai miei amici per alleviare la pesantezza del percorso,  
a chi ha creduto in me,  
e a chi non ha creduto in me,  
per avermi spinto a dimostrare il contrario.*

# Contents

<b>Abstract</b> .....	2
<b>Contents</b> .....	5
<b>Chapter 1: Introduction to the Thesis</b> .....	7
<b>Part I: State of the Art</b>	
<b>Chapter 2: State of the Art</b> .....	12
<b>Part II: Theoretical background</b>	
<b>Chapter 3: Interaction Control</b> .....	21
3.1 The ABLE project .....	21
3.2 Interaction Control .....	25
3.2.1 Robot-Environment Interaction.....	25
3.2.2 Interaction Control .....	28
3.2.3 Passivity.....	30
3.2.4 Coupled Stability.....	34
3.3 Impedance Control .....	38
3.3.1 Masking the low-frequency inertia behavior: limits of applicability of the impedance control.	41
3.4 Admittance Control .....	43
3.4.1 Analyzing passivity of uncoupled apparent dynamics .....	47
3.4.2 Analyzing coupled stability .....	47
3.4.3 Virtual stiffness and damping behavior.....	48
3.4.5 Virtual element combination.....	49
3.4.6 Guidelines for minimal inertia.....	50
3.5 Emulated Inertia Compensation and other strategies to modify the displayed behavior of the robot	54
3.5.1 Presenting the hardware .....	54
3.5.2 Modeling of the system .....	55
3.5.3 Experiments with negative exoskeleton damping and its effect on the human limb.....	57
3.5.4 Compensating for inertial effects .....	58
3.5.5 Emulated inertia compensation .....	62

## **Part III: Analysis of control strategies implemented in lower-limb rehabilitative exoskeletons**

<b>Chapter 4: Control strategies for lower-limb rehabilitative exoskeletons .....</b>	<b>69</b>
4.1 Postural balance control strategies .....	71
4.1.1 Description of the mechanical structure .....	71
4.1.2 Control System .....	72
4.2 Control strategies for lower-limb rehabilitative exoskeletons.....	78
4.2.1 Description of the mechanical structure .....	78
4.2.2 Control system based on human torques estimation .....	80
4.2.3 Control system based on emulated inertia compensation.....	83
4.3 Transparent control applied to exoskeleton devices.....	86
4.4 Mixed control: tutoring-coordination-cooperation.....	95
<b>Chapter 5: Conclusions and future works .....</b>	<b>98</b>
Conclusions .....	98
Future works.....	98
<b>Appendix.....</b>	<b>99</b>
<b>Appendix A: Fundamentals of bipedal locomotion control.....</b>	<b>99</b>
<b>A1. Support Polygon .....</b>	<b>99</b>
<b>A2. Center of Pressure .....</b>	<b>99</b>
<b>A3. Zero-Moment Point (ZMP): theory and stability criterion .....</b>	<b>99</b>
<b>A3.1. The ZMP Notion.....</b>	<b>101</b>
<b>A3.2 Fictitious ZMP .....</b>	<b>103</b>
<b>A4. Gait model: 3D-Linear Inverted Pendulum Model.....</b>	<b>104</b>
<b>A4.1. Cart-Table model-based postural equilibrium control.....</b>	<b>108</b>
<b>Appendix B: The Routh-Hurwitz criterion.....</b>	<b>110</b>
<b>Appendix C: Haptics.....</b>	<b>112</b>
<b>Bibliography .....</b>	<b>114</b>

# Chapter 1

## Introduction

This Thesis was born from the personal curiosity and interest in robotic exoskeletons for rehabilitation purposes. Unfortunately, there was not the possibility to proceed in this direction during the Master Course, therefore, I took the opportunity to invest the time for the Thesis in this journey, to explore and understand how rehabilitation exoskeletons are designed, modeled, controlled, and simulated.

In addition, since the abundant but not very diverse literature about robotic exoskeletons, this Thesis was planned to give a first insight of this exciting field to the future engineering students approaching these themes. Of the about 80 documents among articles, essays, manual passages, I selected the ones I found the most illuminating and oriented to the objective of the Thesis: presenting the main aspect in design, modeling, and control of lower-limb active rehabilitation robotic exoskeletons based on non-human models. I tried the best I could to provide the information necessary to understand the fundamentals and the applications I found most relevant and on point to this objective. I strongly remained on strategies based on non-human models and not exploiting machine learning or artificial intelligence algorithm, to be coherent to what studied during the Course in Mechatronic Engineering. Far complex control strategies employing neurobiological model or physiological signals measuring or AI controlled robots can be found in the literature, and the lecture is warmly advised. However, human models require a minimum study in human muscular, skeletal, tendinous, nervous, even cardiorespiratory systems, which are too far from an engineering student background knowledge, and many physiotherapical applications are shifting towards non-human models based on motion/force sensing. Having followed a single course on machine learning algorithms did not give me enough confidentiality to explore those strategies exploiting such systems.

The analyzed systems are more complex if compared to the aforementioned strategies, but are more reliable and easier to understand, design, and deploy. I focused primarily on rehabilitation exoskeletons for lower limbs, since several control strategies coming from bipedal robots and haptic devices seem to be managed and exploited in this field, giving the opportunity to have a look also to those field, poorly treated in the selected academic path.

The Thesis is articulated as follows:

- Part I is devoted to the State of the Art, to provide context and insight to the engineered rehabilitation problem, and to provide the main aspects to consider in the robotic exoskeleton applications.
- Part II is devoted to the theoretical background, which is fundamental to read since the exoskeleton problem is an interaction control problem not a regulation problem. Since the problem articulates in having a robot coupled to a human, which interact by a force (mechanical energy) exchange, understanding which are the stability conditions to ensure that not only the isolated systems but the coupled systems itself is not unstable, hence, it will not damage (further)

the patient coupled to the robotic device, is paramount importance. There will be analyzed the concept of passivity and coupled stability, representing the aforementioned stability conditions, the interaction control and its two forms of application: the impedance control, which will reveal unsuccessful in the exoskeleton field, and the admittance control.

- Part III presents three control strategies implemented for lower-limb rehabilitation exoskeleton. The first one addresses the problem of monitoring and recovering postural balance. This is one of the main function a lower-limb exoskeleton should have, considering that the user is followed in a rehabilitation therapy to regain control on the impaired limb. The second and the third strategies present two methods to obtain patient compliance without having to rely on biological signals, such as EMG or EEG. In Part III, transparent control is presented, which is a particular operative mode aimed at minimizing the interactions between the exoskeleton and the human, in order to maximize the human range of motion, avoid hindering movements, in a perspective of an exoskeleton worn on daily basis to help in daily-life activities.
- The Appendix is exploited as a theoretical vault. When it was required to know a particular piece of theory, but this would have implied a strong deviation from the current discussion, I placed it in the Appendix. The lecture is kindly advised.



*PART I:*  
*State of the Art*



# Chapter 2

## State of the Art

This section is devoted to presenting the state of the art in rehabilitation exoskeletons, focusing primarily on robotic devices for the rehabilitation of the lower limbs. It is important to provide a context to the reader before exploring the theoretical background in order to understand, at least intuitively, the prior objectives and the main tasks demanded to rehabilitation exoskeleton technologies.

The following discussion is based on the documents [1-3], which present a solid narrative review of the state of the art of these devices based on a vast number of articles published in the last decades. These papers have been fundamental to fix in mind the major requirements asked to robotic exoskeletons, such as ergonomics, safety, stability in the man-machine interaction, human motion intention recognition and prediction to be compliant with the users.

Let the author introduces the argument by focusing on the causes that brought many robotic researchers to explore the vast field of rehabilitation robotic auxiliary support.

Motor dysfunctions can be caused by traumas, surgery, stroke, spinal cord injury, and even aging. They impact physically and mentally on the patients and represent a heavy medical burden both to society and family. In addition, long periods spent lying down in bed or sitting may result in complications, such as pressure ulcers, muscle atrophy, organ dysfunction, edema, osteoporosis, which aggravate the health condition.

The main objective of traditional motor rehabilitation treatments is to make patients regain the independence in daily activities. Physical rehabilitation promotes, indeed, motor recovery in terms of neural plasticity and functional recovery, by suitably dosing and progressively increasing the number of training sessions and the intensity and the number of repetitions of task-oriented movement exercises. Neural plasticity is the capacity of the neurological and nervous system's structures to modify or reorganize the neural and nervous connections in response to events and experience that cause anatomical or functional changes in the brain, even in case of sever lesions of the nervous system or brain damage. Neural plastic rewiring involves the perilesional tissue and injured hemisphere, the contralateral brain, subcortical, and spinal regions [1]. The latter are specifically involved in the lower limbs nervous control.

To meet the increasing demand of professional rehabilitation procedures with daily assistance, robotic devices have been drawn increasing attention to achieve intelligent training and evaluation. Their main contributions in the rehabilitation field are the maximization of afferent inputs from peripheral joints and provide task-specific stimulation to the central nervous system to promote functional recovery [1]. Robotic devices can be distinguished into end-effector and exoskeleton devices.

The robotic end-effector devices use footplates or handles to assist the patient's limb movement. Being connected through the most distal segment, no joints alignment is required.

**DEFINITION 1:** A robotic exoskeleton may be defined as a mechatronic system identified as a wearable man-machine device, made through anthropomorphic design, working in parallel with the human body ergonomically and according to the user's voluntary motion intention, to augment, complement, or substitute the functions of impaired natural human limbs.

Since directly connected to portions of the impaired human limb and replicating its morphology, the exoskeleton's joints must be aligned to the human joint. This characteristic is measured by the matching performance, and it is paramount to construct an ergonomic robotic structure and to guarantee for comfort.

According to the interactions with the human wearer, a further categorization divides the robotic systems into active, passive, active-assisted, resistive, and interactive devices:

- Active devices provide active assistance to the patient's movement by providing assistive torques by means of the actuators.
- Passive devices provide unpowered assistance to the patient's movement, by means of elastic textile and spring-based systems.
- Active-assisted devices complete the movement after the patient began a movement.
- Resistive devices are designed to oppose to the patient's movements.
- Interactive devices exploit control strategies to assist, correct, and provide the complementary torques necessary to complete the initiated movement.

Passive (unpowered) exoskeletons do not contain powered elements and represent the reference point for ergonomic designs. The characteristic bionic design, based on human muscle distribution, tendon-based transmission, and skeleton-based support, joined to the employment of soft materials, such as plastics and elastic textiles, especially for the coupling elements, which connect portions of human limbs to the exoskeleton, allows to adapt well to the singular patients' morphology and results, in general, in dexterous structures.

Active (powered) exoskeletons, on the other hand, must provide the assistive torques in an ergonomic way to aid in reshaping or maintaining the mobility of patient affected by motor dysfunctions while completing training exercises. By restricting the horizon on the active robotic exoskeletons for lower-limb rehabilitation, there are two main categories: the platform-based exoskeletons, or static robots, and the overground robots, divided into crutches-based exoskeletons, and self-balanced exoskeletons (Figure 1-1). Static robots allow rehabilitation treatments in a fixed area. The users generally wear the lower-limb exoskeleton under the protection of weight support structures and exploit treadmills to perform gait recovery exercises, allowing intensive training of the patient's legs without bearing the body weight on them but constraining them on a specific trajectory in space. Crutches-based exoskeletons allow the patients to ambulate in not confined areas. Crutches involve patient's upper limb to help in controlling postural balance. Intelligent crutches present a button panel to adjust the exoskeleton's movement modes and interaction. The Israeli ReWalk series is one of the major exponents of the category. Self-balanced exoskeletons exploit control strategies to automatically adjust movement to maintain or

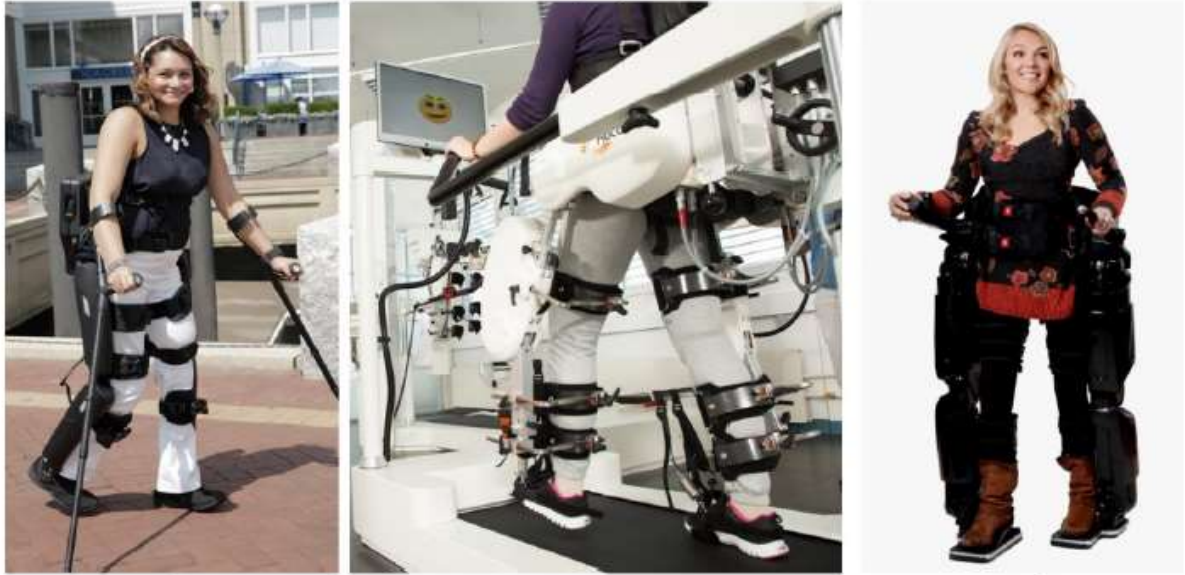


Figure 2-1: Examples of rehabilitation exoskeletons, crutches-based on the left, platform-based in center, self-balance algorithm-based on the right. Reprinted from [2]

recover postural balance of the whole human-exoskeleton system without structural assistance. Exoskeletons Rex and LOPES belong to this category.

Devices	Working Form	Actuator	Control Strategies	Target Parts of Human
Lokomat	Treadmill-based exoskeleton	Motor	Position and impedance	Hip and knee
ALEX III	Overground	Motor	Balance and impedance	Hip, knee and ankle
ReWalk	Overground	Motor	Force and impedance	Hip and knee
Indego	Overground	Motor	Position and force control	Hip and knee
Mindwalker	Overground	SEA-motor	Electroencephalogram (EEG)-based position control	Hip, knee and ankle
BLEEX	Overground	Hydraulic Cylinders	Position and force control	Hip, knee and ankle
Ankle-foot Exoskeleton	Overground	Pneumatic Muscles	Position and force control	Ankle
LOPES	Treadmill-based exoskeleton	Bowden Cable-based Series Elastic Actuator	Torque	Hip, knee and ankle
Rex	Overground	Motor	Balance and force control	Hip, knee and ankle
HAL	Overground	Motor	EMG-based force control	Hip, knee and ankle

Table 2-1: Summary of existing exoskeletons and their related technical details. Reprinted from [2].

Joint actuators make powered exoskeletons to deliver the required power to achieve the auxiliary movement [2]. The ideal drive must be lightweight, small, and provide enough drive torque, while having a good heat dissipation [3]. Electric motor-driven exoskeletons allow fast responses. However, due to the size and weight of batteries, motors, and gear reducers to transform the motor's low-torque high-velocity output into the required high-torque low-velocity input, the exoskeletons are often heavyweight bulky, and not flexible. In addition, being used for rehabilitation purposes, the movements' velocity is often low to prioritize safety during training. Pneumatic actuators are implemented in the form of pneumatic artificial muscles (PAMs). These systems are compliant actuators mimicking human muscles, they are lightweight and present a great power-vs-weight ratio. The produced force output is lower with respect to the electric motors, but still sufficiently high to be used in rehabilitation assistance tasks. The main drawbacks of these actuators are the inevitable hysteresis between the inflation and deflation process, and the nonportable bulky air compressor, the power supply, which allows ambulation within a limited range. Hence, their application is limited to platform-based exoskeletons.

Due to the uniqueness of each human being, it is necessary to perceive human motion and provide it to the exoskeleton to adjust the pre-planned control strategies and joints' trajectories. This process is called human motion intention recognition, or voluntary motion intention recognition, and it is implemented to obtain man-machine interaction and state information, on the basis of which the robotic exoskeleton can "understand" the purpose of the human motion and even predict the possible future movements. Human motion intention recognition is a fundamental technique in control design for exoskeletons, since it lets achieve comfortable assistance and keeps the patient involved during the therapy session, guaranteeing the benefits of neural plasticity, which would not be achieved if the movements were imposed by the machine, i.e., if the mechanical structure dragged the human limb. The intention information acquisition may be based on motion signals, biological (or physiological) signals, and man-machine hybrid signals [2]. Motion signals are kinematic and dynamic signals measured by IMUs, gyroscopes, angle position sensors, and force or torque sensors, embedded in the robotic structure, on links and under the feet soles, in the coupling elements, and eventually placed on the human patients, by means of elastic bands with Velcro®. Intention perception based on biological signals, such as EEG or EMG, respectively, the command from the brain and the execution from the muscles, extracts direct motion intention information and have the quality of reducing the hysteresis of the process. These signals are extracted by means of non-invasive electrode-based sensors, posed on headband for EEG, or on the skin over muscles to extract superficial EMG. The main drawbacks are the high variability, implying performing repeated calibrations at low time distances, the low signal-to-noise ratio implicit in non-invasive sensors, the complex filtering processes, and the time-consuming don process. Other physiological signals of interest are the metabolic cost, which is often measured indirectly, the heart rate, and the respiratory rate [3]. MINDWALKER combines EMG and EEG to derive the motion features to improve accuracy [2]. The third method is based on interaction forces, which are extracted by force sensors placed in the coupling elements, and it establish a man-machine sensor network to utilize both the biological and motion signals.

Data fusion algorithms are often needed to merge and derive information from the multitude of sensors placed in the system.

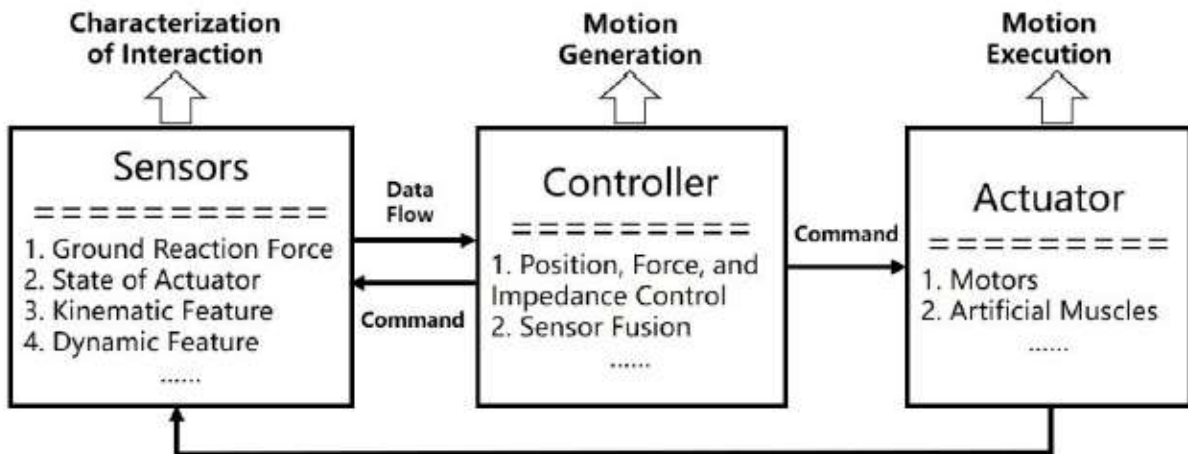


Figure 2-2: Schematic and conceptual scheme for rehabilitative exoskeletons. Reprinted from [2].

The exoskeleton compliant control strategy is based on the result of intention perception. Controlling the joints to assist the human body in accordance with the wearer's motion intention or the physiotherapist's plan was key to ensure that the system generated the desired motion and produced auxiliary effects. Trajectory planning control is adopted when the patient lost entirely or almost entirely motor ability, i.e., the patient's muscles are unable to provide the strength required to move their limb. In these cases, one speaks of passive rehabilitation, without patient's active involvement. Gait trajectory planning algorithm generates periodic joints' trajectories to reproduce specific movements in the operative space. The machine simply drags the human limb in performing repetitive preplanned movements. The control parameters considered can be related to healthy human gait or it is possible to use a mathematical model to generate gait trajectories and compute this way the required parameters. Exoskeleton Rex uses a ZMP-based gait model in order to ensure postural balance too (see Appendices A3 and A4). To involve actively the patient's muscles, it is possible to employ impedance/admittance model in order to design the robot behavior displayed at the port of interaction with the human, i.e., at the coupling element. Advanced methods consider variable and adaptive impedance/admittance parameters to suitably adapt to the movement's stage and context. LOPES II, the exoskeleton employed in the European project Balance (see [30] and section 4.3) presents an admittance controller.

The control of rehabilitation exoskeletons is performed based on kinematics and dynamics of the robot. Hence, the accuracy of the model heavily affects the final performances. Some valid strategies are proposed in Chapter 4, considering different tasks (postural balance and patient compliance), but are based on a simplistic model of the coupled human-exoskeleton system. Due to the high order, strong coupling effects, and nonlinearities, which make difficult to analytically solve the dynamics, many researchers focused on intelligent control based on neural networks, genetic algorithms, fuzzy logic, chaos theory, and other methods. Unfortunately, these methods are not yet mature [3]. Control strategies may consider also a human model, such as muscular-tendinous-skeletal models, or based on several physiological signals. However, due to the implicit complexity, which often requires advanced machine learning techniques or advanced artificial intelligence support, and due to the presence on the market of those model, this Thesis will focus on exoskeletons exploiting non-human models.

Although the rising interest in this technology, the expanding horizon of application possibilities, and the undeniable advantages exoskeletons may bring to the rehabilitation field, it would be incorrect to not

linger on the main and difficult challenges present at these days, that shows how this technology is still in its infancy and it is not yet ready to be broadly commercialized. The first aspect to consider is the significantly low matching performance. The distribution of the exoskeleton's joints cannot mirror the human joints' distribution, causing misalignment during movements, degrading man-machine interactions and ergonomics. The exoskeleton devices are typically redundant to improve flexibility and avoiding limiting the possible range of movements, however, the complex structure composition and hardware lines affect severely the system's performances. To improve ergonomics, wearable passive technology has been taken as a point of reference, since it is characterized by a well-bionic design and the employed materials allows safety and comfortable interface with the human.

The second aspect to consider is the sensor-based feedback at the basis of the exoskeleton control. Motion and force/torque sensors are generally cheaper and easier to embed in the mechanical design. However, although the reliability and stability of the results, voluntary motion intention recognition and prediction based on those signals is affected by a large hysteresis due to signal conversion and decoding process. Human motion intention recognition based on biological signals analysis has good timelines, but data tend to be unstable, and the use process is cumbersome. The explored solutions focus on intelligent controller based on machine learning techniques and more complex models which consider the physical model of the human body.

The third aspect concerns the inevitable tradeoff between the desired low system's weight and the desired high power-to-weight ratio of driving units. Electric motors offer high performances but the weight of power supplies, the motor itself, and transmissions cannot help in reaching lightweight expectations. The use of pneumatic artificial muscle actuators which not only have a high power-to-weight ratio but are also lighter and offer compliance properties is limited due to the dimensions and weight of the air power supply, limiting the application to fixed area exoskeletons. The final aspect to consider is the high deviation between the system motion control and human motion. The complexity of controlling a coupled system characterized by strong autonomy of human motion and strong coupling interactions has made difficult to reach good properties in these terms. A control strategy that aims at making the exoskeleton transparent to the human motion, i.e., make the exoskeleton follow the human movements as a shadow, has been proposed and analyzed in section 4.3. However, it is still troublesome having the exoskeleton "perfectly" following the human motion and providing assisting torques at the same time.



*PART II:*  
*Theoretical background*



# Chapter 3

## Interaction Control

### 3.1 The ABLE project

Before proceeding to a more detailed theoretical discussion of the fundamental concepts and notions to control a lower-limb rehabilitation exoskeleton to ensure postural stability and patient-compliance, at the point to reach even a transparent operative mode of the joints, I consider useful to introduce these arguments by means of an example to highlight the main hindrances to this goal.

In the article [4], Bastide et al. present a simplified and sort of naïve approach to considering an exoskeleton operating in transparent mode when coupled and interacting with a human user and proceed to analyze how “the impact of wearing an exoskeleton, even a “transparent” one, may be non-trivial and could affect the optimality of human motor behavior”. In this experiment, they considered an upper-limb 7 DoFs back drivable exoskeleton called ABLE, whose architecture’s description can be found in [5], and investigated the robot’s “transparency” during elbow flexions and extensions. From a modeling perspective, the human upper limb and lower limb can be both described as compound pendulums with their inertia, friction, and other dissipative effects, subjected to the gravitational field, generally modeled as a linearized stiffness component. Elastic deformations, slacks of the parts, and other phenomena displaying a stiffness behavior are typically neglected.

As shown in the schematic view in Figure 3-1, the exoskeleton and human forearms can be modeled as simple pendulums, with a single DoF, coupled with interacting torque  $\tau_i$ . In the considered model,  $\theta_r$  represents the angular position of the exoskeleton’s “forearm” link, subscript “r” stands for “robot”, and  $\theta_h$  is the angular position of the human forearm. Both angular positions are measured with respect to the vertical.

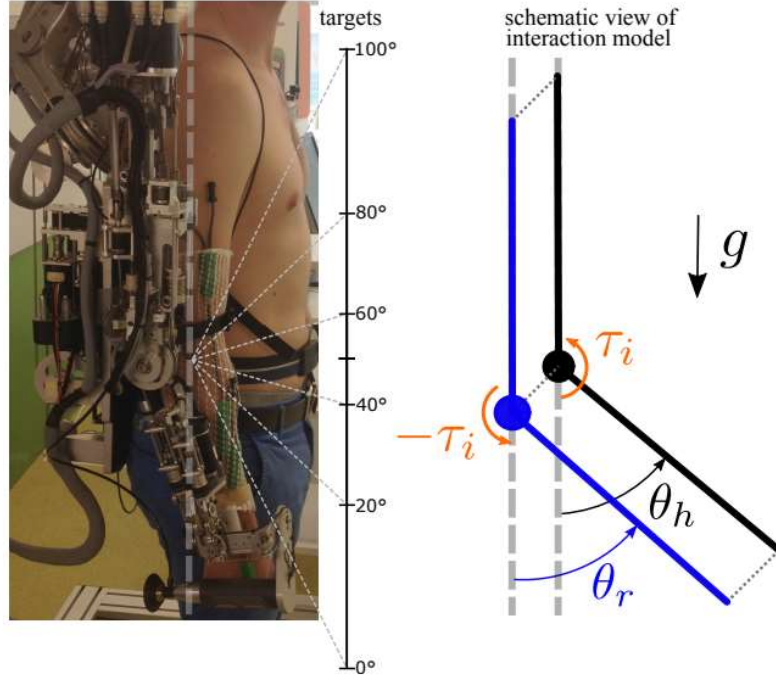


Figure 3-1: Lateral view of ABLE exoskeleton worn by the user (on the left). Schematic view of the interaction model between the exoskeleton and the human forearm. Reprinted from [4]

The equations of motion of the coupled system are given by the equation of motion of the single pendulum systems in the following. Please notice the role of the interacting torque  $\tau_i$  in coupling the two equations.

$$\begin{cases} I_h \ddot{\theta}_h + b_h \dot{\theta}_h + m_h g l_h \sin(\theta_h) = \tau_h + \tau_i \\ I_r \ddot{\theta}_r + b_r \dot{\theta}_r + F_{NL} + m_r g l_r \sin(\theta_r) = \tau_r - \tau_i \end{cases} \quad (3.1)$$

where subscripts  $r$  and  $h$  denote similar quantities related respectively to the robot and the human systems,  $I, b, m, l$  stands for the forearm's axis-specific respectively moment of inertia, coefficient of viscosity, mass, and length,  $F_{NL}$  is the nonlinear friction in the exoskeleton's joint,  $\tau$  is the system's joint torque,  $\theta$  is the joint's angular position, and  $g$  is the gravity acceleration.

Notice that, linearizing the two sinusoidal terms, considering small oscillations approximation ( $\sin \theta \approx \theta$ ), it is possible to rewrite the gravitational load term as:

$$mgl \sin \theta \approx (mgl) \theta = k \theta \quad (3.2)$$

where  $k = mgl$  can be seen as an elastic stiffness linearly approximating the gravitational load on the pendular "mechanisms". For completeness' sake, it is reported the equation of motion of the coupled system considered as whole, since it may be useful to the reader to understand the main aspect of the arguments presented in the following Chapters. By the trivial substitution of  $\tau_i$  in one of the equations of motion in Equation 3.1, one obtains:

$$\tau_h + \tau_r = [I_h \ddot{\theta}_h + b_h \dot{\theta}_h + k_h \theta_h] + [I_r \ddot{\theta}_r + b_r \dot{\theta}_r + F_{NL} + k_r \theta_r] \quad (3.3)$$

Equation 3.3 shows that the torques (i.e., the mechanical energy) provided by the exoskeleton's motor and the human are needed to move both the mechanisms, divided in brackets.

Consider the following assumptions:

- 1) Since two coupled dynamically interacting systems are considered, one should rely on the impedance/admittance control, as presented in sections 3.3 and 3.4. The transparent control law used to drive the exoskeleton is defined as follows:

$$\tau_r = \hat{b}_r \hat{\theta}_r + \hat{F}_{NL} + \hat{k}_r \hat{\theta}_r \quad (3.4)$$

- a. Notice that  $\hat{\theta}_r$  and  $\hat{\theta}_r$  are the angular velocity and position estimated from the motion sensors applied on the exoskeleton's link, while  $\hat{b}_r$ ,  $\hat{F}_{NL}$ ,  $\hat{k}_r = \hat{m}_r g \hat{l}_r$  are estimations of the dynamic parameters of the robot's link.
- b. Notice that the impedance control law **cannot be used to compensate for the exoskeleton's inertia**. In fact, in the case of two dynamically interacting systems coupled together, the inertias are strongly related to both coupled stability and performance. The stability conditions constrain the minimum value of the apparent inertia displayed by the robot to a positive constant. Hence, the apparent inertia cannot be lowered arbitrarily without degrading the stability of the system. In absence of opportune modules introduced in the control scheme with the sole purpose of coping with the inertia of the robot and the apparent inertial behavior shown by the exoskeleton at low frequencies, it is more proper to consider as control law the equation shown in Equation 3.4. Further explanations will be provided in the reading of this Part.
- 2) The estimated quantities are accurate, at the point that there is **perfect compensation**:

$$\begin{aligned} \hat{b}_r &\cong b_r, \\ \hat{\theta} &\cong \dot{\theta}, \\ \hat{F}_{NL} &\cong F_{NL}, \\ \hat{k}_r &\cong k_r \Leftrightarrow \hat{m}_r \cong m_r, \hat{l}_r \cong l_r, \\ \hat{\theta}_r &\cong \theta_r, \end{aligned} \quad (3.5)$$

- 3) Human and robot joint angle accelerations are equal, i.e., assume **perfect tracking** (or, as presented in section 4.3, synchronism):

$$\ddot{\theta}_h = \ddot{\theta}_r = \ddot{\theta} \quad (3.6)$$

Given those assumptions, the equation of motion of the exoskeleton can be simplified as follows:

$$\tau_i = -I_r \ddot{\theta} \quad (3.7)$$

Therefore, substituting in the equation of motion of the human "mechanism", it derives:

$$(I_h + I_r) \ddot{\theta} + b_h \dot{\theta} + k_h \theta = \tau_h \quad (3.8)$$

In the case of coupled systems, impedance/admittance control cannot be used to directly compensate the inertial behavior displayed by the exoskeleton at low frequencies, i.e., the range of frequency to which human movements belong; even lower if one considers that the exoskeletons operate in rehabilitation

therapy, for which the movements are even slower. This is one of the main difficulties encountered in this field, since having a residual inertial behavior felt by the user means that the patient not only has to exert enough muscle torque to move their limb, which is already difficult when in impaired conditions, but the user is also forced to drag the exoskeleton's mechanical structure's residual inertia.

The aforementioned article highlights the main rivals when dealing with exoskeletons' transparency mode:

- 1) Since there are dynamically interacting coupled systems, one should rely on admittance/impedance control, the last cannot be used to compensate adequately for the robot's inertia, since related to coupled stability.
- 2) The transparent control law must compensate perfectly for the exoskeleton's mechanical reactance characteristics.
- 1) It is necessary to have the robot joint accelerations with perfect tracking of human ones.

These are the main arguments discussed in the following Chapters.

## 3.2 Interaction Control

### 3.2.1 Robot-Environment Interaction

In most of robotics applications, a robot is demanded to interact dynamically and mechanically with its environment, being this a manipulator deployed for manipulation and material handling tasks [6] or an exoskeleton designed to assist and support patients' movements during physiotherapy exercises. A dynamical interaction between two systems manifests typically as the exchange of power through the interface between (or the ports of) the two systems, which can be generally divided into the control system (plant + regulator) and the environment, which encapsulates all those systems different from the plant on which the designed controller has no regulation power.

Considering a human analogy, one of the most impressive human abilities is to explore and interact with the objects within the environment, suitably modifying their behavior according to the characteristics of the manipulated object, the goal of the movement, and the constraints imposed by the environment itself. For instance, when we are grasping a brittle object or performing tactile exploration, we spontaneously tend to use the fingers and to perform slow, compliant movements. Instead, when there are no obstacles imposed by the environment there is freedom of movement, we tend to perform fast and stiff (as opposed to compliant) movements. In such examples, based on daily human actions, consciously or not, we cannot plan our movement intentions neglecting the dynamical properties of the environment, such as inertia, stiffness, damping, and the eventual presence of environmental constraints. However, in classical control theory, the environment is typically simplified as source of disturbances, without investing any further its dynamics. That is the reason why early robotic control theory does not address the problem of interaction with the environment, but it focuses mainly on tracking and regulation control problems.

The design of the latter category of controllers, namely the "servo controllers", is mainly concerned with guaranteeing the nominal stability of the system and its tracking capability, thus ensuring the stability of the closed-loop control system based on the nominal plant model, which does not consider eventual disturbances, noise, nor parameter variability, and the minimization of the deviation of the controlled output vector with respect to the reference command vector, so that the error is contained within the tolerance margins required by the application. In this context, the environment the plant is situated in is ordinarily underestimated and not better specified. The possible robot-environment interactions considered are simplistically modeled as state-independent low-magnitude disturbances affecting the plant's controlled output(s) and hindering the servo controller's purposes. According to the required performances, accuracy, and degree of precision, "classical" control strategies are therefore adopted to reject disturbances by bounding or minimizing the effects of the disturbances of the system's outputs. Alternatively, it is possible to exploit more "modern" control techniques, which share the same purpose of classical strategies, but are also concerned with enhancing the system's noise sensitivity and robustness to unmodeled dynamics and parameter uncertainties.

However, quoting Professor Hogan [6]: "Command and control of a vector such as position or force is not enough to control dynamic interaction between systems; the controller must also command and control a relation between port variables". To understand better this passage, please follow the example reported below [7].

**Example 3-1:** Suppose a robotic manipulator for material handling and transportation. A simplified model through which it is possible to represent its dynamic is the one depicted in Figure 3-2.

The dynamic characteristics of the robot are expressed as lumped parameters; the constant mass  $m$  represents the robot's inertia characteristics, which is subjected to the actuators and environment's resulting forces,  $F_a$  and  $F_e$ , respectively, finally, the friction losses are modeled as a damper with damping factor  $b$ , connected between the mass and the ground. Defined with  $x$  the manipulator's position, the (trivial) equation of motion describing the model dynamics in time domain is:

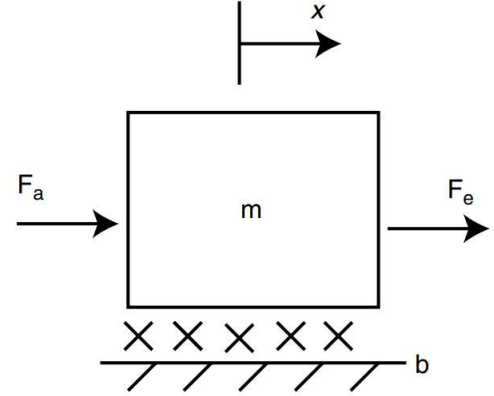


Figure 3-2: Simplified lumped parameter model with inertial, frictional, actuator, and environmental forces. Reprinted from [7]

$$m\ddot{x}(t) = F_a(t) + F_e(t) - b\dot{x}(t) \quad (3.9)$$

which once transposed into frequency domain by applying the Laplace transform is:

$$F_a(s) + F_e(s) = (ms^2 + bs)X(s) \quad (3.10)$$

Consider a proportional-integral motion control law (Laplace variable  $s$  is omitted for visual simplicity):

$$F_a = K_P(X_{ref} - X) + \frac{K_I}{s}(X_{ref} - X) \quad (3.11)$$

posing  $X_{ref}$  as the Laplace transform of the reference position of the manipulator,  $K_P$  and  $K_I$  are the proportional and integral gain, respectively.

In isolation ( $F_e = 0$ ), the closed-loop transfer function is:

$$\frac{X}{X_{ref}} = \frac{K_P s + K_I}{ms^3 + bs^2 + K_P s + K_I} \quad (3.12)$$

Exploiting the Routh-Hurwitz stability criterion (see Appendix B), a condition for isolated/nominal stability is the following upper bound on the integral gain:

$$K_I < \frac{bK_P}{m} \quad (3.13)$$

Suppose that the manipulator grasps and picks up an arbitrarily large mass  $m_e$  in its environment. The above stability condition is no more sufficient to guarantee the stability of the coupled system, the simple act of grasping an object can lead to instability. The manipulator grasping and keeping the object can be modeled as the previous system rigidly coupled to a mass  $m_e$  with a mass-less coupling element, which equivalently corresponds to increase the lumped mass parameter from  $m$  to  $(m + m_e)$ . A more proper condition for the coupled stability is therefore:

$$K_I < \frac{bK_P}{(m + m_e)} \quad (3.14)$$

Therefore, in control design, the value of  $K_I$  must be chosen sufficiently low to satisfy the condition expressed by Equation (3.14). However, for any fixed controller gains, interaction with a large mass  $m_e$ , such that  $K_I \in (\frac{bK_P}{(m+m_e)}, \frac{bK_P}{m})$ , will always destabilize a system due to the change of the stability condition itself.

Example 3-1 shows that just ensuring the nominal stability of the manipulator in isolation is not sufficient to guarantee interaction stability, even considering one of the simplest models of manipulator and environment. Therefore, the requirements in designing interaction controllers must differ from those of servo controllers.

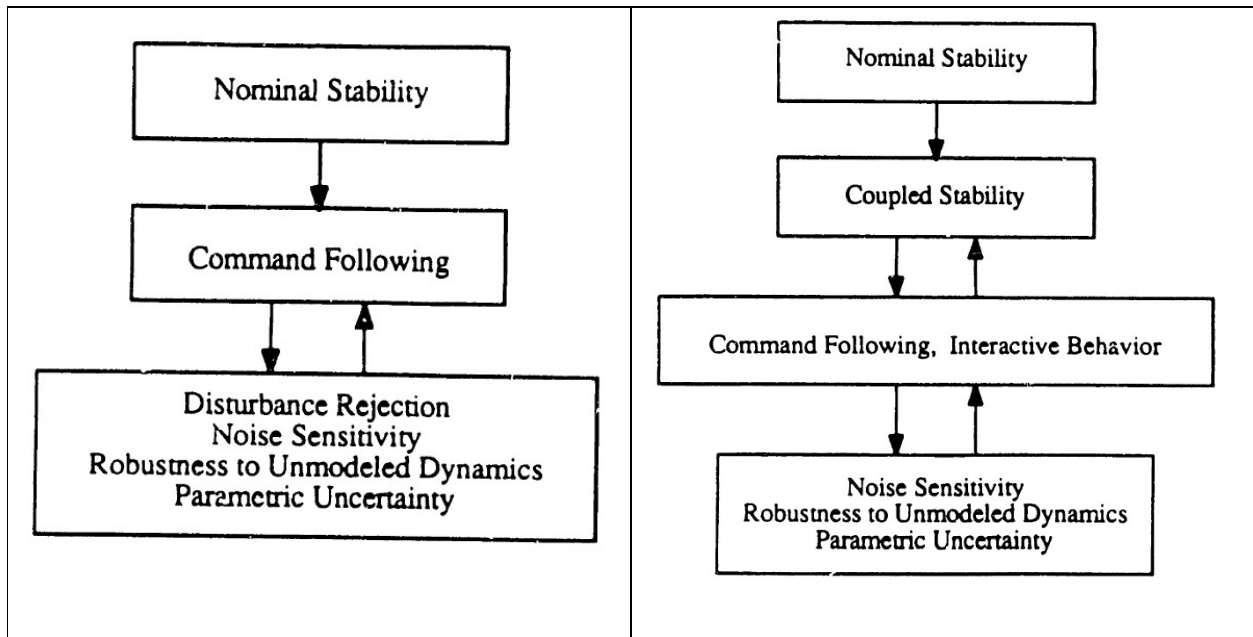


Figure 3-3: Comparison of the design requirements for a servo controller (on the left) and an interaction controller (on the right). Reprinted from [8]

Figure 3-3 provides a simple comparison of the hierarchy of design requirements for a servo controller and for an interaction controller. As it can be seen, nominal stability is still the main requirement to meet, to ensure that the systems in isolation, i.e., when not interacting with each other, are stable. However, a new requirement appears at the second place for interaction controllers. Coupled stability addresses the stability of a feedback-controlled system (the robot) which is expected to interact extensively with its environment [8]. Readers with great intuition will have understood that it is paramount to know the properties and dynamical characteristics of the environment to be able to consider and ensure coupled stability. Indeed, in interaction controller design, the environmental forces cannot be undervalued and treated as external disturbances for two main reasons. First, the environmental forces encountered in these applications have high magnitudes that may equal or overcome the robot's nominal capacity. Secondly, in these applications, environmental forces depend on the state of the system. Conversely, the environmental disturbances considered in classical regulation problems have small magnitudes compared with the plant's capacity and are typically assumed state-independent [9]. The concept, the criteria, and the conditions of coupled stability are addressed in section 3.2.4. Let me anticipate that the first design procedures associated to coupled stability are often "too much" conservative. Although, on one hand, it is more cautious to assess this system's property with respect to every possible environment the robot is likely to

interact with, on the other hand, however, it is possible to restrict the set of possible environments to those that are more likely to encounter. In this way, designers are able to manage a margin within which trading performance against coupled stability. Notice that also the interactive behavior has been added to the performance specifications since stability itself is an insufficient requirement to this purpose.

### 3.2.2 Interaction Control

Interaction control is the general approach aimed at the regulation of the robot's dynamic behavior at its ports of interaction with the environment, also called interactive behavior.

From bond graph theory, an "interaction port" can be defined as a physical interface through which two coupled systems exchanges power. Such interface is defined by a set of power-conjugate variables, namely effort  $e$  and flow  $f$ , such that the power exchanged through the port is defined as:

$$P = e^T f \quad (3.15)$$

The dynamic relationship between power variables *at a port* is called "impedance", if it maps the flow input (vector) to the effort output (vector), or "admittance", if it maps an effort input (vector) to a flow output (vector). Notice that one is the causal dual of the other, i.e., the role of input and output are exchanged, and that, since they are referred to specific ports, they are called port functions and not transfer functions, which, in contrary, relates inputs and outputs at arbitrary locations. Using the definition proposed by H.M. Paynter (1961), reported in [8]:

**DEFINITION 2:** "[Impedance and admittance] are causal dynamic operators which map an input time function  $\mathbf{u}(t)$  onto an output time function  $\mathbf{y}(t)$  such that the present value of the output  $\mathbf{y}(t)$  may depend on the entire past history of the input  $\mathbf{u}(t - \tau)$  for  $0 < \tau < \infty$ , and such that  $\mathbf{u}^T(t)\mathbf{y}(t)$  is the instantaneous power flow into the system."

In electric domain, the voltage corresponds to an effort while the current to a flow, for which the electric impedance can be defined as:  $Z(t) = v(t)/i(t)$  and the electric admittance can be defined as:  $Y(t) = i(t)/v(t)$ . The analogous in mechanical domain, where the force (torque) corresponds to an effort, while the linear velocity (angular velocity) to a flow, can be defined as [7]:

**DEFINITION 3:** “Mechanical impedance at a port (denoted  $Z$ ) is a dynamic operator that determines an output force (torque) time function from an input velocity (angular velocity) time function at the same port.”

**DEFINITION 4:** “Mechanical admittance at a port (denoted  $Y$ ) is a dynamic operator that determines an input velocity (angular velocity) time function from an output force (torque) time function at the same port.”

The mechanical impedance can be approximated as a dynamic extension of a stiffness, considering also the inertial and frictional/dissipative effects, while its dual, the mechanical admittance, can be considered a dynamical extension of a compliance. An example of mechanical impedance of the second order is the model of a linear mass-spring-damper system which receives in input a certain velocity and provides in output a suitable force.

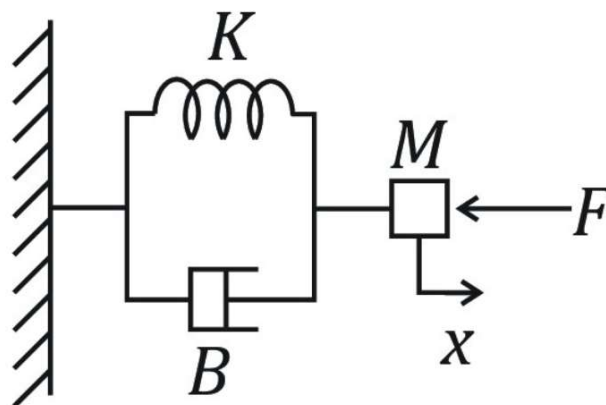


Figure 3-4: Linear mass-spring-damper system. The impedance function describing this system is:  $Z(s) = \frac{F(s)}{v(s)} = ms^2 + bs + k$ , while the admittance function describing this system is:  $Y(s) = \frac{v(s)}{F(s)} = \frac{1}{ms^2 + bs + k}$

Why am I bothering with control strategies based on port functions instead of the more classic exploit of motion and force control techniques? Unfortunately, since the robot and the environment meet at an interaction port, motion and force control strategies require the complete characterization of both systems to be correctly designed. Acquiring the knowledge of the properties and dynamic characteristics of the environment can be troublesome. In fact, to correctly identify the environment, it is necessary to stably interact with the environment, even though the most complete knowledge of the environment is necessary to have a stable interaction. In addition, considering the possible applications, a robot manipulator should be designed to ensure coupled stability for a variety of environments, further complicating the design.

On the other hand, dynamic port behavior is exclusively a property of the considered system [7], i.e., the robot, and it is completely independent of the other systems interfaced with. Thus, since it defines the relationship of the power-conjugate port variables without determining either, impedance operator completely describes the robot's interactive behavior without providing a model describing how reaction forces are generated in association with environment deformation [11].

The problem now shifts to develop a well-characterized model of the robot. Should it be an impedance or an admittance? Hogan proved in [7] that if one system can be modeled as an impedance, the system coupled to it must behave as an admittance, and vice versa. Therefore, the behavior of the robot can be derived as the dual behavior of the environment. In the specific case of a manipulator, it mainly interfaces with movable objects, being these inertias or surfaces, and kinematic constraints.

Inertia is a trivial case of admittance function, in fact, it receives in input a force and gives as output an acceleration. A kinematic constraint imposes zero motion in one or more directions independently of the applied force, thus it cannot be represented as an impedance. In conclusion, the environment's properties can be modeled as an admittance, hence, the robot manipulator should behave as an impedance. In [12], the author presented a model of a manipulator with a control law based on impedance control:

$$\mathbf{F} = \mathbf{K}(\mathbf{X} - \mathbf{X}_0) + \mathbf{B}(\mathbf{V}) \quad (3.16)$$

where  $\mathbf{X}$  and  $\mathbf{V}$  are respectively the manipulator's position and velocity vectors,  $\mathbf{X}_0$  represents the commanded position vector,  $\mathbf{F}$  represents the force applied by the environment,  $\mathbf{K}(\cdot)$  defines the force-displacement relationship, finally  $\mathbf{B}(\cdot)$  defines the force-velocity relationship. In the article, it is proved that until  $\mathbf{K}(\cdot)$  is the gradient of a potential function and  $\mathbf{B}(\cdot)$  is suitably chosen to obtain the stable positioning of an arbitrary small mass, then the manipulator is able to stably interact with every dissipative environment.

However, this model is valid under strong ideally assumptions, such as the links are rigid bodies, actuators are pure torque sources. Under such hypotheses, the control law presented above can compensate also gravity effects and the joint frictions. In practicality, non-idealities such as actuators and transmission dynamics, the elasticity of joints and links, as well as the delays due to data elaboration, mar the model applicability.

Due to the large links' inertias summed to the motor's inertias, amplified by the gear ratio, which tend to dominate the robot's behavior, it is more feasible to make the robot behave as an admittance. In addition, admittance behavior and control are easier to implement in real hardware.

### 3.2.3 Passivity

From the explored literature on impedance and admittance control implemented in rehabilitative exoskeleton systems, many documents underline the paramount importance of guaranteeing both the system's isolated and coupled stability. For completeness and number of citations, the main work about these concepts is the Doctoral Thesis of James Edward Colgate (1988), which "addresses the control of dynamically interacting systems" [8].

To explore the isolated stability of a system, we can employ the concept of "Passivity". Passivity is related to the concept of availability in Thermodynamics. As every engineer student with a little background in Physics knows, from a merely thermodynamic point of view, every system of engineering interest is by its nature "passive". Let's consider the following example.

**Example 2:** Consider a generic thermodynamic system interacting with the atmosphere (the environment). Suppose that the system undergoes a (possibly irreversible) process from initial state 1 to final state 2. By combining the first and the second laws of thermodynamics we have that:

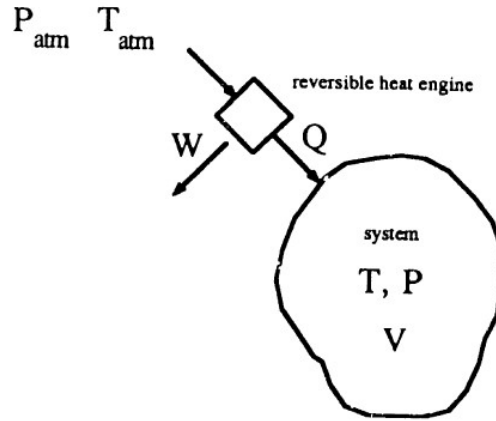


Figure 3-1: General thermodynamic system interacting with atmosphere. Reprinted from [8].

$$W_{1 \rightarrow 2} \leq \int_1^2 T dS - (U_2 - U_1) \quad (3.17)$$

where  $W_{1 \rightarrow 2}$  is the work performed during the state change,  $T$  is the temperature,  $S$  is the entropy of the system,  $U_i, i = 1, 2$  is the internal energy of the system at state  $i$ . The useful work is defined as the amount of  $W_{1 \rightarrow 2}$  which is not spent to displace the atmosphere, hence:

$$(W_{1 \rightarrow 2})_{useful} \leq \int_1^2 T dS - \int_1^2 P_{atm} dV - (U_2 - U_1) \quad (3.18)$$

where  $V$  is the system's volume. For a reversible process, the integrals at second member can be maximized. Since the atmosphere is at constant pressure  $P_{atm}$  and temperature  $T_{atm}$ , the process will be both isobaric and isothermal. Thus:

$$(W_{1 \rightarrow 2})_{useful} \leq -[(U_2 + P_{atm}V_2 - T_{atm}S_2) - (U_1 + P_{atm}V_1 - T_{atm}S_1)] \quad (3.19)$$

Define the property  $\Phi = U + P_{atm}V - T_{atm}S$ . It has minimum value in correspondence of the state  $(P, T) = (P_{atm}, T_{atm})$ . It then follows:

$$(W_{1 \rightarrow 2})_{useful} \leq -(\Phi_2 - \Phi_1) \quad (3.20)$$

Prof. Joseph Keenan defined in 1951 the availability of the system  $\Lambda$  as:

$$\Lambda = \Phi - \Phi_{min} \quad (3.21)$$

Therefore, it immediately follows that the amount of useful work that can be extracted from a system is superiorly bounded by the difference between the availability in the initial state and the last state:

$$(W_{1 \rightarrow 2})_{useful} \leq \Lambda_1 - \Lambda_2 \quad (3.22)$$

The first and the second laws of thermodynamics ensure the existence of a lower bound  $\Phi_{min}$ . Therefore, systems for which  $\Phi$  is bounded from below can supply only finite amount of useful work and are termed

“passive”.

Hypothetically speaking, supposing the existence of systems for which  $\Phi$  is not bounded, the availability would be infinite, i.e., it is possible to extract infinite useful work, and should be properly termed “active”. However, it should be immediately clear to the reader that such systems are nothing else than perpetual motion machines of the second kind, therefore, they cannot exist.

In everyday problems, however, it is common for engineers to face with “active” devices, such as electric motors, amplifiers, and power sources. That happens since most of those “active” devices’ models are based on a limited set of observations, hence, the mathematical equations with which we try to describe a system have limited range of validity. In addition, for most of those system, pushing forward the bounds of validity does not add much to the utility of the result. For instance, a battery is generally represented as a pure voltage source, intended as a pure power source, able to provide voltage indefinitely. However, battery discharging is a daily life experience. That sort of “modeling error” resides in the used time scale. When analyzing a circuit, the phenomena we are interested in have generally small time constants. Hence, the time scale of interest is too short for the battery to discharge significantly, thus the battery is modeled as not discharging at all.

Now focus on finite-dimensional passive linear time-invariant n-port systems described as follows:

$$\begin{aligned}\dot{\mathbf{x}} &= A_{k \times k} \mathbf{x} + L_{k \times n} \mathbf{u} \\ \mathbf{y} &= C_{n \times k} \mathbf{x} + D_{n \times n} \mathbf{u}\end{aligned}\quad (3.23)$$

Notice that  $\mathbf{u}$  and  $\mathbf{y}$  are power-conjugate variables, i.e., generalized efforts and flows associated to the  $n$  interaction ports. Some assumptions must be taken:

- Suppose the system is a minimal representation, meaning that the system is both controllable and observable.
  - The controllable constraint means there exists always a finite controlled input  $\mathbf{u}(t)$ ,  $t \in [0, T]$ ,  $T < \infty$ , able to take the system from the initial states  $\mathbf{x}_A$  to the final states  $\mathbf{x}_B$ . Considering passive systems, the transition will produce or consume a finite energy quantity, therefore the analysis can be focused only on one initial state.
  - The observability constraint allows to join the external (input/output) and the internal (state-based) analyses of passivity. To be fair to the reader, the following dissertation focuses mainly on the input/output passivity criterion, since it is the one presented more often in various articles [14-19,28,29].
- Some assumptions about the inputs:
  - The set of inputs is closed under concatenation, meaning that if  $\mathbf{u}_1(t)$ ,  $t \in [t_1, t_2]$  and  $\mathbf{u}_2(t)$ ,  $t \in [t_2, t_3]$  are admissible inputs, so is  $\mathbf{u}_1$  followed by  $\mathbf{u}_2$ .
  - The set of inputs is translation invariant, i.e., if  $\mathbf{u}(t)$  is an admissible input, so is  $\mathbf{u}(t + \tau)$ .
  - The set of inputs is bounded. In mathematical terms:

$$\int_{-\infty}^t \|\mathbf{u}(t)\|^2 dt < +\infty \quad \text{or} \quad \mathbf{u}(t) \text{ is } L^2(-\infty, t]$$

The complex-variable approach provides a method to examine passivity based on the properties of the driving point impedance matrix (hybrid impedance/admittance matrix), which relates  $\mathbf{u}(s)$  and  $\mathbf{y}(s)$ :

$$\mathbf{y}(s) = Z(s)\mathbf{u}(s) \quad (3.24)$$

with  $Z(s) = D + C(sI - A)^{-1}L$ , if we consider the same state-space representation presented above (Equation 3.23).

In network analysis, systems presenting a single port of interaction, such as an electrical system presenting just a couple of terminals, are called 1-port systems. The most general passivity criterion for linear 1-port system is the following:

**Passivity of LTI 1-port (a):**

An LTI 1-port is passive iff:

$$\operatorname{Re}\{Z(s)\} \geq 0 \text{ for } \sigma \geq 0 \quad (3.25)$$

In other words,  $Z(s)$  is a real rational function in  $s$ . If it satisfies also the previous condition, it is called positive real function. Of course, this criterion is computationally heavy, since requires to evaluate the real part of  $Z(s)$  at each point in the right half  $s$ -plane. An equivalent but computationally lighter method can be found considering the following equivalent conditions.

**Passivity of LTI 1-port (b):**

A linear time-invariant 1-port is passive iff:

1.  $Z(s)$  has no poles in the right half plane,
2. Any imaginary poles of  $Z(s)$  are simple and have positive real residues,
3.  $\operatorname{Re}\{Z(j\omega)\} \geq 0$ .

Equation (3.25) states that right half plane poles and zeros are prohibited, since  $\operatorname{Re}\{Z(s)\}$  must take negative values in the neighborhood of any singularity:

- Condition 1 affirms that the contour cannot enclose any poles.
- Condition 2 affirms that imaginary poles are acceptable only if the negative real part occurs to the left of the pole only.

By combining conditions 2 and 3, we obtain the canonical statement of passivity:

**Passivity of LTI 1-port (c):**

A linear time-invariant 1-port is passive iff:

1.  $Z(s)$  has no right half plane poles.
2.  $Z(s)$  has a Nyquist plot which lies wholly within the closed right half plane.

The direct consequence of passivity is that the phase of  $Z(s)$  is limited between  $\pm 90^\circ$ . Since the phase of  $Z(s)$  corresponds to the phase shift between the output waveform and the input waveform, defined the average power travelling through a port of interaction as the product of the input (output) flow and the output (input) effort, in the case in which both are pure sinusoids, we have that if the phase of  $Z(s)$  is:

- $\angle Z(s) = 0^\circ$ , the average value of product  $u(t)y(t)$  is positive, thus the system consumes energy.
- $\angle Z(s) = \pm 90^\circ$ , the average value of product  $u(t)y(t)$  is zero, thus the system does not consume nor produce energy. Such systems are termed “lossless”.
- $\angle Z(s) \in (90^\circ, +90^\circ)$ , the average value of product  $u(t)y(t)$  is negative, thus the system produces energy.

### 3.2.4 Coupled Stability

In classical control theory, the environment is often omitted and in those rarely cases in which it is considered, it is typically simplified as a source of disturbances, without investigating further its dynamics. Therefore, the early robotic literature does not address the interaction with the environment.

Later, research moved on the study of the kinetic and dynamic properties of the environment the manipulator is deployed in, and it is forced to interact with. The results of these studies were the impedance and admittance control strategies, which are based on the environment’s behavior to determine and design coherently to the application context the behavior of the whole robot-environment coupled system, allowing to perform tasks such as the manipulation of small masses and use of grasped tools. The robotic and control literature that focuses on such control strategies have defined four levels of coupled stability property:

- A) Target dynamics
- B) Closed loop system, assuming rigid links with pure torque sources at the joints,
- C) Closed loop system, assuming that additional dynamic effects (such as the actuator bandwidth limitations and the transmission dynamics) are important, but are included in the manipulator model,
- D) Closed loop system, while accounting for modeling uncertainties, such as unmodeled dynamics or parametric errors.

Professor Fasse developed a method to ensure the stability of closed-loop systems coupled to *passive* environment without posing restriction on linearity properties in his Master’s degree Thesis in 1987. He there defined coupled stability as [8]:

**Definiton 5:** A system is said to have the coupled stability property if:

1. The system is stable when isolated.
2. The system remains stable when coupled to any passive environment which is also stable when isolated.

The motivations for restricting the possible environments to only the passive environments are very interesting. First, most of the environments on interest are passive, such as rigid bodies or approximal to that, rigid surfaces, spring-like element, compliant surfaces, etc. Secondly, passive systems are mathematically well defined and treatable, as presented in the previous section. Thirdly, with respect to the restriction of the input and output's magnitude as proposed originally by Kazerooni, the choice of considering just passive environments is more "natural". Finally, all those reflections may be extended also to some "active" classes of systems.

Let delimit the analysis of coupled stability to the case of interactions between 1-port systems. The considered plant may or may not present a feedback branch, and it is linear time-invariant. The considered environment has a linear dynamics and it is passive according to passivity criterion (c). Without considering any specific application, the analysis of coupled stability must return the property of stability for any possible linear passive environment.

The linear nature of the two systems can be described by a transfer function constituted by the ratio of two rational polynomial in  $s$ . In addition, since the transfer functions are defined by the ratio of power-conjugate variables (flow  $v(s)$  and effort  $f(s)$ ) measured at the interaction port, it is more correct to term these functions as port functions. In the following,  $P(s)$  will denote the driving point impedance of the plant, and  $E(s)$  will denote the port function of the environment.

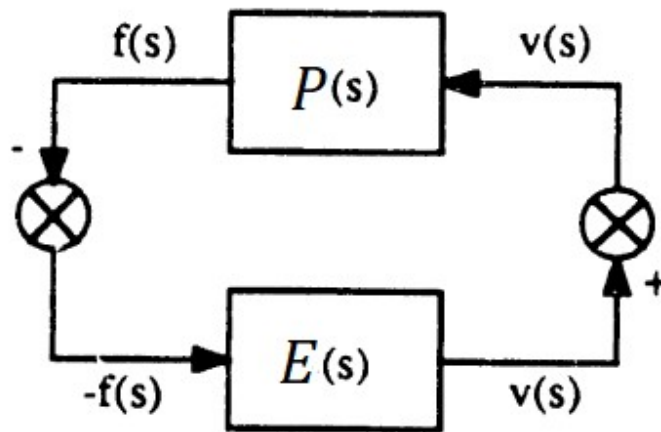


Figure 3-2: Block diagram representation of coupled system. Reprinted from [8].

From the block diagram in Figure 3-6, it is possible to obtain the following system of equations:

$$\begin{cases} f(s) = P(s)v(s) \\ v(s) = -E(s)f(s) \end{cases} \quad (3.26)$$

which corresponds to the following state-space representation:

$$\mathbf{0} = \begin{bmatrix} -1 & E(s) \\ -P(s) & -1 \end{bmatrix} \begin{bmatrix} v(s) \\ f(s) \end{bmatrix} \quad (3.27)$$

To ensure that the coupled system is stable, the roots of the characteristic equation,  $1 + P(s)E(s) = 0$ , must be lay in the closed left half plane (LHP). To study the poles' locations and, hence, determine the stability of the system, it is possible to use the Nyquist stability criterion, considering as open-loop transfer function the product  $P(s)E(s)$ .

Before proceeding with the discussion, however, it is necessary to make some assumptions:

- $P(s)$  is BIBO stable, i.e., the input and output of  $P(s)$  are suitably bounded, such that there exists a state-space representation of  $P(s)$  so that, denoted the plant's state vector with  $\mathbf{x}_P$ :

$$\begin{aligned}\dot{\mathbf{x}}_P &= A_P \mathbf{x}_P + B_P \mathbf{v} \\ \mathbf{f} &= C_P \mathbf{x}_P + D_P \mathbf{v}\end{aligned}\tag{3.28}$$

for which the (zero-state) system output response can be written as:

$$\left. \frac{f(s)}{v(s)} \right|_{\mathbf{x}(0)=0} = P(s) = D_P + C_P (sI - A_P)^{-1} B_P\tag{3.29}$$

The above equation is equivalent to impose  $P(\infty) < \infty$ , i.e., the output response is bounded from above.

- The eigenvalues of  $A_P$  have real part strictly negative:  $Re\{\lambda(A_P)\} < 0$ .
- The first two hypotheses combined determine that the poles of  $A_P$  lie in the closed LHP, and the plant is stable.
- The environment is passive according to the third presented passivity criterion (c):
  - $E(s)$  has no poles in the right-half plane (RHP),
  - $E(s)$  has a Nyquist plot which lies wholly within the closed RHP.

Hence, there are no constraints posed on the magnitude of  $E(s)$ , but its phase must be contained in the range  $\left(-\frac{\pi}{2}; \frac{\pi}{2}\right)$ .

From the plant's point of view,  $E(s)$  acts as a compensator able to change the plant's magnitude by a factor between 0 and  $\infty$ , and the plant's phase by  $\pm 90^\circ$ . To stably interact with *all* passive environment, the plant must have a phase margin of  $\pm 90^\circ$  and gain margin  $(0, \infty)$ . In other words, the mappings of the Nyquist contour through  $P(s)$  must lie in the closed right-half plane.

This conclusion, taken together with the nominal stability of  $P(s)$ , i.e., when the plant is isolated from the environment, is a necessary and sufficient condition to ensure coupled stability, and, according to third passivity criterion presented in section 3.2.3, for  $P(s)$  to represent the driving point impedance of a

**Definiton 6:** A necessary and sufficient condition to ensure the coupled stability of a LTI stable plant coupled at a single port to a LTI stable passive environment is that the driving point impedance of the plant be positive real or, equivalently, that the plant be passive.

passive system. The definition of coupled stability [8] is provided in the next page.

The analysis conducted until now assumed that the plant was passive. This restriction is far away from reality since most of the times the plant is an active system. What happens if we add an active term  $u$  to the previous plant representation?

It is possible to intuitively understand that until the new term is independent of the states of the plant or the environment, it does not affect the system stability. The driving point impedance can be considered as a Thévenin or Norton equivalent impedance seen at that port. Therefore, the presence of a general Thévenin or Norton equivalent source does not change the stability result.

Another extension is that, as long as it has the equivalent impedance of a passive system, also the environment can be active.

### 3.3 Impedance Control

In this section, I address the main characteristics of the impedance control strategy. As previously mentioned, impedance is a port function that maps an input flow onto an output effort and in the mechanical domains, the mechanical impedance is the dynamic operator relating the input velocity (angular velocity) to the output force (torque) of the specified interaction port.

Fortunately, both coupled stability and performance of the controlled system are tied to the dynamic port behavior. In fact, the stability of the coupled system can be guaranteed by suitably shaping the impedance function, which governs the dynamic port behavior of the system, and performance for interactive systems is measured by the port behavior. Therefore, both goals can be reached by implementing an interaction controller which tries to minimize the deviations of the port behavior with respect to a desired behavior. It is important to recall that in the requirements hierarchy presented in Figure 3-3, coupled stability must always be prioritized against performance and that whenever it is possible to restrict the range of possible encounterable environments to a small and manageable set, a tradeoff between these two requirements can be managed.

The dynamic model of a robot subjected to environment's contact forces can be described as it follows [11]:

$$\mathbf{M}(\mathbf{q})\ddot{\mathbf{q}} + \mathbf{C}(\mathbf{q}, \dot{\mathbf{q}})\dot{\mathbf{q}} + \mathbf{G}(\mathbf{q}) = \boldsymbol{\tau}_{act} + \mathbf{J}^T(\mathbf{q})\mathbf{F}_c, \quad \mathbf{q} \in \mathbb{R}^n \quad (3.30)$$

where  $\mathbf{F}_c \in \mathbb{R}^m$  is the vector of generalized contact forces exerted by the environment on the system. It is important to point out that it is not describing a kinematic constraint, since contact can happen in any direction.

Since interactions with the environment are commonly evaluated in the task space, it is useful to consider the dynamic model of a robot in contact in Cartesian coordinates:

$$\mathbf{M}_x(\mathbf{q})\ddot{\mathbf{x}} + \mathbf{C}_x(\mathbf{q}, \dot{\mathbf{q}})\dot{\mathbf{x}} + \mathbf{G}_x(\mathbf{q}) = \mathbf{J}_a^{-T}(\mathbf{q})\boldsymbol{\tau}_{act} + \mathbf{F}_{c_a}, \quad \mathbf{x} \in \mathbb{R}^{m=n} \quad (3.31)$$

where:

- $\mathbf{M}_x(\mathbf{q}) = \mathbf{J}_a^{-T}(\mathbf{q})\mathbf{M}(\mathbf{q})\mathbf{J}_a^{-1}(\mathbf{q})$
- $\mathbf{C}_x(\mathbf{q}, \dot{\mathbf{q}}) = \mathbf{J}_a^{-T}(\mathbf{q})\mathbf{C}(\mathbf{q}, \dot{\mathbf{q}})\mathbf{J}_a^{-1}(\mathbf{q}) - \dot{\mathbf{M}}_x(\mathbf{q})\mathbf{J}_a^{-1}(\mathbf{q})$
- $\mathbf{G}_x(\mathbf{q}) = \mathbf{J}_a^{-T}(\mathbf{q})\mathbf{G}(\mathbf{q})$
- $\mathbf{F}_{c_a} = \mathbf{T}_a^{-T}(\phi)\mathbf{F}_c$ , where  $\mathbf{T}_a(\phi)$  is the transformation mapping the geometric Jacobian matrix to the algebraic Jacobian matrix:  $\mathbf{J}_a(\mathbf{q}) = \mathbf{T}_a(\phi)\mathbf{J}(\mathbf{q})$

keeping the same matrix properties the correspondent matrices have in joint space:

- $\mathbf{M}_x > 0$ , if  $\mathbf{J}_a$  non-singular
- $\dot{\mathbf{M}}_x - 2\mathbf{C}_x$  is skew-symmetric, if  $\dot{\mathbf{M}} - 2\mathbf{C}$  is skew-symmetric.

and assuming no redundancy to avoid complications on the Jacobians computations.

The control law is obtained in two phases. First, it is necessary to impose the target port behavior with respect to the desired trajectory  $[\mathbf{x}_d, \dot{\mathbf{x}}_d, \ddot{\mathbf{x}}_d]^T$ :

$$\mathbf{M}_m(\ddot{\mathbf{x}} - \ddot{\mathbf{x}}_d) + \mathbf{D}_m(\dot{\mathbf{x}} - \dot{\mathbf{x}}_d) + \mathbf{K}_m(\mathbf{x} - \mathbf{x}_d) = \mathbf{F}_{c_a} \quad (3.32)$$

which mainly consists in defining a desired behavior for the interaction forces imposed by the environment at the port. The three scalar matrices at first member are the desired (or apparent) inertia,  $\mathbf{M}_m$ , the desired damping,  $\mathbf{D}_m$ , and the desired stiffness,  $\mathbf{K}_m$ .  $\mathbf{M}_m$  and  $\mathbf{K}_m$  are positive definite while  $\mathbf{D}_m$  is semi-positive definite. In general, it is preferable to build them as diagonal matrices to have decoupled equations.

Second, as already mentioned in the example with the upper-limb exoskeleton ABLE (section 3.1), the design aims at the compensation of the “real” robot’s dynamics in order to impose the desired and controllable impedance behavior. The inverse dynamic control strategy proposes a control law able to validate this goal.

$$\mathbf{u} = \mathbf{J}_a^{-T}(\mathbf{q})[\mathbf{M}_x(\mathbf{q})\mathbf{a} + \mathbf{C}_x(\mathbf{q}, \dot{\mathbf{q}})\dot{\mathbf{x}} + \mathbf{G}_x(\mathbf{q}) - \mathbf{F}_{c_a}] \quad (3.33)$$

Notice that this control law requires to deploy a force/torque sensor to measure the actual value of  $\mathbf{F}_{c_a}$ , which cannot always be possible to frame on the designed robot’s structure.

Thus, the complete control law is obtained by guaranteeing the loop closure on  $\ddot{\mathbf{x}} = \mathbf{a}$ :

$$\mathbf{a} = \ddot{\mathbf{x}} = \ddot{\mathbf{x}}_d + \mathbf{M}_m^{-1}[\mathbf{D}_m(\dot{\mathbf{x}}_d - \dot{\mathbf{x}}) + \mathbf{K}_m(\mathbf{x}_d - \mathbf{x}) + \mathbf{F}_{c_a}] \quad (3.34)$$

By substituting in (3.33) and simplifying:

$$\begin{aligned} \mathbf{u} = & \mathbf{M}(\mathbf{q})\mathbf{J}_a^{-1}(\mathbf{q})\{\ddot{\mathbf{x}}_d - \dot{\mathbf{J}}_a(\mathbf{q})\dot{\mathbf{q}} + \mathbf{M}_m^{-1}[\mathbf{D}_m(\dot{\mathbf{x}}_d - \dot{\mathbf{x}}) + \mathbf{K}_m(\mathbf{x}_d - \mathbf{x})]\} + \mathbf{C}(\mathbf{q}, \dot{\mathbf{q}})\dot{\mathbf{q}} \\ & + \mathbf{G}(\mathbf{q}) + \mathbf{J}_a^T(\mathbf{q})[\mathbf{M}_x(\mathbf{q})\mathbf{M}_m^{-1} - \mathbf{I}]\mathbf{F}_{c_a} \end{aligned} \quad (3.35)$$

Notice that  $[\mathbf{M}_x(\mathbf{q})\mathbf{M}_m^{-1} - \mathbf{I}]$  is the matrix weighting the measured contact forces. Although the interactions happen in the task space and, therefore, the control design is based on the dynamic analysis and desired behavior in the operational space, the final implementation is always in the joint space [11]. Hence considering the following identity:

$$\mathbf{J}_a^T(\mathbf{q})[\mathbf{M}_x(\mathbf{q})\mathbf{M}_m^{-1} - \mathbf{I}] = [\mathbf{M}(\mathbf{q})\mathbf{J}_a^{-1}(\mathbf{q})\mathbf{M}_m^{-1} - \mathbf{J}_a^T(\mathbf{q})] \quad (3.36)$$

the last Cartesian quantity is eliminated, and the control law can be implemented fully at the joint level.

The last aspect to cover to give the reader enough information about the impedance control to understand the following examples and the exoskeleton control strategies presented in Part III is how to choose a suitable impedance model, i.e., how to decide the values of matrices  $\mathbf{M}_m$ ,  $\mathbf{D}_m$ , and  $\mathbf{K}_m$ .

Probably, during the previous presentation, the reader has already wondered more than once why there is not a loop devoted to torque control and torque error. Actually, such control loop is not necessary with the aim of impedance control, since the generated contact forces are indirectly controlled by controlling the position. Consider for instance the mechanical machining application, such as milling. The contact forces are generated as long as the tool or the tool’s head is kept in touch with the workpiece surface. Therefore, by planning a virtual trajectory,  $\mathbf{x}_d$ , passing inside the workpiece’s surface, the machine will push more or less intensely against the object’s surface, controlling in this way the contact forces’ intensity.

However, due to the absence of a direct regulation of the contact forces, it is important to avoid large impact forces due to the geometry of the environment, intended as position and orientation.

Another important consideration to make is to match the dynamic characteristics of the environment (especially its estimated stiffness) in a complementary way [6,11], i.e., if the environment behaves as an admittance, due to the presence of large inertias and kinematic constraints, then the ideal behavior of the robot is the one of an impedance, and vice versa. A simple way to approach this problem is to make the robot mimic the behavior of a human arm [13].

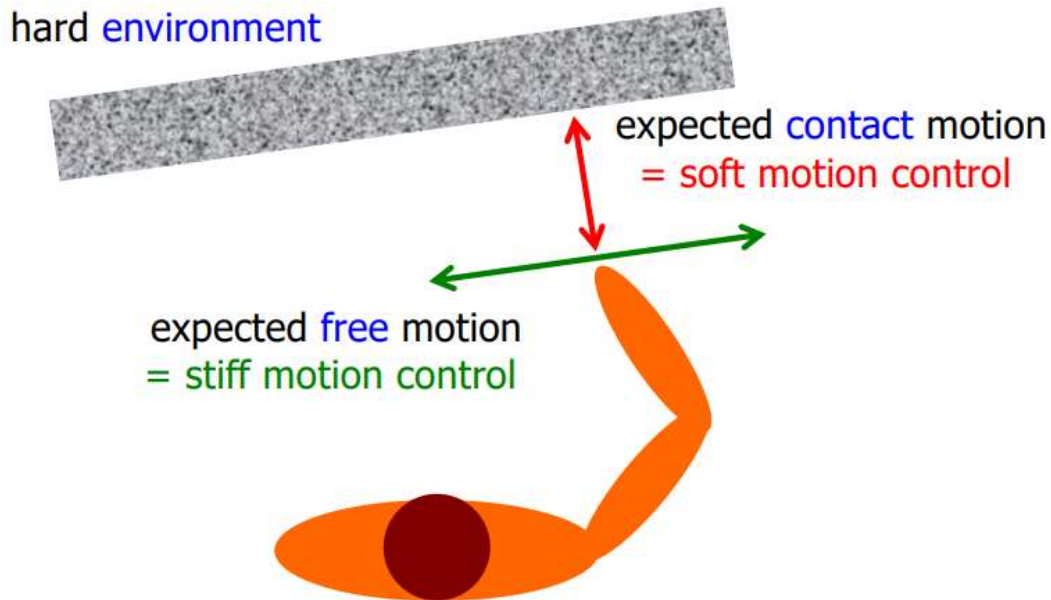


Figure 3-7: Analogy between the movement of a human arm and a robot arm. In the direction along which a contact is expected, motion is slower to avoid damage. In the direction along which there are no constraints, motion is faster and stiffer. Reprinted from [13].

In fact, in condition of “free” motion, when no contact is expected, we generally move fast and stiff. Otherwise, in “guarded” motion, the movement is slower and more compliant. Thus, following the analogy, in those Cartesian directions  $i$  where contact is expected, it is important to minimize the intensity of contact forces, by providing large apparent inertia values,  $M_{m,i}$ , and small desired stiffness values,  $K_{m,i}$ . When motion is supposed to be free, we want to have large  $K_{m,i}$  and small  $M_{m,i}$ , in order to have a good tracking of the virtual trajectory. Damping coefficients,  $D_{m,i}$ , are decided to shape the transient behavior.

Ideally, by a suitable choice of  $M_m$ ,  $D_m$ , and  $K_m$ , it is possible to obtain a robotic device which shows zero damping, stiffness, and apparent inertia. Recalling the ABLE example presented at the beginning of Part II, it was proposed a control law which tries to zero the damping and gravitational load characteristic of the exoskeleton’s simplified model.

However, despite it is possible to have a perfect compensation<sup>1</sup> of damping and gravitational effects, it is particularly difficult to obtain a “perfect compensation” of the inertia characteristic of a robot shown at a port.

---

<sup>1</sup> I don’t like the words “perfect compensation” as it is practically impossible to obtain

### 3.3.1 Masking the low-frequency inertia behavior: limits of applicability of the impedance control

Many notable authors and peak exponents in the field has shown why impedance control is ineffective to mask arbitrarily the inertia characteristics such as [7, 8, 12, 30].

An intuitive explanation can be provided without disturb these important authors and just focusing on equation Equation (3.36). As presented before, factor  $[\mathbf{M}_x(\mathbf{q})\mathbf{M}_m^{-1} - \mathbf{I}]$  is the matrix weighting the measured contact forces in Cartesian space. It depends on the inertia matrix of the robot in Cartesian space and the apparent inertia. If the system is simplified to a 1-DOF case, posing the correspondent mass in Cartesian space  $m_x$  and apparent mass  $m_m$ , the factor reduces to:

$$\left[ \frac{m_x}{m_m} - 1 \right] = \frac{m_x - m_m}{m_m} \quad (3.37)$$

It is immediate to understand that the apparent inertia shown by the robot at its port of interaction,  $m_m$ , cannot be zero, otherwise, the actuator should deliver an infinite torque, leading definitely to instability and the damaging the object in contact/coupled with the system. Thus, a robot controlled via an impedance control law will inevitably show an inertial characteristic at the port of interaction that cannot be arbitrarily lowered. The same consideration can be done in joint space, rewriting the factor as  $[\mathbf{J}_a^{-T}(\mathbf{q})\mathbf{M}(\mathbf{q})\mathbf{J}_a^{-1}(\mathbf{q})\mathbf{M}_m^{-1} - \mathbf{I}]$ .

Furthermore, Hogan [7] and Colgate [8] proved that even considering the physical equivalent of the system in Figure 3-2 controlled by a (simple) impedance control with proportional force feedback,  $K_f$ , is inefficient to reduce apparent inertia. The equation of motion for the uncontrolled system is:

$$m\ddot{x} + b\dot{x} + F_n(x, \dot{x}) = F_a + F_e \quad (3.38)$$

where  $F_n(x, \dot{x})$  represents a nonlinear friction action applied to the mass.

A simple impedance control law with proportional force feedback is given by

$$F_a = K(r - x) + B(\dot{r} - \dot{x}) + K_f[F_e + K(r - x) + B(\dot{r} - \dot{x})] \quad (3.39)$$

The resulting equation of motion of the controlled system is given by:

$$\frac{(m\ddot{x} + b\dot{x} + F_n(x, \dot{x}))}{1 + K_f} = F_e + K(r - x) + B(\dot{r} - \dot{x}) \quad (3.40)$$

which is appealing, since it scales all the dynamic characteristics of the system of a factor  $1/(1 + K_f)$ .

However, as shown in [8],  $K_f$  must be lower than the unity ( $K_f \leq 1$ ), otherwise, the system starts exhibiting **negative** stiffness, mass, and damping parameters, and such negative viscous-elastic behavior upon contact leads to coupled instability.

In conclusion, this section presented the impedance control strategies applied to a robotic manipulator interacting with the environment. A general control design has been presented in order to highlight the main design characteristics, the operative principles, and the main hinderances.

Moving towards robotic exoskeleton applications, being the device designed for transparent control, being this designed for physical rehabilitation, even if in an agility enhancement context (section 3.5), an impedance controller will always be unable to cope with the apparent inertial behavior displayed by the exoskeleton at low frequency; the actuators' torques will be spent to compensate other effects, such as gravity, friction, and other dissipative effects, and to make the end-effector or the ports of interaction follow a pre-planned (virtual) trajectory. Hence, as told by the results obtained in section 3.1, the patient inside an impedance-controlled exoskeleton should exert enough muscle force/torque to move their limb plus the mechanism's inertia.

This result is exactly at the antipodes of the objective of whatsoever wearable exoskeleton technology, especially in the rehabilitation field and in the possibility of implementing a transparent operative mode at the robot's joints. An exoskeleton that requires the impaired patient to exert more muscular strength that they have to move the entire coupled system, when the human is not even able to exert enough force to perform a free-body exercise, has not met its requirements.

From the transparent operative mode perspective, Equation (3.4) and (3.37) testify the impossibility of eliminating the interaction forces, due to the inability in compensating the inertial behavior of the machine. Hence, the exoskeleton will be always lagging with respect to human movements, and it will be felt as a ballast, hindering their movements.

## 3.4 Admittance Control

In this section, there will be a brief presentation of the admittance control, in order to provide to the reader the final piece of theoretical mosaic that will be adopted in the continuation of the Thesis. The main concepts are taken from article [10], which is the most complete article found by the author about admittance control implemented in robotic exoskeleton applications, adding a specific focus on human-robot interaction.

The mechanical admittance has been defined before:

**Definition 4:** Mechanical admittance at a port (denoted  $Y$ ) is a dynamic operator that determines an input velocity (angular velocity) time function from an output force (torque) time function at the same port.

Mechanical admittance is the causal dual of mechanical impedance, in terms of inverted input and output roles, hence, if a mechanical impedance may be thought as a generalized stiffness, the model of a spring taking into account internal dissipation effects and the mass of the spring itself, producing a mechanical effort in response to a mechanical flow in input, a mechanical admittance can be thought as a generalized compliance, producing an output (angular) velocity in response to a force (torque).

Conversely to the impedance control, which controls motion after a force has been measured, the admittance control controls force after motion or deviation from a set point is measured [10]. Admittance control is mainly employed to control large non-backdrivable high friction devices, being these used for wearable robotics or in industrial environments. Being based on kinematic signal sensing and treating the robot as a large inertia instead of a stiff object, admittance control is easier to design with respect to its dual, since IMUs and other kinematic sensors are easier to deploy, cheaper, and less sensitive to drift and temperature changes than of force or torque sensors, despite being more prone to the parasitic dynamics and friction effects of the device itself.

The most complete general admittance control scheme found by the author is [10]. The general physical setup considered in the presentation is explained below. According to the received low-power control input, an actuator generates mechanical power. As already shown in Part I, such actuator can be an electromechanical drive or a hydraulic or pneumatic motor. The mechanical power is exploited to move the robot's link via a transmission system. Close to the interaction port, a force sensor is mounted to measure the interaction forces with the user. Obviously, it has non-zero inertia and it is often attached to a tool, handle, or cuff designed to improve the quality of interaction with the environment. Hence, it is possible to imaginarily divided the robot into two subsystems. The pre-sensor subsystem has the purpose to generate the forces (torques) to move the system. The post-sensor subsystem consists of the parts between the sensor and the interaction port itself, whose dynamics will be measured by the sensor and will be considered as a known time-invariant impedance effect of the interaction dynamics, and it should display pure inertial behavior. The user's impedance, denoted  $Z_h$ , is generally unknown and not included in the post-sensor dynamics. The force sensor will detect the interaction forces that arise while the post-sensor subsystem interacts with the environment and the admittance controller will attempt to impose a target admittance behavior at the port of interaction described by a virtual dynamical model.



To explain the reason behind the introduction of such many subsystems, in particular three different regulators, two in feedforward, one in feedback, and the presence of so many observers, I chose to guide the reader in a journey, starting from a baseline model, i.e, a model able to explain coupled instability, and progressively expanding the control scheme to the one presented above. The reader's attention should focus on the reflection the apported improvements have on the robot performance.

Consider a simple 1-DOF linear dynamical model of a robot. The inertial characteristics are grouped in lumped mass parameter  $m_r = m_r' + k_r^2 m_m$  and in lumped damping factor  $b_r = b_r' + k_r^2 b_m$ , where subscript "m" indicates the dynamical characteristics of the motor, reflected to the shaft side by  $k_r^2$ , and apex " ' " indicates the actual dynamical characteristics of the robot's link. Assume to have ideal force and velocity sensors,  $S_f = S_v = 1$ , no acceleration sensor,  $S_a = 0$ , and no feedforward regulators,  $G_f = C_{ff} = 0$ . The post-sensor impedance effect is purely inertial,  $Z_{ps} = m_{ps}s$ . The external force applied to the system, eventually by the human, is  $F_{ext}$ , eventually produced by the human impedance. The coupling element is rigid.

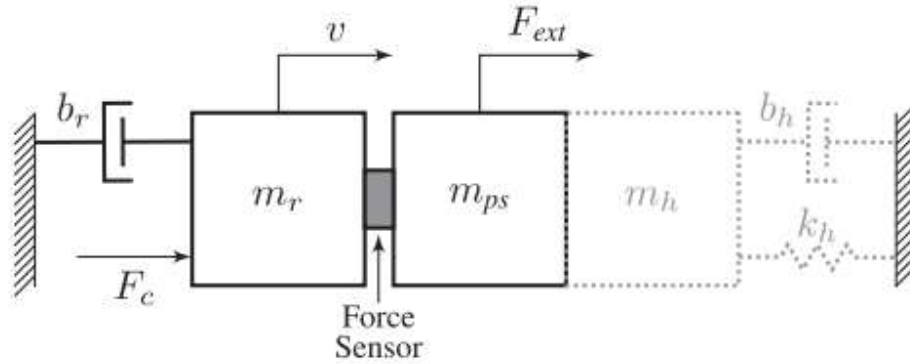


Figure 3-9: Schematic view of a rigid robot. The gray dotted part represents the human passive dynamics. Reprinted from [10].

The equation of motion of the system in Figure 3-9 in Laplace domain is given by:

$$(m_r s + b_r) v(s) = F_{ext}(s) - m_{ps} s v(s) + F_c(s) + k_r F_{dst}(s) \quad (3.41)$$

Recalling what discussed in section 3.3, the baseline controller is based on target dynamics, desired as purely inertial:

$$Y_v(s) = \frac{1}{m_v s} \quad (3.42)$$

and proportional-integral control law:

$$F_c(s) = k_r \left( k_p + \frac{k_I}{s} \right) (v_d(s) - k_r v(s)) \quad (3.43)$$

noticing that the desired velocity is obtained as output of the target admittance model:

$$v_d(s) = k_r Y_v(s) (F_{ext}(s) - m_{ps} s v(s)) \quad (3.44)$$

Combining Equations (3.41) to (3.44), the apparent admittance describing the input-output characteristics between the sensing port and the interaction port facing the environment is:

$$\begin{aligned} \bar{Y}_a(s) &= \frac{1}{s} \frac{m_v s^2 + k_r^2 k_p s + k_r^2 k_I}{m_v(m_r + m_{ps})s^2 + (b_r m_v + k_r^2(m_{ps} + m_v)k_p)s + k_r^2(m_{ps} + m_v)k_I} \\ &= \frac{1}{s} \frac{m_v s^2 + K_p s + K_I}{a_2 s^2 + a_1 s + a_0} \end{aligned} \quad (3.45)$$

The baseline apparent admittance  $\bar{Y}_a(s)$  presents three poles, one valued zero from the purely inertial target behavior, and two stable (possibly complex-conjugate) poles from the PI-feedback controller, making the robot stable when isolated. By looking at the Bode plot of  $\bar{Y}_a(j\omega)$  in Figure 3-10, at low frequencies, there is a constant difference between magnitudes of  $\bar{Y}_a$  and target behavior  $Y_v$  caused by the post-sensor inertia  $m_{ps}$ . At high frequencies, the magnitude of  $\bar{Y}_a(j\omega)$  approaches the robot dynamics  $Y_r$ , unfortunately introducing a phase lag in the frequency range of the transition.

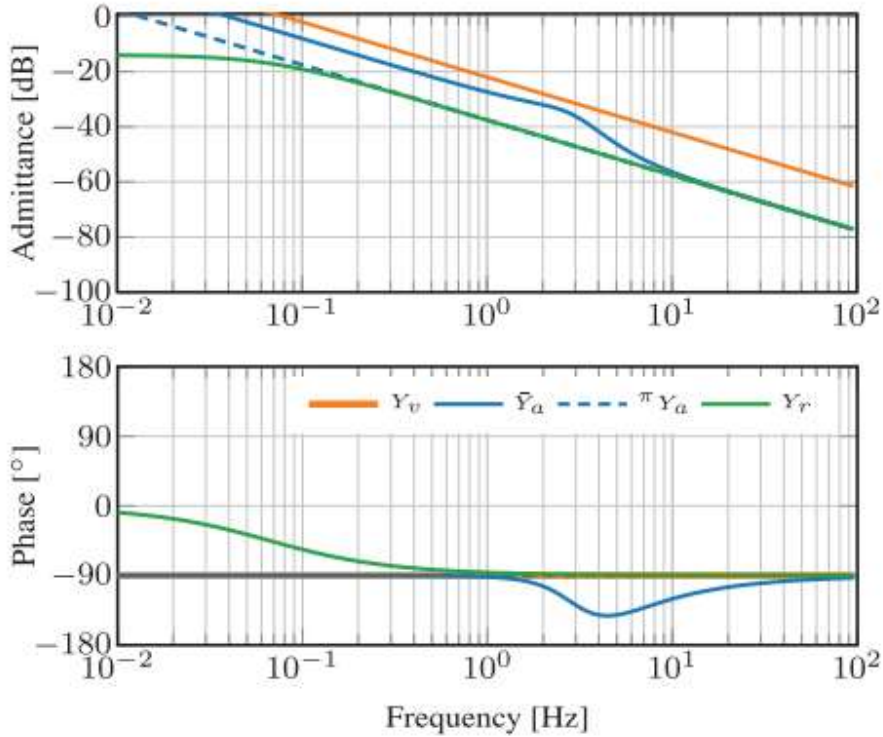


Figure 3-10: Bode plot showing the behavior and performance of the admittance controlled system. Reprinted from [10].

### 3.4.1 Analyzing passivity of uncoupled apparent dynamics

Substituting  $s = j\omega$  in Equation (3.45), we obtain:

$$\bar{Y}_a(j\omega) = \frac{(m_v\omega^2 - K_I) - jK_P\omega}{a_1\omega^2 + j(a_2\omega^3 - a_0\omega)} = \frac{N_a(j\omega)}{D_a(j\omega)} \quad (3.46)$$

The positive real condition becomes:

$$\begin{aligned} \mathcal{R}\{N_a\}\mathcal{R}\{D_a\} + \mathcal{J}\{N_a\}\mathcal{J}\{D_a\} &\geq 0, \forall \omega \\ [(K_P + b_r)m_v^2 - K_P m_r m_v]\omega^4 + [-K_I b_r m_v]\omega^2 &\geq 0, \forall \omega \\ c_1\omega^4 + c_2\omega^2 &\geq 0, \forall \omega \end{aligned} \quad (3.47)$$

Passivity condition requires that both coefficients  $c_1$  and  $c_2$  be non-negative. Thus, imposing that a positive virtual inertia  $m_v > 0$ , the passivity conditions are reduced to:

$$m_v \geq \frac{K_P}{K_P + b_r} m_r \approx m_r \quad (3.48)$$

$$-b_r K_I \geq 0 \quad (3.49)$$

Since  $b_r \geq 0$  and  $k_r \gg 1$ , and  $k_I \geq 0$  to ensure uncoupled stability, it is necessary to impose  $k_I = 0$  to respect condition (3.49), meaning that it is necessary to sacrifice low-frequency performance in favor of passivity.

The integral behavior of the PI controller introduces a phase lag in the low frequency range, so any amount of extra phase lag makes the apparent admittance active (section 3.2.3). Wondering more on condition (3.48), it testifies that the apparent inertia must be equal or higher of the actual robot's inertia. Thus, it is impossible to achieve passive inertia reduction with admittance control based on pure virtual inertia and using a feedback control only. The passivity criterion requires to use low values for integral gain and transmission ratio, which is in conflict with good disturbance rejection and performance.

### 3.4.2 Analyzing coupled stability

Analyze the diagram depicted in Figure 3-11. This diagram is called “ez-width”, and it describes the stabilizing range of stiffness and damping of the passive environment, in our case, the passive human impedance characteristics, that guarantees coupled stability. In simpler words, they describe coupled stability boundaries.

Since all the curves pass through the origin at varying of the human limb's inertia, it is possible to conclude that admittance-controlled systems would never be stable for interaction with pure springs, or pure mass-spring combination. Since real environments will always show a form of dissipative behavior, this result is not alarming.

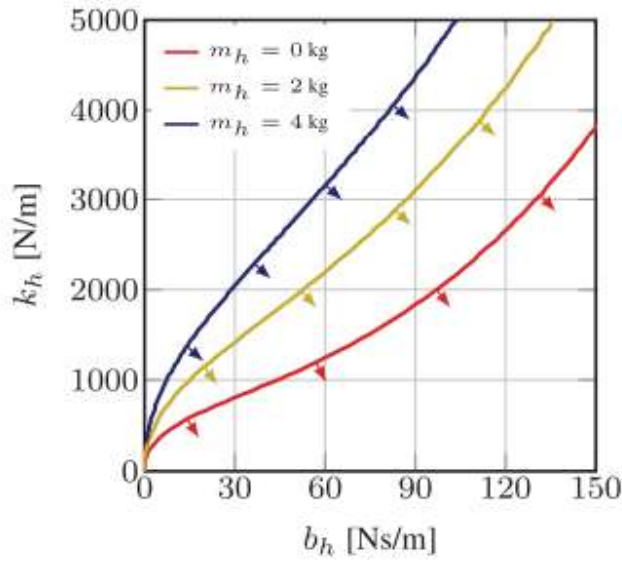


Figure 3-11: The ez-width of the baseline apparent inertia  $\bar{Y}_a$  coupled to a second-order impedance. It increases for higher value of the human limb inertia  $m_h$ . The arrows indicate the stable interaction area. Reprinted from [10]

### 3.4.3 Virtual stiffness and damping behavior

It is possible to design admittance controllers with pure damping and pure stiffness target behavior, able to maintain the exoskeleton passive and making it have decent performance. By taking a look to the Bode plots of the two types of controllers in Figure 3-12, it is shown that robot's displayed behavior is close to the target behavior in low-frequency range within the feedback controller bandwidth. As expected, the robot starts showing its inertial behavior for frequencies above the feedback controller bandwidth, due to its intrinsic behavior.

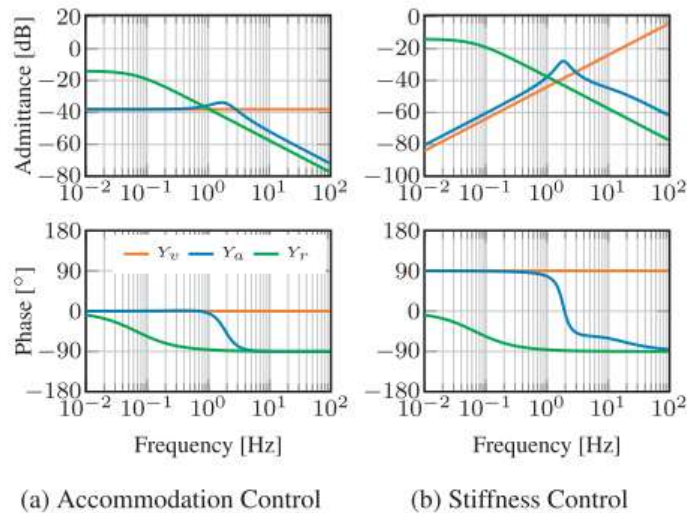


Figure 3-12: Admittance control apparent dynamics  $Y_a$  for uncoupled (a) passive pure damping control ( $b_v = 80$  Ns/m) and (b) passive pure stiffness control ( $k_v = 1$  kN/m).

A purely damping target dynamics is modeled as it follows:

$$Y_v = \frac{1}{b_v} \quad (3.50)$$

Substituting this equation in place of (3.42), following the same procedure aforementioned, the passivity conditions for the coupled system are:

$$b_v \geq 0 \quad (3.51)$$

$$m_r K_I \leq (K_p + b_r)(K_p + b_v) \quad (3.52)$$

Integral gain  $k_i$  should be still low in value, the robot should be lightweight, and either the proportional gain, the virtual damping, or the robot's damping should be high enough to ensure passive behavior.

If it is required the exoskeleton displays purely stiff behavior, the target dynamics are modeled as:

$$Y_v = \frac{s}{k_v} \quad (3.53)$$

Substituting this equation in place of (3.42), following the same procedure aforementioned, the passivity condition for the coupled system consists of:

$$k_v \geq 0 \quad (3.54)$$

if all the other parameters are positive.

The apparent stiffness  $k_{app}$  of the device is the equivalent of the series of two springs characterized respectively by the virtual stiffness and the reflected integral gain stiffness:

$$k_{app} = \left( \lim_{s \rightarrow 0} \left( \frac{Y_a(s)}{s} \right) \right)^{-1} = \left( \frac{1}{k_v} + \frac{1}{K_I} \right)^{-1} \quad (3.55)$$

To point out the obvious, the apparent behavior cannot track perfectly the target behavior.

### 3.4.5 Virtual element combination

For combination of mass-spring-damper elements, i.e., when the display of complex dynamic behavior by the exoskeleton is required, e.g., to compensate some of the dynamics of the coupled system, the passivity and coupled stability conditions are a combination of the previous ones. The table 3-1 tries to rank the coupled stability robust conditions for different combinations of haptic elements (virtual stiffness  $k_v$ , virtual damping  $b_v$ , and virtual inertia  $m_v$ ).

Table 3-1: Conditions that need to be greater or equal to zero for different haptic elements combinations

Element(s)	Condition(s)	Effective influence	Coupled stability ranking
$k_v$	$c_k$	$k_v \geq 0$	1
$b_v$	$c_b$	$k_i \leq \dots$	3
$m_v$	$c_{m1}, c_{m2}$	$k_i = 0, m_v \geq \dots$	7
$m_v, b_v$	$c_b + c_{m1}, c_{m2}$	$k_i \leq \dots$ (lower than for pure damper), $m_v \geq \dots$	4
$k_v, b_v$	$c_k + c_b$	$k_i \leq \dots$ (higher than for pure damper)	2
$m_v, k_v$	$c_{mk} = c_s + c_{m1} + \delta_{mk}, c_{m2}$	$k_i \leq \dots$ (lower than for mass-damper), $m_v \geq \dots$	6
$m_v, b_v, k_v$	$c_{mk} + c_b, c_{m2}$	$k_i \leq \dots$ (higher than for mass-spring, lower than mass-damper), $m_v \geq \dots$	5

### 3.4.6 Guidelines for minimal inertia

Previous section gives an insight into the modification of the robot's interacting behavior in terms of damping and stiffness. The following section will provide a practical example and some important experimental results. Masking the inertial behavior displayed by the exoskeleton is a piece of cake, since inertia is involved not only in performance but also in coupled stability conditions. Section 3.5 addresses this complex issue and introduces a control strategy based on emulated inertia compensation able to modify the displayed inertial behavior of the exoskeleton.

However, it is possible to provide some guidelines to improve a naïve admittance controller performance, making more similar to the one presented in Figure 3-8.

First of all, it is suggested to **use feed-forward control** if the robot can be used in torque (current) control mode. Feedforward control consists of two regulation contributions: an inertia and damping compensation, in the form of impedance  $C_{ff} = \mu_{ff}s + b_{ff}$ , and force gain  $G_f > 0$ . The passivity conditions become:

$$m_v \geq \frac{(K_p + \beta_{ff}k_r^2)m_r - (K_p + b_r)\mu_{ff}k_r^2}{(G_fk_r + 1)(K_p + b_r)} \quad (3.56)$$

$$0 \leq (\beta_{ff}k_r^2 - b_r)K_I \quad (3.57)$$

From condition (3.57), imposing  $\beta_{ff}k_r^2 \geq b_r$ , it is possible to exploit integral gain  $k_i$  to ensure good admittance tracking performance at low frequencies. From condition (3.56), instead, feedforward inertia parameter  $\mu_{ff}$  partially compensate the robot's inertia, facilitating the performance of the feedback controller. Despite  $\beta_{ff}$  increases the robot's inertia contribution, the positive force gain  $G_f$  helps in reducing this inconvenient effect.

The use of feedforward control allows to have high transmission ratios in achieving low virtual inertia. In fact, for  $k_r \gg 1$ , condition (3.56) is reduced to:

$$\mu_{ff} \geq \frac{k_p + \beta_{ff}}{k_p + b_m} m_m \quad (3.58)$$

remembering that  $m_r = m'_r + k_r^2 m_m$ .

The use of feedforward expands the coupled stability margins and improves the admittance tracking performance also at frequencies outside the feedback controller bandwidth [10].

Without the feedforward control, the high-frequency inertia would always fall to the robot's total inertia  $m_r + m_{ps}$ . Using a feedforward control the high-frequency apparent inertia becomes:

$$m_{app} = \left( \lim_{s \rightarrow \infty} (sY_a) \right)^{-1} = m_{ps} + \frac{m_r}{\frac{\mu_{ff}}{m_v} k_r^2 + G_f k_r + 1} \quad (3.59)$$

Notice that for  $G_f \rightarrow \infty$ ,  $m_{app}$  cannot be lower than  $m_{ps}$ .

The second suggestion is to **avoid low-pass filtering of force sensor measurements** if the target behavior is purely inertial. The noise and aliasing reduction effects would be traded for the additional phase lag, reduction of coupled stability boundaries, limiting high-frequency admittance tracking performance, marring the inertia masking activity. Suppose to have a Butterworth filter of order  $n$ :

$$S_f(s) = B_n^{-1}(s) \quad (3.60)$$

posing  $B_n(s)$  the Butterworth polynomial of order  $n$ . To the degree of the polynomial corresponds an introduction of additional poles, each contributing with a  $n\pi/2$  rad phase lag to the virtual admittance  $Y_v$ . Even a single-pole low-pass filter with time constant  $\tau_f > 0$  would increase the inertia lower bound, changing the passivity condition (3.48) to:

$$m_v \geq m_r \frac{K_p}{K_p + b_r} + K_p \tau_f \quad (3.61)$$

with  $k_I = 0$ .

If force filtering is inevitable, then the filter bandwidth should be the highest possible and the order of the filter the lower possible.

The third aspect involves **compensating for the post-sensor inertia in the low-frequency range**. In fact, post-sensor dynamics cannot be masked by the admittance controller nor the feedforward control. It is necessary to introduce a compensator in the form of a low-pass filter impedance:

$$\hat{Z}_{ps} S_a = \frac{\mu_c}{\tau_c s + 1} \quad (3.62)$$

where  $\mu_c$  is the compensation inertia and  $\tau_c$  is the filter time constant. The apparent inertial behavior at low frequencies becomes:

$$Y_{a,low\ freq} \approx \frac{1}{s} \lim_{s \rightarrow 0} (sY_r) = \frac{1}{s(m_v + m_{ps} - \mu_c)} \quad (3.63)$$

and the passivity criterion changes into:

$$m_v \geq \frac{K_p}{K_p + b_r} (m_r + \mu_c) \quad (3.64)$$

Being  $\mu_c$  a design parameter, it is possible not only to compensate the post-sensor dynamics by setting  $\mu_c = m_{ps}$ , but also create a negative inertia bound. This allows to set a “negative” inertial behavior for the robot, reducing the inertia felt that the human coupled to it, i.e., modifying the haptic sensations the human will feel once coupled to such exoskeleton.

It is also suggested to consider a **mass-damper admittance target behavior**. A small amount of damping ( $b_v$ ) is hardly felt by the user and allows to introduce a useful phase lead at lower frequencies, expanding coupled stability margins and providing a passive behavior.

The passivity condition on virtual inertia is untouched, i.e., adding virtual damping will not reduce the lower bound of the virtual inertia, but it changes condition (C2) and introduces a new (although trivial) condition:

$$K_I \leq b_v \frac{(K_p + b_v)(K_p + b_r)}{b_r m_v + b_v m_r} \quad (3.65)$$

$$b_v K_I^2 \geq 0 \quad (3.66)$$

The new condition leaves  $k_I$  tunable to obtain good low-frequency admittance tracking capabilities.

When the introduction of a feedforward control is not possible, it is preferable to modify the velocity reference by **adding a feedforward acceleration gain to the admittance target model**:

$$Y_v = (s k_a + 1) Y'_v \quad (3.67)$$

where  $k_a$  is the feedforward acceleration gain and  $Y'_v$  is the originally intended target admittance. Passivity conditions change to:

$$m_v \geq \frac{(K_p + k_a K_I) m_r - k_a (K_p^2 + K_p b_r)}{K_p + b_r} \quad (3.68)$$

$$0 \leq (k_a K_I - b_r) K_I \quad (3.69)$$

For high transmission ratios,  $k_r \gg 1$ , the condition (3.69) will be reduced to:

$$k_a \geq 0 \quad (3.70)$$

ensuring passivity for any positive value of  $k_a$ .

Having elevated values of  $k_p$  and  $k_I$  is important to increase the velocity loop bandwidth, since a higher bandwidth pushes the phase lag into the high-frequency range, and higher PI gains ensure more disturbance rejection at the motor side, which suppresses unwanted friction and parasitic dynamics. However, having high values of  $k_p$  and  $k_I$  conflicts with all the passivity conditions explored before. To increase the controller bandwidth, it is possible to add **differential velocity control** or **reduce time delays**. It is possible to substitute the PI velocity controller with a PID velocity or PDD<sup>2</sup> position controller with form:

$$C_{fb} = k_P + \frac{k_I}{s} + \frac{k_D s}{\tau_d s + 1} \quad (3.71)$$

where  $k_D$  is the differential gain and  $\tau_d$  is the time constant of the low-pass filter, implemented to band-limit the differentiation and having a proper and implementable transfer function. Passivity conditions change to:

$$m_v \geq \frac{K_P m_r + b_r K_I \tau_d^2 - b_r K_D}{K_P + b_r} \quad (3.72)$$

where  $K_D = k_D k_r^2$ .

The lower bound on the virtual inertia will increase for nonzero  $K_I$  and  $\tau_d$ . This solution introduces a new condition:

$$m_v \geq m_r \frac{K_P \tau_d + K_D}{(K_P + b_r) \tau_d + K_D} \approx m_r \quad (3.73)$$

which testifies that passive inertia reduction cannot be achieved.

Although the band-limited differential control action has almost no effect on the passivity conditions, it allows to expand the bandwidth of the controller and increases drastically the coupled stability margins.

## 3.5 Emulated Inertia Compensation and other strategies to modify the displayed behavior of the robot

The following text analyzes and reports one of the examples I found most clarifying of the main aspects in designing a robotic active exoskeleton, together with the document about the ABLE upper-limb exoskeleton. The peculiarity of the presented project is its purpose of enhancing the wearer's agility, i.e., empowering the kinematic response of human lower limbs, in terms of gait speed and quick reactions accelerations to cope to unexpected external perturbation, while keeping a special attention to comfort during walking and to maintaining user's control authority intact. Despite the relevance and applicability of results, this represents a limited research trend [17], giving that most of the research focuses on muscular strength enhancement strategies, being those aimed at power augmentation to assist in load-carrying activities in industrial or military applications, enhancing soldiers' walking speed, or complementing the patient's exerted torques in completing a physiotherapy training exercise.

As shown in many studies, see [19] and [20] for instance, bipedal walking behavior can be approximated as an inverted pendulum swing. It has been proved that when walking at a selected speed, the swing leg behaves as a pendulum oscillating close to its natural frequency, to minimize the metabolic cost of walking. To enhance agility, the exoskeleton should increase the natural frequency of the legs, allowing the users to walk comfortably at higher speeds. However, coupling the exoskeleton to the human involves modifying its dynamical properties by adding the mechanism's inertia, weight, friction, and other dissipative effects [17].

### 3.5.1 Presenting the hardware

The experimental platform exploited in [14-17] is a 1-DOF knee-exoskeleton, mounted on a fixed base, to assist users in knee flexions and extensions. The single port of interaction consists of a custom-made ankle brace, coupling *rigidly* the user to the machine. It is mounted on a sliding bracket to accommodate any lengths of user's shank and to eliminate any displacement's non-radial components. However, due to construction limits, it was not possible to mount a torque or interacting force sensor on the ankle brace. It is mounted between the major pulley and the lightweight exoskeleton's leg, measuring the resulting torque due to the human and the motor contributions. This is the actual port of interaction considered in the modeling of the controlled system. The system is designed for high backdriveability, i.e., the possibility to follow the user's movements without transmission backlash. For this reason, the exoskeleton drive consists of an AC servo motor as actuator and a cable-driven transmission. Cable-transmission is similar to gear transmission, but it presents two pulleys with different radius instead of gears and coupling is based on cable instead of indentation. This solution is particularly suitable to impedance control

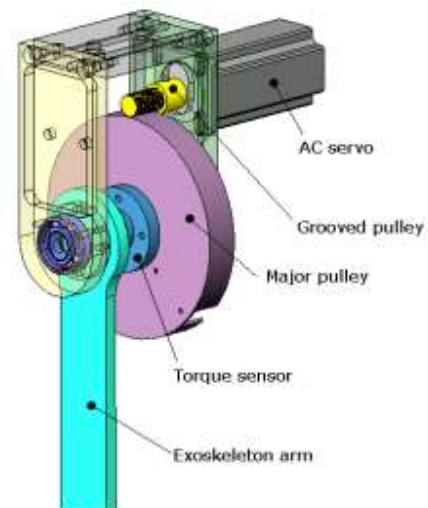


Figure 3-3: 3D model of the exoskeleton's motor, drive, and leg assembly. Reprinted from [14].

application since it is particularly prone to transmission backlash and friction. Cable-transmission is affected by axial cable compliance, which reduces the bandwidth of the mechanism, however, human movements are contained in a small low-frequency bandwidth, hence, this drawback does not result particularly significant.

The exoskeleton is design to display an active impedance by using virtual negative parameters. The control scheme is non-human, i.e., it is not based on a human model, such as model of the human muscular, skeletal, and tendinous systems, the Hill's muscle model, or neuromechanical models, as in [18]. Not relying on physiological signal, the control system is based on kinematic and dynamic signals, with the advantage of fast user adapting capacity although lower intrinsic patient-based customization.

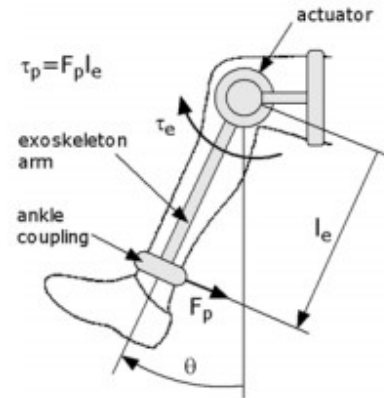


Figure 3-14: Picture of the 1-DOF knee exoskeleton exploited in these set of experiments (on the left). Model representation (on the right). Reprinted from [14].

### 3.5.2 Modeling of the system

With reference to Figure 3-13, it is not surprising that the human shank can be modeled as a simple pendulum, exactly as we considered a simple pendulum in the case of the human arm in the example ABLE. Extending the reasoning, every human limb can be modeled as a compound pendulum, in the same way we model manipulators. The dynamical model of the human shank in time domain is described as follows:

$$\tau_h(t) = I_h \ddot{\theta}_h(t) + b_h \dot{\theta}_h(t) + m_h g l_h \sin(\theta_h(t)) \quad (3.74)$$

It is possible to linearize the model using small oscillations approximation,  $\sin \theta_h \approx \theta_h$ . Using Laplace transform to pass in the frequency domain, and posing  $k_h = m_h g l_h$ , the dynamical model of the human shank becomes:

$$\tau_h(s) = s^2 I_h \theta_h(s) + s b_h \theta_h(s) + k_h \theta_h(s) \quad (3.75)$$

Therefore, the impedance model of the human shank is:

$$Z_h(s) = \frac{\tau_h(s)}{\dot{\theta}_h(s)} = I_h s + b_h + \frac{k_h}{s} \quad (3.76)$$

The exoskeleton's target impedance is:

$$Z_e^d = I_e^d s + b_e^d + \frac{k_e^d}{s} \quad (3.77)$$

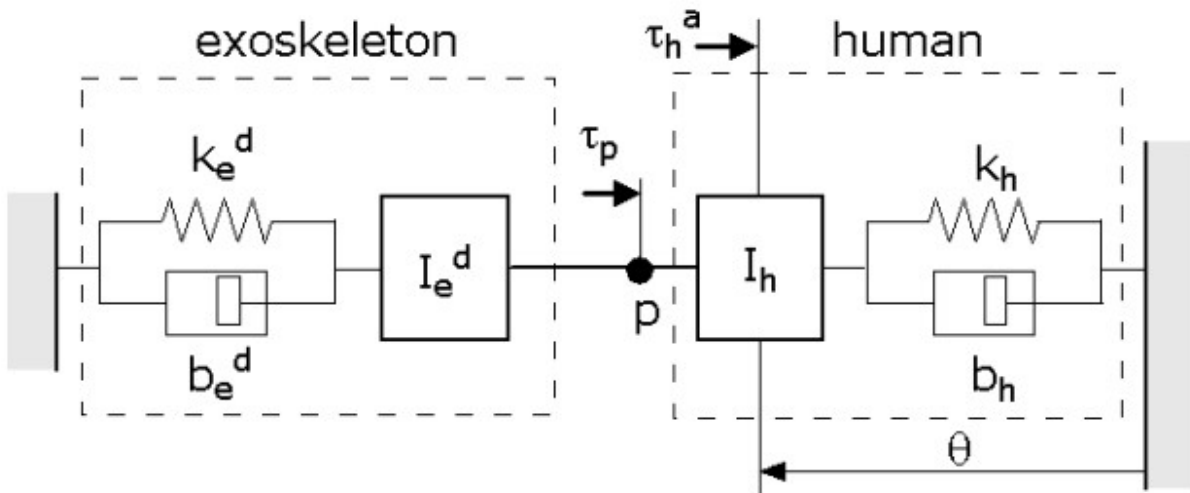


Figure 3-15: Linear model of the coupled 1-DOF human-exoskeleton system. Reprinted from [14].

The linear model of the coupled 1-DOF human-exoskeleton system is given in Figure 3.15, and the equation of motion of the coupled system is:

$$\left[ (I_h + I_e^d)s + (b_h + b_e^d) + \frac{(k_h + k_e^d)}{s} \right] \dot{\theta}(s) = \tau_h^a(s) \quad (3.78)$$

where  $\tau_h^a$  is the net muscle torque under exoskeleton assistance. Remember that since the systems are rigidly coupled:  $\theta_h = \theta_e = \theta$ .

The exoskeleton is indeed used to induce a modification of the human's shank impedance, by modifying coherently its impedance's parameters, so that the muscle torque in input to the coupled system can be modulated, and aiming to increase user's agility, lowered.

With a variance-accounted-for (VAR) factor equal to 87.7%, the system shows a high degree of linearity.

Therefore, it is possible to adopt a simple PID controller to regulate the exoskeleton.

The block diagram of the admittance control scheme is presented in Figure 3-16. The input of the system is the torque  $\tau_p$  measured at the port of interaction,  $P$ , which is the input to the virtual admittance scheme to generate the reference velocity trajectory, and complete kinematic trajectory is obtained by integrating it twice. Reference position time-integral is used to zero the steady-state error. The current in output of the controller is transformed in torque by the motor dynamics, which is used as input of the real exoskeleton plant and its simulated model. A state observer is exploited to produce an estimate of the actual kinematic trajectories, to be compared to the ideal reference ones. It contains the exoskeleton plant model used in

simulations to gain the simulated kinematic trajectories, which must be the most accurate possible, and a PID filter to adjust the result.

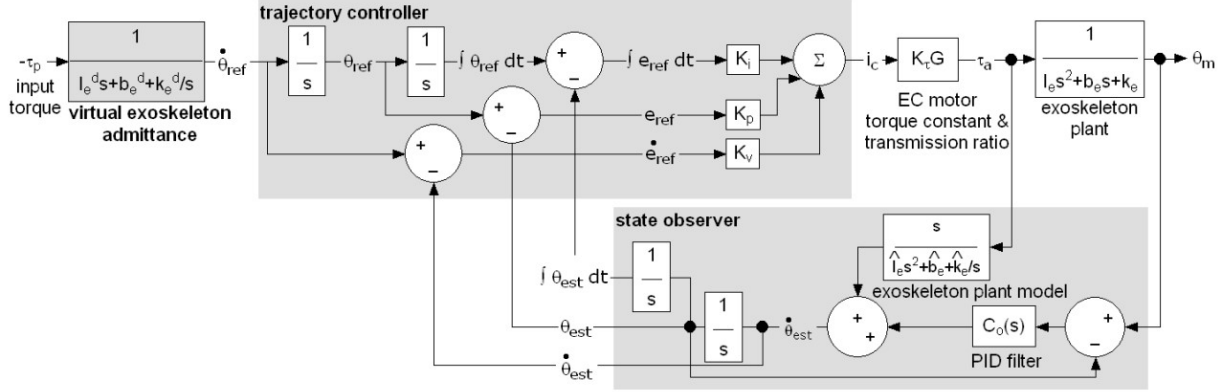


Figure 3-16: Block diagram of the admittance control scheme

### 3.5.3 Experiments with negative exoskeleton damping and its effect on the human limb

The foundation hypothesis on the study of negative virtual damping is the imposition of an energy source behavior to the exoskeleton to help human's motion agility, in the terms of reduction of average time employed to complete knee extension/flexion movement, from resting position to a set target. In fact, posing  $b_e^d < 0$ , Equation (3.78) becomes:

$$\left[ (I_h + I_e^d)s + (b_h - |b_e^d|) + \frac{(k_h + k_e^d)}{s} \right] \dot{\theta}(s) = \tau_h^a(s) \quad (3.79)$$

$$\left[ (I_h + I_e^d)s + b_h + \frac{(k_h + k_e^d)}{s} \right] \dot{\theta}(s) = \tau_h^a(s) + |b_e^d| \quad (3.80)$$

The interesting aspect in investigating negative virtual damping is that it is a velocity-dependent term, therefore, the exoskeleton should not intervene when the system is at rest or in quasi-static motion.

Two possibilities are presented: constant negative damping or state-dependent negative damping.

If the virtual damping factor is constant negative, the exoskeleton will provide energy facilitating starting motions but making difficult to decelerating since the human equivalent impedance's damping is reduced ( $b_{eq} = b_h + b_e^d = b_h - |b_e^d|$ ).

A solution to this issue is to consider the kinematic state of the human lower limb, in order to extrapolate an estimation of the user's movement intention, called voluntary movement intention, to modulate  $b_e^d$  accordingly.

The ratio of kinetic energy variation of the human and human limb's inertia can be used as voluntary motion intention estimation. The ratio is equal to the product of the measured angular velocity and the measured angular acceleration,  $\dot{\theta}_m \ddot{\theta}_m$ . The sign of  $\ddot{\theta}_m$  allows to identify subject's motion intentions. In fact, supposing the user keeps control over the limb motion for the entire duration of the movement:

- $\dot{\theta}_m \ddot{\theta}_m > 0$  assesses the intention to increment the limb's velocity. Consequently,  $b_e^d$  will be tuned negative.
- $\dot{\theta}_m \ddot{\theta}_m < 0$  assesses the intention to decrease the limb's speed. Consequently,  $b_e^d$  will be increased. According to the situation,  $b_e^d$  will either remain negative or become positive, increasing the equivalent damping coefficient.

The idea to modulate the impedance/admittance characteristic is used in several applications, such as [29, 21], with different equations.

In the article [14], the state-dependent damping factor is designed equal to:

$$b_e^d(\dot{\theta}_m, \ddot{\theta}_m) = B_e^o \left[ \left( \frac{1 + \delta_e}{2} \right) \tanh(\lambda_e \dot{\theta}_m \ddot{\theta}_m) + \left( \frac{1 - \delta_e}{2} \right) \right] \quad (3.81)$$

In this way,  $b_e^d$  is bounded:  $b_e^d \in [B_e^o; -\delta_e B_e^o]$ . In detail:

- $B_e^o$  is the damping factor and it is generally negative.
- $\delta_e \in [-1; 1]$ .
- $\lambda_e$  is the coefficient representing the convergence ratio towards the asymptotic values of tanh, hence the bounding values of the possible virtual damping values.

These values are obtained by trial and error procedure, according to the users' feedback about the ability to keep control on their movements. For instance, a wide negative-to-positive virtual damping transition has been reported as "felt unnatural" [14] due to the large accelerations involved.

Experimental results shown that, on average, subjects were able to reduce the time to complete the motion by 16%. The first  $b_e^d$  strategy is more successful to this goal. The most likely hypothesis is that the users spontaneously increase their joint stiffness, to compensate to the lacking of natural "damping".

In the article [15], the same equip tested also the effect of gravity compensation by posing negative virtual stiffness  $k_e^d < 0$ , such that  $k_h^d < k_h$ . Remember that stiffness  $k$  is used as linearization of the effect of gravity.

In the same article, it is shown the ability of a variable impedance/admittance exoskeleton in reducing muscular effort, based on EMG activity. The exoskeleton assists in quickening the dynamic response of the human limb, compensating the slower response of the nervous system, showing great potentiality in human ability enhancement and physical rehabilitation.

### 3.5.4 Compensating for inertial effects

As shown in the previous section, an impedance/admittance controller employing negative virtual parameters can easily compensate for the exoskeleton's weight and friction effects. Nevertheless, it has been highlighted the main problem arising from impedance control applied to mask the exoskeleton's dynamics while coupled to the human: the difficulty in eliminating the inertial term of the mechanism due to stability issues. The hardly modifiable inertial behavior displayed by the exoskeleton work against agility enhancement, decreasing gait speed. At selected gait speed, the swing leg, i.e., the leg performing the step, oscillates with a frequency close to its natural frequency to reduce the metabolic cost of walking. Adding the exoskeleton's inertia to the human leg reduces its natural frequency, leading to an increase of metabolic cost of walking. To compensate that effect, the user will spontaneously decrease its swing frequency to get closer to the natural frequency of the leg, resulting in an increasing of swing time and stride time during walking, finally, reducing gait speed [16].

One may think to apply the same compensation strategy based on negative virtual parameter estimation as for weight and friction compensation, so generating a negative virtual inertia to mask the exoskeleton displayed inertial behavior. Unfortunately, as the reader should expect, it is not so simple. There exists a relationship between the exoskeleton's virtual inertia and sensor non-collocation for which the system would become unstable if the virtual inertia, is lower than the servo motor's inertia reflected on the shaft of the exoskeleton's arm. This result is due to the relationship between exoskeleton's virtual inertia and sensor non-collocation, i.e., neglecting the dynamical characteristics of the sensor system, such as the housing's inertia.

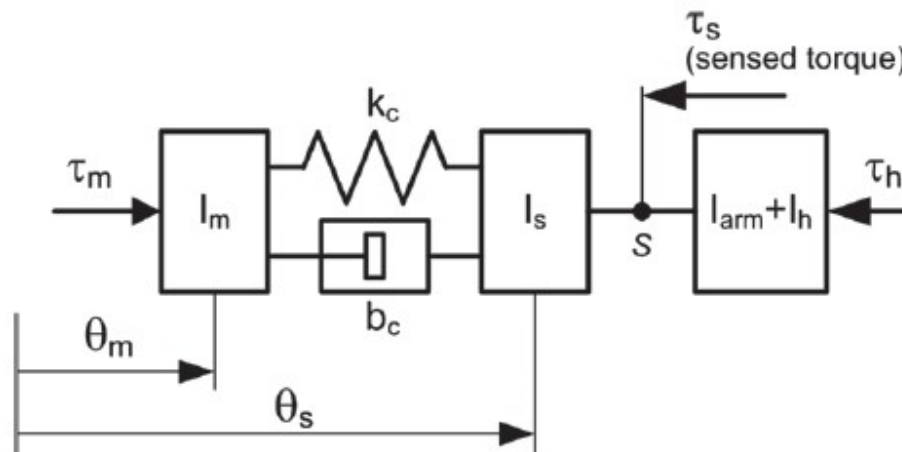


Figure 3-17: Simplified model of the exoskeleton drive mechanism and inertial load. The servo motor and the torque sensor are non-collocated. Reprinted from [16]

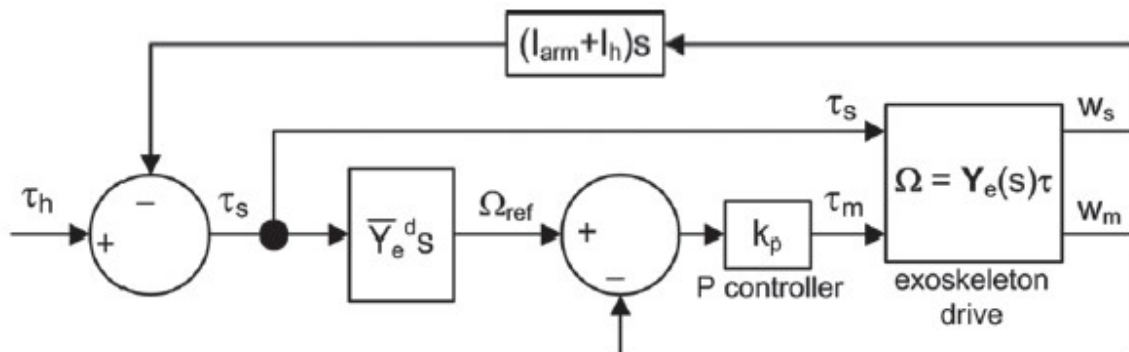


Figure 3-18: Block diagram of the admittance controller and proportional velocity tracker and the exoskeleton drive dynamics. Reprinted from [16].

Consider the simplified model in Figure 3-17 representing the exoskeleton's mechanism rigidly coupled to the human limb. The exoskeleton drive is represented as the servo motor's inertia reflected on the output shaft  $I_m$ , connected by the cable transmission to the output inertia  $I_s$ , which comprises the mechanical components mounted between the cable and the torque sensor, such as the pulleys' inertia and the torque sensor's housing. The cable transmission is modeled by means of a spring with stiffness  $k_c$  and a damper  $b_c$  representing the dissipating effects of transmission. The port  $S$  is the location of the torque sensor,

measuring torque  $\tau_s$ , mounted uphill the exoskeleton's leg, and whose dynamics is neglected. That one is rigidly coupled to the human leg through the ankle brace, namely port of interaction  $P$ . Therefore, the two moments of inertia can be summed,  $I_{arm} + I_h$ . Due to the difference in modeling employed in the control strategies showed in Part III, it is important to point out that, to the purpose of this demonstration, the human leg is modeled as a rigid body with moment of inertia  $I_h$ . The input torques are the exoskeleton's actuator's one,  $\tau_m$ , and the net human muscle torque,  $\tau_h$ . The outputs are the velocities of the exoskeleton's drive, namely, the servo motor's angular velocity reflected on the output shaft,  $\omega_m = \dot{\theta}_m$ , and the output shaft's own angular velocity,  $\omega_s = \dot{\theta}_s$ . The relationship between the input torques and the output velocities can be expressed as a 2-port admittance in the Laplace domain,  $\mathbf{Y}_e(s)$ :

$$\begin{aligned} \begin{bmatrix} \omega_s(s) \\ \omega_m(s) \end{bmatrix} &= \mathbf{Y}_e(s) \begin{bmatrix} \tau_s(s) \\ \tau_m(s) \end{bmatrix} \\ &= \begin{bmatrix} Y_e^{ss}(s) & Y_e^{sm}(s) \\ Y_e^{ms}(s) & Y_e^{mm}(s) \end{bmatrix} \begin{bmatrix} \tau_s(s) \\ \tau_m(s) \end{bmatrix} \end{aligned} \quad (3.82)$$

where apices  $i, j$  in  $Y_e^{ij}$  are referred to the output angular velocity and the input torque, respectively, so that, for instance:

$$Y_e^{sm}(s) = \frac{\omega_s(s)}{\tau_m(s)}$$

It should be point out that the formulation above is not the canonical definition of admittance for a MIMO system, but for the sake of the demonstration, it is a good approximation.

The equations of motion of the coupled systems are:

$$\tau_m - \tau_s = I_m \dot{\omega}_m + b_c(\omega_s - \omega_m) + k_c(\theta_s - \theta_m) \quad (3.83)$$

and

$$\tau_h + \tau_s = (I_{arm} + I_h) \dot{\omega}_s \quad (3.84)$$

Now consider the minimal admittance controller provided in Figure 3-18. That controller consists of two components. The first component is the virtual admittance model  $\bar{Y}_e^d(s)$ , which represents the desired exoskeleton's drive behavior, and to the purpose of demonstration, since the exoskeleton displays an inertial behavior, there will be considered as desired dynamics those of a pure inertia:

$$\bar{Y}_e^d(s) = \frac{1}{I_e^d s} \quad (3.85)$$

The virtual admittance model receives the measured torque at port  $S$ ,  $\tau_s$ , as input, and generates the angular velocity  $\omega_{ref}$  as output, which is used as reference signal in the second component of the controller, which consists of the proportional control law for velocity tracking:

$$\tau_m = k_p(\omega_{ref} - \omega_m) = k_p(\bar{Y}_e^d \tau_s - \omega_m) \quad (3.86)$$

being  $k_p$  the proportional gain.

The exoskeleton's drive admittance under closed-loop control is obtained as it follows. From Equation (3.82), it follows:

$$\omega_s = Y_e^{ss} \tau_s + Y_e^{sm} \tau_m \quad (3.87)$$

and

$$\omega_m = Y_e^{ms} \tau_s + Y_e^{mm} \tau_m \quad (3.88)$$

Thus, plugging Equation (3.88) into Equation (3.86):

$$\tau_m = \frac{k_p (\bar{Y}_e^d - Y_e^{ms})}{1 + k_p Y_e^{mm}} \tau_s \quad (3.89)$$

Finally, plugging Equation (3.89) into Equation (3.87), it is now possible to derive the equation for the exoskeleton's drive admittance under closed-loop control:

$$Y_e^s(s) = \frac{\omega_s(s)}{\tau_s(s)} = Y_e^{ss}(s) + \frac{k_p Y_e^{sm}(s) (\bar{Y}_e^d(s) - Y_e^{ms}(s))}{1 + k_p Y_e^{mm}(s)} \quad (3.90)$$

In other words,  $Y_e^s$  represents the admittance function between port of interaction  $S$  and the output of the exoskeleton's drive.

The inertial load acting on the exoskeleton drive is given by:

$$Z_L(s) = (I_{arm} + I_h) s \quad (3.91)$$

The admittance presented to the muscle torque,  $\tau_h$ , is equal to admittance of the coupled system, consisting of the product of the closed-loop drive admittance  $Y_e^s(s)$  and the load  $Z_L(s)$ . To find the range of values of  $\bar{I}_e^d$  the coupled system remains stable, it is sufficient to apply the Nyquist stability criterion to open-loop transfer function of the coupled system ( $b_c = 0$  for simplicity):

$$\begin{aligned} G(s) &= Z_L(s) Y_e^s(s) = \\ &= \frac{I_{arm} + I_h}{I_s} \frac{s^3 + \frac{k_p}{I_m} s^2 + \frac{k_c}{I_m} s + \frac{k_p k_c}{\bar{I}_e^d I_m}}{s^3 + \frac{k_p}{I_m} s^2 + \frac{k_c(I_m + I_s)}{I_m I_s} s + \frac{k_p k_c}{I_m I_s}} \end{aligned} \quad (3.92)$$

To test for right half-plane poles, apply the Routh Hurwitz criterion to the characteristic polynomial of  $G(s)$ . The obtained Routh array is:

$$\left[ 1, \frac{k_p}{I_m}, \frac{k_c(I_m + I_s)}{I_m I_s}, \frac{k_p k_c}{I_m I_s} \right] \quad (3.93)$$

Since there are no changes in sign,  $G(s)$  has no right half-plane poles.

Thus, to establish the stability of the closed-loop system, it is sufficient to investigate if the Nyquist contour of  $G(s)$  does not encircle of  $-1$ , which corresponds to the following conditions:

$$\operatorname{Re}\{G(j\omega)\} > -1 \quad (3.94)$$

$$\operatorname{Im}\{G(j\omega)\} = 0 \quad (3.95)$$

Writing:

$$G(j\omega) = \frac{a(\omega) + jb(\omega)}{c(\omega) + jd(\omega)} \quad (3.96)$$

those conditions are equivalent to

$$\frac{a(\omega)c(\omega) + b(\omega)d(\omega)}{c^2(\omega) + d^2(\omega)} > -1 \quad (3.97)$$

$$\frac{b(\omega)c(\omega) - a(\omega)d(\omega)}{c^2(\omega) + d^2(\omega)} = 0 \quad (3.98)$$

Solving those conditions for  $\bar{I}_e^d$  and  $\omega$  yields to the following stability condition:

$$\bar{I}_e^d \geq \frac{I_m(I_{arm} + I_h)}{I_s + I_{arm} + I_h} \quad (3.99)$$

A fair assumption is that the output inertia is lower than the two moments of inertia,  $I_s \ll I_{arm} + I_h$ , so condition (3.99) can be reduced to:

$$\bar{I}_e^d \geq I_m \quad (3.100)$$

Although condition (3.100) is the solution of a particular case, this result recurs in many other similar applications, leading to the following important conclusion. The apparent inertia  $\bar{I}_e^d$  cannot be arbitrarily lower, otherwise the coupled system will become unstable. The admissible range of values for  $\bar{I}_e^d$  is inferiorly limited by the servo motor's inertia,  $I_m$ . In conclusion, it is not possible to adopt a negative apparent inertia to compensate for the inertias of the exoskeleton arm or human limb.

Notice that even if the sensor port  $S$  would be mounted, and therefore, result coincident with the port of interaction  $P$  between the human limb and the exoskeleton arm, it is still impossible to adopt a negative apparent inertia in the admittance model since the stability condition would be:

$$\bar{I}_e^d \geq \frac{I_m I_h}{I_s + I_{arm} + I_h} \quad (3.101)$$

### 3.5.5 Emulated inertia compensation

A question arose while studying these documents: "If it is not possible to eliminate the inertia from the problem, is it actually possible to minimize it or circumvent the issue?"

The solution proposed in [16] presents a complementary control method aimed at masking the inertias of both the exoskeleton's arm and the human limb. It is called "emulated inertia compensation" and it consists of an approximate form of inertia compensation based on positive feedback of angular

acceleration. It is adopted also in other exoskeletons control strategies, such as in [21]. Human motion is relatively slow, if compared with electrical or mechanical systems, hence, in frequency domain, the entire range of motion is contained in a low-frequency bandwidth. For the experiment set, knee joint motion occurs in at frequencies less than 2 Hz. Thus, providing an acceleration feedback that is low-pass filtered at a cutoff frequency near the maximum frequency of the leg motion is sufficient to assist human movement. It cannot result in an exact cancellation of the inertia parameters, but it can increase the pendulum frequency of the leg, resulting in an overall increment of the leg's swing speed.

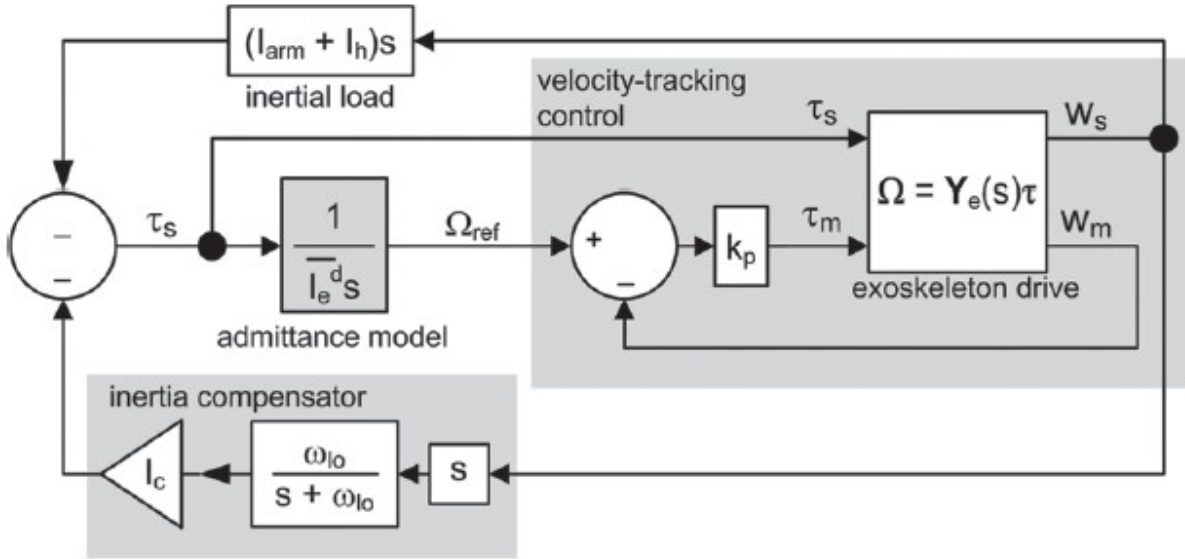


Figure 3-19: Admittance controller with emulated inertia compensator. Reprinted from [16].

The addition of the emulated inertia compensator to the previous minimal control scheme is illustrated in Figure 3-19. Its transfer function is:

$$H_i(s) = I_c \frac{\omega_{lo}}{s + \omega_{lo}} s \quad (3.102)$$

consisting of a low-pass filter,  $LPF(s) = \frac{\omega_{lo}}{s + \omega_{lo}}$ , with  $\omega_{lo}$  cutoff frequency, operating on the fed back angular acceleration of the output's shaft,  $s\omega_s$ , and a constant negative gain  $I_c$ , which is the new degree-of-freedom in the design that allows to obtain a “negative” apparent inertia.

To find the range of values of the new inertia compensation gain  $I_c$ , apply the Nyquist stability criterion to the open-loop transfer function of the new formed coupled system:

$$G_i(s) = [H_i(s) + Z_L(s)]Y_e^s(s) \quad (3.103)$$

The stability analysis for this system yields to the following condition (see Appendix B of [3] for more details):

$$I_c \geq -(I_h + I_{arm} + I_m) \quad (3.104)$$

This stability condition testifies that it is possible to choose a negative value for  $I_c$  to compensate the inertias of the human limb and the exoskeleton drive and arm, without bringing the system to instability. In addition,  $I_c$  is a constant value independent of the inertia compensator cutoff frequency,  $\omega_{lo}$ , leading to

a design for stability which is not constrained by the maximum frequency in the human motion bandwidth, and the proportional gain,  $k_p$ , is decoupled from the stability condition and can be used to tune the system to obtain the required performance.

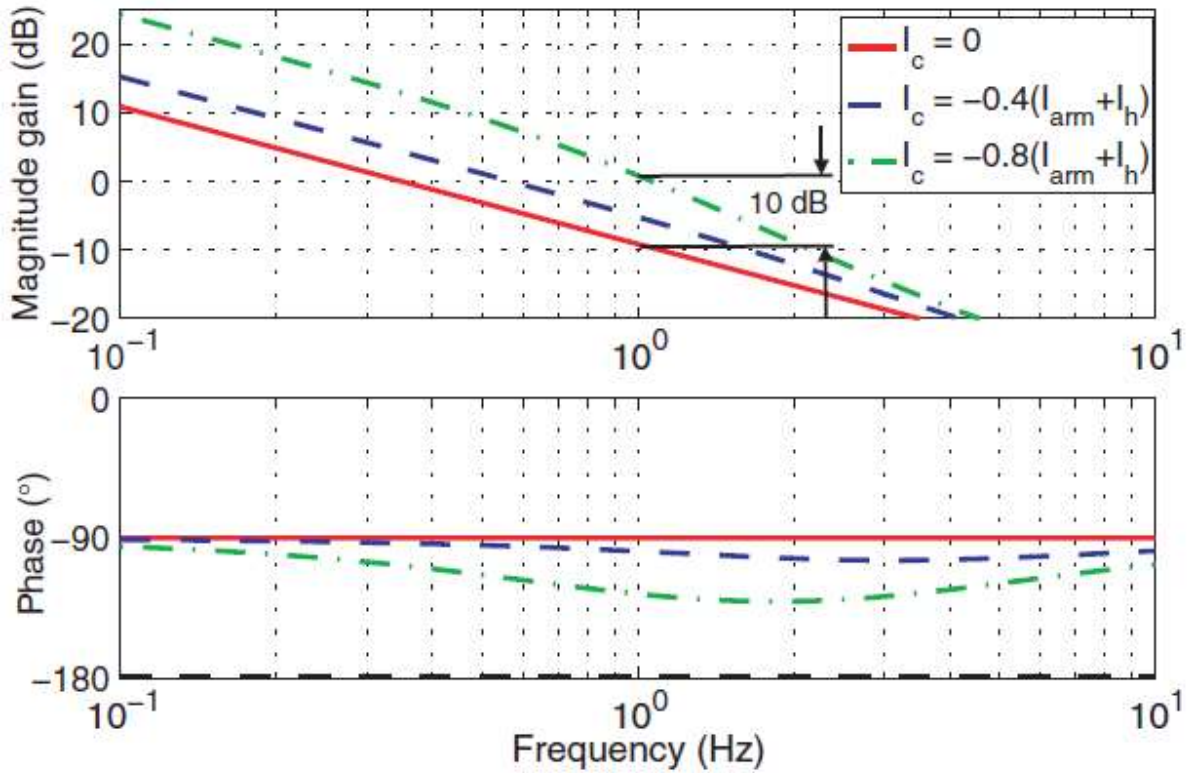


Figure 3-20: Bode plot of the closed-loop admittance  $Y_e^h(j\omega)$  of the coupled system exoskeleton drive/inertia compensator/inertial load. Reprinted from [16].

Figure 3-20 provides the frequency-response plots of the closed-loop admittance  $Y_e^h(s)$  for different values of  $I_c$ :

$$Y_e^h(s) = \frac{\omega_s(s)}{\tau_h(s)} = \frac{Y_e^s(s)}{1 + [H_i(s) + Z_L(s)]Y_e^s(s)} \quad (3.105)$$

which represents the admittance of the coupled system presented to the human muscle torque  $\tau_h$ .

At low frequencies, the emulated inertia compensation produces a virtual increase in the magnitude of the admittance of the system and, for increasing frequencies, all admittance functions' magnitudes converge to the bounding plot  $I_c = 0$ . Notice that for  $I_c = -0.8(I_{arm} + I_h)$ , the increased admittance is about 10 dB at 1 Hz, which corresponds to a virtual reduction in load inertia of about 68%. The haptic sensation felt by the user will be the leg less resistant to movement or "lighter" when moving the leg.

### 3.5.5.1 Emulated inertia compensator

The low-pass filter adopted in the emulated inertia compensator can be more complex than the one adopted above, such as Butterworth filters with order superior to two [21].

The cutoff frequency must be wisely selected. For values superior to 2 Hz, the higher frequency components in the acceleration feedback mar the control of voluntary leg moments. Instead, lower values will introduce phase lag, reducing the reliability of the inertia compensator.

Due to the presence of the inertia compensator, the admittance model will be used only to mask damping and weight. Assistance to the user will be provided only by the inertia compensator.

For  $I_c = 0$ , the inertia felt by the user is equal to the sum of the moment of inertia of the exoskeleton leg and the apparent inertia of the admittance model,  $\bar{I}_e^d + I_{arm}$ . So, it is possible to have partial compensation of the human limb's inertia only for  $I_c > \bar{I}_e^d + I_{arm}$ .



*PART III:*  
*Analysis of control strategies*  
*implemented in lower-limb rehabilitative exoskeletons*



# Chapter 4

## Control strategies for lower-limb rehabilitation exoskeletons

Every exoskeleton for lower-limb rehabilitation must be able to allow a sane and safe rehabilitation therapy program, by involving actively the patient's muscles in the planned movements, in order to recover the original nervous structure. Nevertheless, it can be argued that is important to have an exoskeleton that is able to perform passive rehabilitation exercises for the initial stages of the therapy, when the muscles of the patients are unable to provide enough force to move the limbs, and in such case, movements imposed by the robot are allowed and welcome.

Focusing on the recovery of the normal functionalities of the lower limbs, being the main structures involved in postural balance, the exoskeleton must be able to detect and recognize when the patient loses the equilibrium, and there is a risk of falling. In that case, the exoskeleton should intervene "more aggressively", i.e., having more control authority on the movement than the patient, providing the required torques to recover balance, but avoiding any type of damage to the patient's body. The velocity of the transition from the normal operative state to the "risk state" must be rapid but not abrupt.

Robotic exoskeleton for human-robot interaction can be classified according to the usage planned for the interaction torques. When the muscles of the patient are no longer able to provide muscular strength, due to (almost) complete paralysis of the limb, the exoskeleton is expected to generate sufficient actuator torques so that the interaction forces, constituting the main input to the passive dynamic of the human limb, can be used to impose the limb movement. These types of exoskeletons are no longer considered for rehabilitation purposes and belong more properly to the power augmentation device category. Such robotic devices are employed for patients suffering of severe paralysis or cerebral palsy, in order to make the human regain the ability to walk. When the muscles of the patients are able to provide muscular forces, but not in the measure to allow the limb movements, the exoskeleton is expected to generate the complementary assisting torque that allows the wearer to complete the movement while keeping them actively involved for neuroplastic recovery of the impaired limb. The actual amount of energy provided by the exoskeleton to the user is always lower than the energy required to passively move the limb. When the patient is in (almost) healthy conditions, and it is required that the exoskeleton intervenes only when specific situations or conditions arise, i.e., the exoskeleton is expected to operate in transparent mode, the exoskeleton's actuators should provide enough torque to compensate just for its dynamics and zero the interaction forces while following the human limb movement. In such case, the interaction forces are expected to be null.

In this Chapter, there will be presented different strategies to control lower-limb rehabilitative exoskeletons. The first one will focus on guaranteeing postural balance while performing the pre-planned training exercise, based on the studies conducted by Professors Menga and Ghirardi. The second part will focus on strategies to ensure patient-compliance while the patient performs the planned movements. Those readers that managed to read and resist the theoretical background provided in Part II (kudos to you!)

should find this part easy to understand and interesting since it is a different implementation of the main concepts. The third and fourth parts focus on transparent control, a particular and poorly researched control strategy that makes the exoskeleton follow the human limb movements as a shadow to hide its presence while there are no risks detected. This strategy aims at making the exoskeleton imperceptible while its assistance is not required.

## 4.1 Postural balance control strategies

This section focuses on the studies conducted by Professors Menga and Ghirardi on an exoskeleton able to monitor and recover postural balance. The following paragraphs will analyze first the mechanical structure, providing an in-depth description of the mechanism and the sensor used.

### 4.1.1 Description of the mechanical structure

The lower-limb exoskeleton considered in these set of experiments is a heavyweight exoskeleton, weighting about 80 kg, fixed to the ground, and designed to assist patients' movements during sit-to-stand exercises, to keep them actively involved during the training sessions, by controlling the offered compliance through an admittance controller and the postural balance by a kinematic trajectory tracker, in order to intervene more aggressively when falling risks have been identified. The robot leaves the control authority of only one joint to the human, allowing a focused training on a specific joint.

The mechanical structure is composed of two length-adjustable legs, each with three joints at the corresponding heights of the human joints, a saddle and a backrest, which were needed to introduce the opportune constraint on the symbolic software computing the exoskeleton's dynamics. Coupling is obtained through belts. The exoskeleton allows movements in the sagittal and frontal planes but constraints rotations along the z-axis, i.e., the vertical axis. Hence, it has two DOFs at the hip and ankle joints, and only one DOF at the knee joint. The joints are actuated by brushless motors, which have the optimal performances at high velocities. Harmonic gear reducers convert the high motor velocities into the high torques required in the rehabilitation application. Three types of sensors are used to collect the necessary signals: the EMG sensors, the velocity sensors, and the pressure sensors. The EMG sensors are placed on patient's skin at the location of antagonist muscles to collect the superficial EMG signals, measure of the patient's efforts. This type of sensor requires a lot of time to don on the patient, good skin conditions, and calibration must be performed at every application even for the same patient at a few hours distance. In addition, it has been proven that the measured EMG signals also contain the echoes of the primary nervous signal, containing all the signals for the lower limbs, coming from the spinal cord, requiring an intelligent filter to cut out the unnecessary signal. The velocity sensors are placed on the output of the shaft and measures the reflected velocity signals. The pressure sensors consist of load cells located under the feet of the mechanical structure to measure the pressure distribution to determine the location of the center of pressure (CoP), that is the point of application of the ground reaction force according to Vukobratovic's theory (see Appendix A3). The modeling and simulation of this exoskeleton platform is based on a Autolev (MotionGenesis) model, which exploits the Kane's method to derive the equations of motion of the robotic structure. The Kane's method is a method developed by Harvard's Professor Kane, which allows to use the constraint equations to reduce the number of equations to consider is solving the dynamic problem of a mechanical system.

The dynamical model of the exoskeleton is linearized though the Kane's method and it is described as follows:

$$\mathbf{M}(\boldsymbol{\theta})\ddot{\boldsymbol{\theta}} + \mathbf{C}(\boldsymbol{\theta}, \dot{\boldsymbol{\theta}})\dot{\boldsymbol{\theta}} - \mathbf{G}(\boldsymbol{\theta})\boldsymbol{\theta} = \boldsymbol{\tau} - \boldsymbol{\tau}_{dist} \quad (4.1)$$

where  $\mathbf{M}$  is the configuration-dependent linearized inertia matrix,  $\mathbf{C}$  is the linearized matrix that takes into account the centrifugal, gyroscopic, and Coriolis effects,  $\mathbf{G}$  is the linearized gravitational effect vector,  $\boldsymbol{\tau}$  is the vector of the actuators' torques, and  $\boldsymbol{\tau}_{dist}$  is the vector of the external disturbances.

For further information and details about the modeling of the considered exoskeleton and the Kane's method, refer to documents [22-24]



Figure 4-1: Frontal view of the prototype exoskeleton coupled with human user. Reprinted from [24]

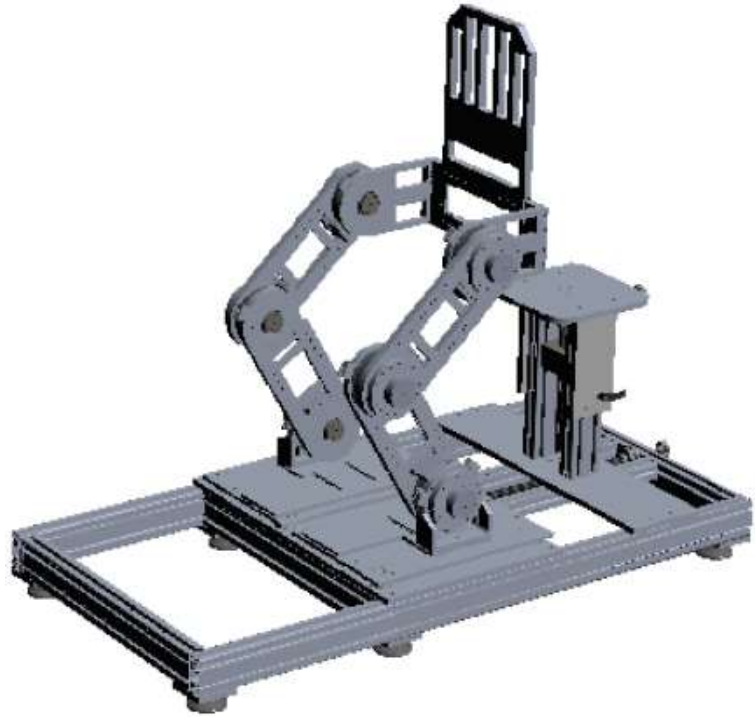


Figure 4-2: CAD model of the prototype exoskeleton for sit-to-stand exercises. Reprinted from [25]

### 4.1.2 Control System

The control system exploited in this system, presented in articles [24,25], is particularly complex and it will be briefly discussed in the following to let the reader understand how it is complex to integrate postural balance control laws, coming from the control literature of autonomous bipedal robots, to rehabilitative exoskeletons, which are coupled to a human being, hence, they must consider also safety, compliance, and their rehabilitative mission.

The controller's inputs as presented before are the superficial EMG signals, the velocity signals, and the pressure signals. The ulterior input signal is the simulation-generated reference trajectory signal for the desired position and velocity of the center of gravity (COG), the zero-moment point (ZMP), and the trunk rotation, both in the sagittal and frontal planes. This solution is adopted to consider the future possibility of set one between several exercises to be performed during the training session.

The block diagram of the control loop is provided in Figure 4-3. The internal loop is a classic velocity tracking loop. The deviation of the measured joints velocities,  $\dot{\theta}(t)$ , with respect to the reference joint velocities computed and provided by the external control loop,  $\dot{\theta}_{ref}(t)$ , is used as input of a PD controller to generate the intensity of the actuators' torques. The control law is reported in the following:

$$\tau(t) = k_p (\dot{\theta}_{ref}(t) - \dot{\theta}(t)) + k_D (\ddot{\theta}_{ref}(t) - \ddot{\theta}(t)) \quad (4.2)$$

where  $k_p$  and  $k_D$  are respectively the proportional and derivative gain. The value of  $k_p$  can be tuned to have a sufficiently extended controller's bandwidth, a lower rise time, and a lower steady-state error, in absence of an integral action. The value of  $k_D$  can be selected to restrict the transient's overshoot, increasing the stability margins, counteracting the effect of high-valued  $k_p$ , and increasing the pass-band frequency range. However, high values of  $k_D$  lead to an amplification of noise.

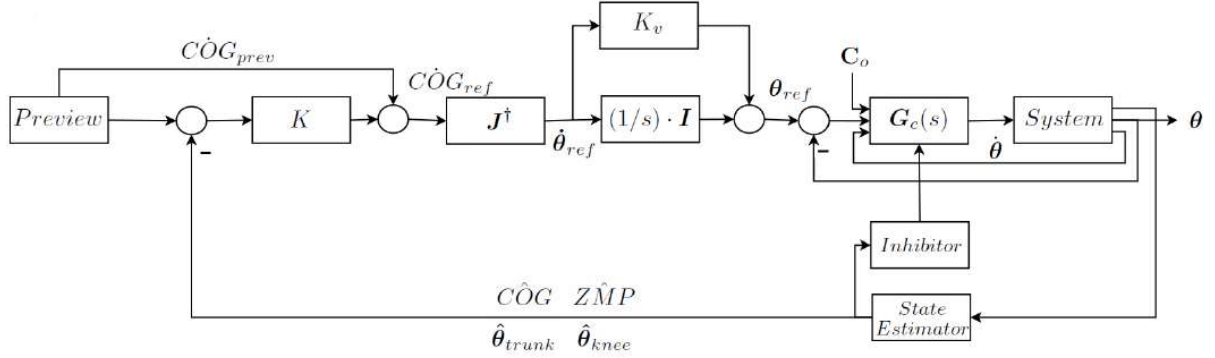


Figure 4-3: Block diagram of the postural control loop for each plane. Reprinted from [25].

The external loop consists of several blocks that will be discussed in the following. The mission of the external loop is to monitor the postural balance while the patient performs some movements, in order to intervene to help in balance recovery when the initial state of a falling is detected, by deriving the estimation of the ZMP, and to generate the reference joint velocities,  $\dot{\theta}_{ref}$ . In addition, the admittance control module allows to generate a contribution,  $\dot{\theta}_p$ , to the reference joint velocities starting from the measured EMG signal and the arbitrary parameters of the virtual admittance model, which can be left to assign to the physician according to the patient's progress in rehabilitation.

The Preview block is responsible for generating the desired kinematic trajectories of the COG, the ZMP, and the trunk sagittal rotation, according to the exercise selected during the training session.

The reference trajectories for the COG and the trunk are given by periodic mathematical functions, while the reference ZMP signal is computed according to Equation (A19):

$$ZMP_{ref_x} = COG_{ref_x} - \frac{COG_z}{g} CO\ddot{G}_{ref_x} \quad (4.3)$$

$$ZMP_{ref_y} = COG_{ref_y} - \frac{COG_z}{g} CO\ddot{G}_{ref_y} \quad (4.4)$$

In addition, the reference velocities of the COG and the trunk are provided as feedforward signals to maximize the robustness of the system.

The target admittance model,  $Y_{des}(s)$ , is the dynamic operator mapping the muscular efforts of the patient, testified by the measured EMG signals, to the joint velocities due to the patient's movements. It has the form of a damper-spring system:

$$\mathbf{Y}_{des}(s) = \frac{\hat{\theta}_p(s)}{EMG_m(s)} = diag\left(\frac{1}{b_i s + k_i}\right) \quad (4.5)$$

where  $k_i$  and  $b_i$  are respectively the desired stiffness of joint  $i$  and the desired damping factor of joint  $i$ . The desired damping factor is used also to filter the noise on the measured EMG signals. Fortunately, the dynamics of each joint can be decoupled from the others, hence, the target admittance model has the form of a diagonal matrix.

The inhibitor block is responsible for decreasing the target admittance, by increasing the stiffness  $k_i$  of the joint  $i$  of the robot, when the actions of the patient move the ZMP near the equilibrium tolerance region.

An extension of Choi's theory for estimation of the ZMP based on the ground projection of the COG is considered in the state estimator [27]. This extension considers that it is impossible to avoid noise in the measurements, and that the ZMP can be derived directly from the COP (see Appendix A2), while the COG can be derived only indirectly from the joint kinematics and the load distribution measured by the load cells. The solution proposed in [27] consider an extended system able to estimate and robustly control the COG and the ZMP, taking into account the external and the patient's movement-induced internal disturbances acting on the exoskeleton Figure 4-4. The modified Choi's equations become:

$$e_c = c_d - \hat{c} - \hat{\delta}_c \quad (4.6)$$

$$e_p = p_d - \hat{p} - \hat{\delta}_p \quad (4.7)$$

$$e_{cv} = \dot{c}_d - \hat{c} \quad (4.8)$$

$$u = \dot{c}_d + k_c e_c - k_p e_p + k_{cv} e_{cv} \quad (4.9)$$

where  $c$  indicates the position of the COG on the ground,  $p$  is the location of the ZMP,  $e_c$ ,  $e_p$ , and  $e_{cv}$  are respectively the error on the position of the COG on the ground, the error on the location of the ZMP, and the error on the velocity of the projected COG,  $k_p$ ,  $k_c$ , and  $k_{cv}$  are the controller gains on the position of the ZMP, the position and velocity of the projected COG. Subscript  $d$  defines the desired quantities. The quantities  $\hat{\delta}_p$  and  $\hat{\delta}_c$  represents the estimated difference between the position measured and desired of the ZMP and the COG, respectively.

The outputs of the state estimator are:  $\widehat{ZMP}_{xy}$ ,  $\widehat{COG}_i$ ,  $\widehat{COG}_i$ ,  $\hat{\theta}_{trunk_{xy}}$  and  $\hat{\theta}_{trun_{xy}}$ . The estimations of the trunk kinematic quantities are obtained from the system's kinematic.

The external loop presents a PD controller too. The inputs are the preview signals and the estimated signals. The output signals are controlled actions on the selected coordinates in the operative space. They can be expressed as (omitting time variable  $t$  for visual simplicity):

$$u_{COG_i} = k_{p_i} (COG_{ref_i} - \widehat{COG}_i) - k_{z_{1xy}} (ZMP_{ref_{xy}} - \widehat{ZMP}_{xy}) + k_{v_i} (\dot{COG}_{ref_i} - \widehat{COG}_i), \quad i = x, y \quad (4.10)$$

$$u_{trunk_j} = k_{p_j} (\theta_{trunk_{ref}} - \hat{\theta}_{trunk_j}) + k_{v_j} (\dot{\theta}_{trunk_{ref}} - \hat{\theta}_{trunk_j}), \quad j = x, y \quad (4.11)$$

where  $k_{p_i}$  and  $k_{v_i}$  are the COG's position and velocity gains,  $k_{z_{1xy}}$  is the gain on the ZMP position,  $k_{p_j}$  and  $k_{v_j}$  are the gains on the trunk's angular position and velocity.

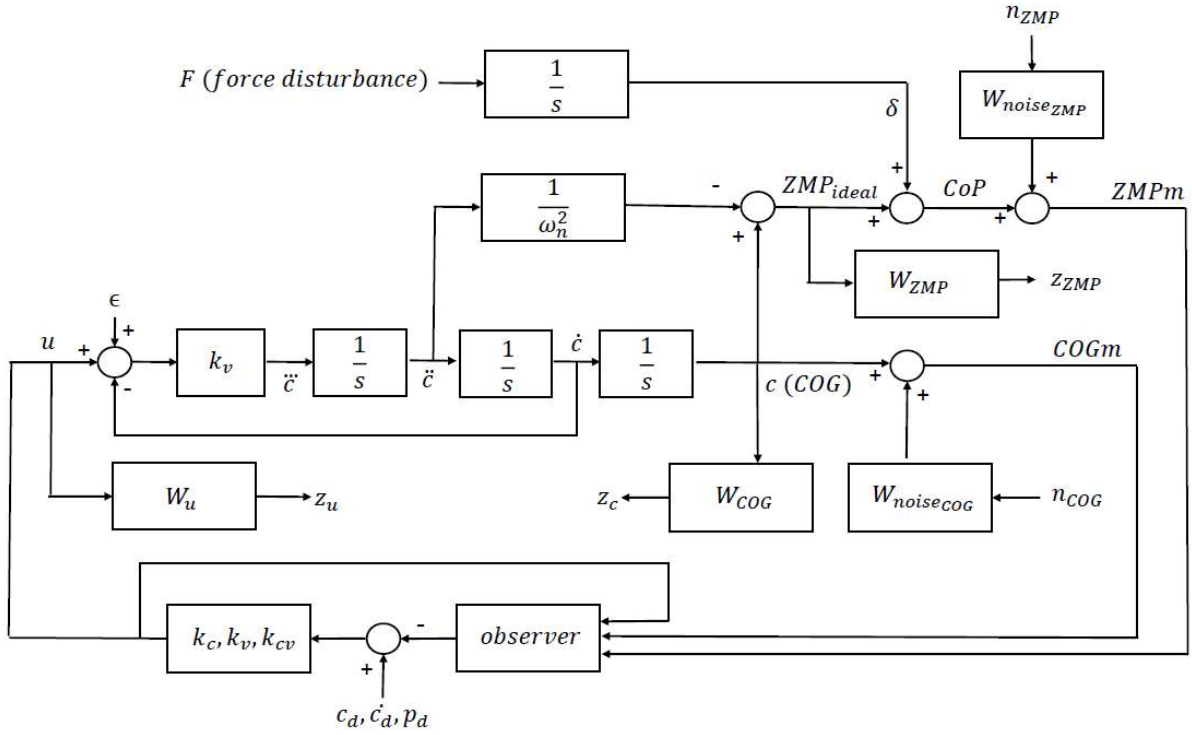


Figure 4-4: Block diagram for the extended robust estimation system of ZMP-COG according to the modified Choi's theory. Reprinted from [27].

These output signals are then summed to the feedforward signals, obtaining:

$$u_{COG_i} = \dot{C}\dot{O}G_{ref_i} + k_{p_i}(COG_{ref_i} - \widehat{COG}_i) - k_{z_{xy}}(ZMP_{ref_{xy}} - \widehat{ZMP}_{xy}) + k_{v_i}(\dot{C}\dot{O}G_{ref_i} - \widehat{\dot{C}\dot{O}G}_i), \quad (4.12)$$

$$i = x, y$$

$$u_{trunk_j} = \dot{\theta}_{trunk_{ref_j}} + k_{p_j}(\theta_{trunk_{ref}} - \hat{\theta}_{trunk_j}) + k_{v_j}(\dot{\theta}_{trunk_{ref}} - \hat{\dot{\theta}}_{trunk_j}), \quad (4.13)$$

$$j = x, y$$

To control properly the postural balance in both the sagittal and frontal planes, the vector  $u_{COG_i}$  is decomposed in the two components ( $u_{COG_x}, u_{COG_y}$ ), and it is considered also the command related to the height of the center of gravity:

$$u_{COG_z} = \dot{C}\dot{O}G_{ref_z} + k_{p_z}(COG_{ref_z} - \widehat{COG}_z) + k_{v_z}(\dot{C}\dot{O}G_{ref_z} - \widehat{\dot{C}\dot{O}G}_z) \quad (4.14)$$

To univocally determine the posture or a movement of the coupled system, the controlled input on the sagittal plane will be expressed by Equation (4.15), and on the frontal plane by Equation (4.16):

$$\mathbf{u}(t) = \begin{bmatrix} u_{COG_x} \\ u_{COG_z} \\ u_{trunk_y} \end{bmatrix} \quad (4.15)$$

$$\mathbf{u}(t) = \begin{bmatrix} u_{COG_y} \\ u_{COG_z} \\ u_{trunk_x} \end{bmatrix} \quad (4.16)$$

The real-time Jacobian matrix that transforms the controlled input in the operative space,  $\mathbf{u}(t)$ , into the reference velocities in the joint space,  $\dot{\boldsymbol{\theta}}_{ref}$ , is the 3-by-3 matrix given by:

$$\mathbf{J} = \begin{bmatrix} J_{COG_i} \\ J_{COG_z} \\ J_{trunk_j} \end{bmatrix}, \quad i = x, y; j = y, x \quad (4.17)$$

so that:

$$\begin{bmatrix} u_{COG_i} \\ u_{CO_z} \\ u_{trunk_j} \end{bmatrix} = \begin{bmatrix} J_{COG_i} \\ J_{COG_z} \\ J_{trunk_j} \end{bmatrix} \begin{bmatrix} \dot{\theta}_{ref\_ankle_i} \\ \dot{\theta}_{ref\_knee} \\ \dot{\theta}_{ref\_hip_j} \end{bmatrix}, \quad i = x, y; j = y, x \quad (4.18)$$

Therefore, to obtain the reference joint velocities,  $\dot{\boldsymbol{\theta}}_{ref}$ , it is necessary to exploit the inverse of the Jacobian, so that:

$$\dot{\boldsymbol{\theta}}_{ref}(t) = \mathbf{J}^{-1}\mathbf{u}(t) + \dot{\boldsymbol{\theta}}_p \quad (4.19)$$

To ensure that the Jacobian matrix is invertible, i.e., it is nonsingular and has maximum rank, the authors added an ulterior component, the controlled input to the knee joint, to the control input  $\mathbf{u}(t)$ , so that:

$$\mathbf{u}(t) = \begin{bmatrix} u_{COG_i} \\ u_{COG_z} \\ u_{trunk_j} \\ u_{knee} \end{bmatrix}, \quad i = x, y; j = y, x \quad (4.20)$$

where

$$u_{knee}(t) = \dot{\theta}_{ref\_knee} + k_p (\theta_{preview\_knee} - \hat{\theta}_{knee}) + k_d (\dot{\theta}_{preview\_knee} - \hat{\dot{\theta}}_{knee}) \quad (4.21)$$

The relationship between the new component of  $\mathbf{u}(t)$  and  $\dot{\theta}_{ref\_knee}$  can be expressed as:

$$u_{knee}(t) = \lambda[0 \ 1 \ 0]\dot{\boldsymbol{\theta}}_{ref} \quad (4.22)$$

posing  $\lambda \in [0.2; 0.5]$  in order to reduce the priority of controlling the knee joint.

The extended Jacobian matrix is then:

$$\mathbf{J}_{ext} = \begin{bmatrix} J_{COG_i} \\ J_{COG_z} \\ J_{trunk_j} \\ \lambda[0 \ 1 \ 0] \end{bmatrix}, \quad i = x, y; j = y, x \quad (4.23)$$

allowing to solve the singularities of the Jacobian matrix and the complications arisen from the angular position of the knee and the height of the COG during the real-time synthesis.

Since the extended Jacobian matrix is rectangular, i.e., the exoskeleton is redundant, instead of computing the inverse of the Jacobian, the pseudoinverse of the Jacobian matrix is considered:

$$J_{ext}^{\dagger} = (J_{ext}^T J_{ext})^{-1} J_{ext}^T \quad (4.24)$$

All things being equal, the controller is designed to leave only one joint passive to be controlled by the patient, in order to keep them neurologically involved during the physical recovery. However, as presented in section 4.4, it is possible to introduce a transparency level parameter, whose tuning is left to the physiotherapist, in order to modulate the patient's control authority over the whole coupled system.

## 4.2 Control strategies for lower-limb rehabilitative exoskeletons

In this section, it will be provided two examples of control strategies for lower-limb rehabilitation exoskeletons based on patient-compliance. The kinematic trajectories of the joints must be prepared in advance according to the desired physiotherapeutic exercise.

The following strategies are based on documents [28] and [21].

### 4.2.1 Description of the mechanical structure

The lower-limb rehabilitation exoskeleton exploited in the experiments in [28] is lightweight and it has three 1-DOF joints per leg, located in correspondence to the hip, the knee, and ankle. The hip and the knee joints are actuated by brushless DC electric motors, which meet the requirements of power-vs-weight, the ankle joint is left passive. The coupling elements are bandages and link human's thigh and shank to the robot's corresponding ones. Each of these components accommodates pockets for two uniaxial force sensors used to acquire real-time human-exoskeleton interaction force data. A real-time control system is needed to process real-time data.

Human-robot interaction (HRI) may be classified into physical (pHRI), based on force interaction, and cognitive (cHRI), based on user's feelings in controlling the coupled system. The haptic feelings are perceived since at the port of interaction, i.e., the bandage location, the muscles and fat in the human leg create a soft coupling between the exoskeleton and the skeleton (Figure 4-5), which can be modeled as a parallel of linear spring and linear damper attached to the surface of the links, allowing the torques generated by the actuators to assist the human in their movement.

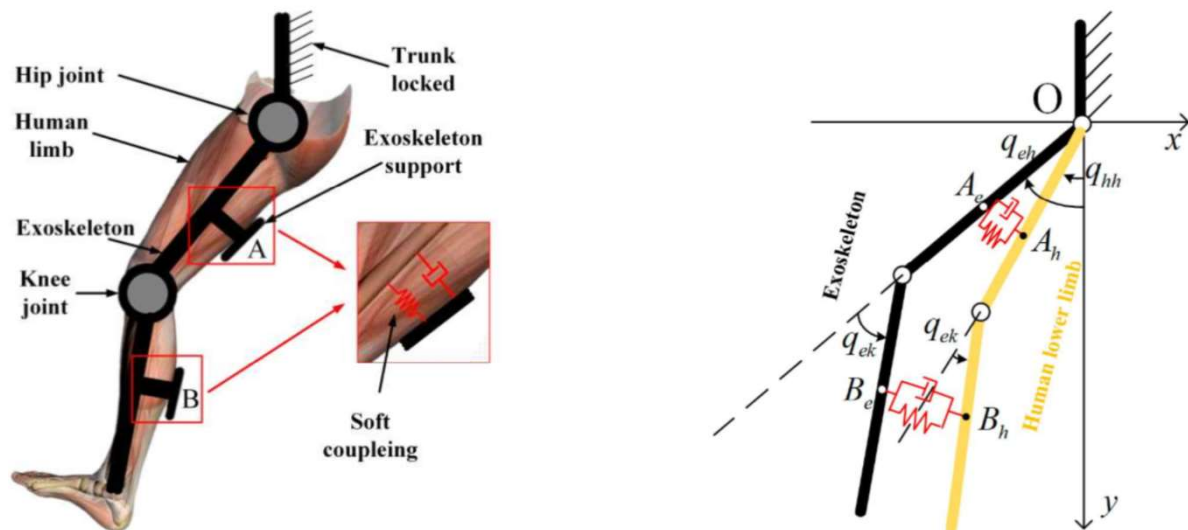


Figure 4-5: The coupling model of human lower limb and exoskeleton (on the left) and its model representation on the right (yellow, the human limb; black, the exoskeleton). Notice the model description for the soft coupling. Reprinted from [28].

With reference to Figure 4-5, the Euler-Lagrange equations of motion of the human leg can be described as:

$$\mathbf{M}_h(\mathbf{q}_h)\ddot{\mathbf{q}}_h + \mathbf{C}_h(\mathbf{q}_h, \dot{\mathbf{q}}_h)\dot{\mathbf{q}}_h + \mathbf{G}_h(\mathbf{q}_h) = \mathbf{T}_h \quad (4.25)$$

where  $\mathbf{q}_h = [q_{hh}, q_{hk}]^T$  is the state vector of human joint angle, where the first index “h” stands for “human”, and the second indices “h” and “k” stand respectively for “hip” and “knee” joints,  $\mathbf{T}_h = [T_{hh}, T_{hk}]^T$  is the human muscle torques vector,  $\mathbf{M}_h \in \mathbb{R}^{2 \times 2}$  is the inertia matrix of the single human lower limb,  $\mathbf{C}_h \in \mathbb{R}^{2 \times 2}$  is the centrifugal and Coriolis force matrix,  $\mathbf{G}_h \in \mathbb{R}^2$  is the gravitational torque vector.

In a similar way, the Euler-Lagrange equations of motion of the exoskeleton leg can be described as:

$$\mathbf{M}_e(\mathbf{q}_e)\ddot{\mathbf{q}}_e + \mathbf{C}_e(\mathbf{q}_e, \dot{\mathbf{q}}_e)\dot{\mathbf{q}}_e + \mathbf{G}_e(\mathbf{q}_e) = \mathbf{T}_e \quad (4.26)$$

Having two ports of interactions means that when the two systems are coupled, two sets of interaction forces are generated. Interaction force is a key aspect of rehabilitative exoskeletons since allows to transfer part of the torques generated by the actuators to the patients to assist in their movement execution. However, the interaction forces represent a resistance for exoskeleton’s actuators. Thus, the dynamical equation of the human-exoskeleton coupled system is:

$$\begin{cases} \mathbf{M}_h(\mathbf{q}_h)\ddot{\mathbf{q}}_h + \mathbf{C}_h(\mathbf{q}_h, \dot{\mathbf{q}}_h)\dot{\mathbf{q}}_h + \mathbf{G}_h(\mathbf{q}_h) = \mathbf{T}_h + \mathbf{J}_{hh}^T \mathbf{F}_h + \mathbf{J}_{hk}^T \mathbf{F}_k \\ \mathbf{M}_e(\mathbf{q}_e)\ddot{\mathbf{q}}_e + \mathbf{C}_e(\mathbf{q}_e, \dot{\mathbf{q}}_e)\dot{\mathbf{q}}_e + \mathbf{G}_e(\mathbf{q}_e) = \mathbf{T}_e - \mathbf{J}_{eh}^T \mathbf{F}_h - \mathbf{J}_{ek}^T \mathbf{F}_k \end{cases} \quad (4.27)$$

where  $\mathbf{J}_{hh}, \mathbf{J}_{hk}$  are the Jacobian matrices for the human limb, while  $\mathbf{J}_{eh}, \mathbf{J}_{ek}$  are the Jacobian matrices for the exoskeleton. The interaction forces are  $\mathbf{F}_h$  and  $\mathbf{F}_k$  applied to the thigh links and the shank links, respectively. Since these are the reaction forces opposed by the parallel of the linear spring and linear damper, they can be defined as:

$$\mathbf{F}_h = \begin{bmatrix} F_{hx} \\ F_{hy} \end{bmatrix} = b_A \begin{bmatrix} \dot{x}_{Ae} - \dot{x}_{Ah} \\ \dot{y}_{Ae} - \dot{y}_{Ah} \end{bmatrix} + k_A \begin{bmatrix} x_{Ae} - x_{Ah} \\ y_{Ae} - y_{Ah} \end{bmatrix}, \quad (4.28)$$

$$\mathbf{F}_k = \begin{bmatrix} F_{kx} \\ F_{ky} \end{bmatrix} = b_B \begin{bmatrix} \dot{x}_{Be} - \dot{x}_{Bh} \\ \dot{y}_{Be} - \dot{y}_{Bh} \end{bmatrix} + k_B \begin{bmatrix} x_{Be} - x_{Bh} \\ y_{Be} - y_{Bh} \end{bmatrix}, \quad (4.29)$$

posing  $k_i, b_i, i = A, B$  the stiffness and the damping coefficient of the soft coupling connecting respectively the thigh and the shank links. The coordinates of the four contact points can be expressed as:

$$\begin{cases} x_{Ah} = l_{Ah} \cos(q_{hh}) \\ y_{Ah} = l_{Ah} \sin(q_{hh}) \\ x_{Ae} = l_{Ae} \cos(q_{eh}) \\ y_{Ae} = l_{Ae} \sin(q_{eh}) \end{cases} \quad (4.30)$$

$$\begin{cases}
x_{Bh} = l_{hh} \cos(q_{hh}) + l_{Bh} \cos(q_{hh} + q_{hk}) \\
y_{Bh} = l_{hh} \sin(q_{hh}) + l_{Bh} \sin(q_{hh} + q_{hk})
\end{cases}
\quad (4.31)$$

$$\begin{cases}
x_{Be} = l_{eh} \cos(q_{eh}) + l_{Be} \cos(q_{eh} + q_{ek}) \\
y_{Be} = l_{eh} \sin(q_{eh}) + l_{Be} \sin(q_{eh} + q_{ek})
\end{cases}$$

where  $l_{hh}, l_{hk}$  are the length of the thigh and the shank of the human limb;  $l_{eh}, l_{ek}$  are the length of the thigh and the shank of the exoskeleton leg;  $l_{Ah}, l_{Bh}$  denote the distance from the human hip joint and the knee joint to point  $A_h$  and  $B_h$ ;  $l_{Ae}, l_{Be}$  denote the distance from the human hip joint and the knee joint to point  $A_e$  and  $B_e$ .

#### 4.2.2 Control system based on human torques estimation

Defined the dynamical model we are going to use, the main aspect to take into account is how to exploit interaction forces to transfer partial of the total torques generated by the actuators in order to provide the complementary energy to sustain movement.

Suppose the human is completely unable to generate any muscle torque and, therefore, the exoskeleton's actuators must generate the torques to move both its leg and drive the human lower limb. A situation in which the exoskeleton is required to impose the movement is often found in power augmentation exoskeletons aimed at providing bipedal locomotion to patients affected by lower limb total paralysis [29] or in tutoring state (see section 4.4). According to Equation (4.27), the interaction forces, collectively called interaction torques  $\mathbf{T}_i$ , are the only input to the human leg system, i.e.,  $\mathbf{T}_i$  assumes its maximum value possible and it is called standard interaction torque,  $\mathbf{T}_{id}$ :

$$\mathbf{M}_h(\mathbf{q}_h)\ddot{\mathbf{q}}_h + \mathbf{C}_h(\mathbf{q}_h, \dot{\mathbf{q}}_h)\dot{\mathbf{q}}_h + \mathbf{G}_h(\mathbf{q}_h) = \mathbf{T}_{id} \quad (4.32)$$

Alternatively, if the human limb retains some muscle strength, the inputs driving the human limb are both  $\mathbf{T}_h$  and  $\mathbf{T}_i$ . Notice that the variation in intensity of  $\mathbf{T}_i$  depends on whether the human torques are directed along the interaction torques, in which case  $\mathbf{T}_i$  decreases, decreasing the effort on the actuators, or the human torques does not follow the interaction torques, in which case  $\mathbf{T}_i$  increases, and the effort required to the actuators will increase as well.

There is not a sensor that is able to measure directly the torque generated by human muscle, or, at least, there exists not a non-invasive sensor for such function. However, it is possible to measure indirectly the exerted human torque by measuring the changes in the interaction forces using the uniaxial force sensors. In addition, such signals show also intention of motion.

As a result, by measuring the real-time interaction forces exchanged between the robot and the human, and comparing them to the standard interaction force in Equation (4.32), it is possible to derive an estimation of the real-time human muscle torque  $\tilde{\mathbf{T}}_h$ :

$$\tilde{\mathbf{T}}_h = \mathbf{T}_{id} - \mathbf{J}_{hh}^T \mathbf{F}_h - \mathbf{J}_{hk}^T \mathbf{F}_k \quad (4.33)$$

The designed controller is an admittance controller used to extrapolate the human intention of motion from the measured interaction forces and control the coupled system to make the human leg swing to the desired angle. The control authority over the movement is under the user's intentions, the controller will adjust the reference rehabilitation training trajectory to provide suitable assistance according to the user's intention of motion.

The control law used to regulate the interaction between the coupled systems is given by two control loops, one external and one internal (Figure 4-6).

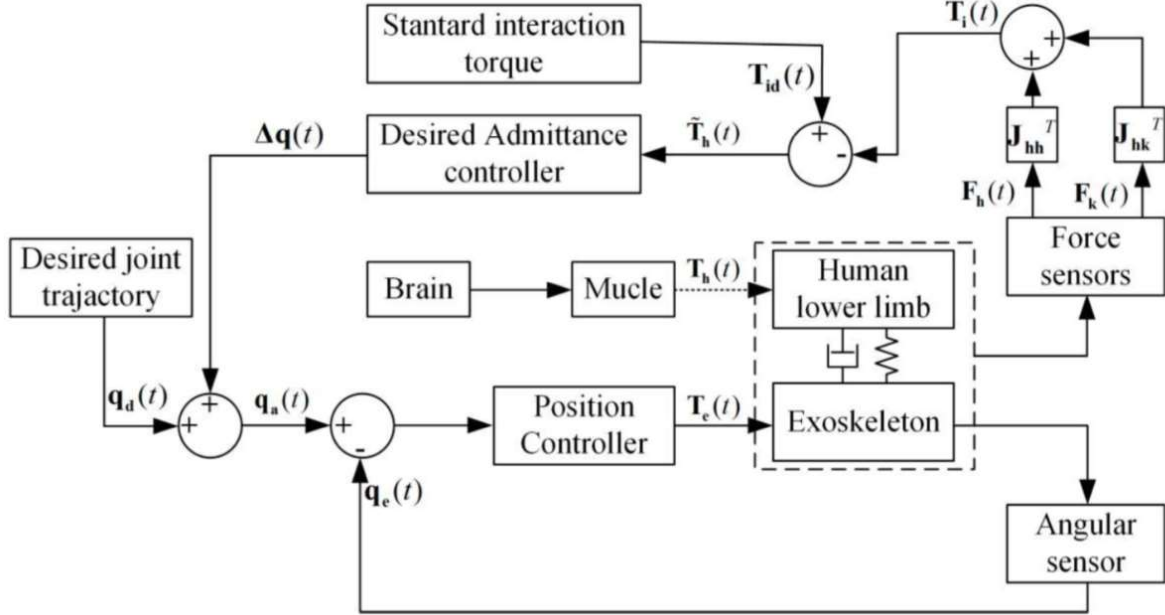


Figure 4-6: Block diagram of the control system and the plant. Notice that the human torque input is represented but cannot be verified without other sensors. Notice that differently from the system in section 3.5, the admittance controller generates a deviation from the desired joint trajectory, not the reference trajectory. Reprinted from [28].

The external control loop consists of the target admittance dynamical model, whose characteristics are the target rotatory inertia matrix,  $\mathbf{M}_d$ , the target rotatory damping matrix,  $\mathbf{B}_d$ , and the target rotatory stiffness matrix,  $\mathbf{K}_d$ . The estimated voluntary torque command vector  $\tilde{\mathbf{T}}_h$  is given by Equation (4.32). The kinematic trajectories adjustments are given by  $\Delta\mathbf{q}(t)$  and its first and second time-derivative.

$$\begin{cases} \tilde{\mathbf{T}}_h(t) = \mathbf{M}_d \Delta \ddot{\mathbf{q}}(t) + \mathbf{B}_d \Delta \dot{\mathbf{q}}(t) + \mathbf{K}_d \Delta \mathbf{q}(t) \\ \Delta \mathbf{q}(t) = \mathbf{q}_a(t) - \mathbf{q}_d(t) \end{cases} \quad (4.34)$$

Notice that the desired trajectories for the given training exercise  $\mathbf{q}_d(t)$  are precomputed, as well as the standard interaction force  $\mathbf{T}_{id}$ , once the main dynamical characteristics of the human limb have been obtained.

The internal control loop consists of a position control loop. The actuator torques  $\mathbf{T}_e(t)$  depend on the deviation between the reference trajectories  $\mathbf{q}_a(t)$  and the observed trajectories  $\mathbf{q}_e(t)$ , which are obtained through the angle signal feedback branch.

Considering that this exoskeleton is aimed at assisting patients in rehabilitation therapy, it is valid to assume that the human muscle strength is small, at least at the very beginning of the therapy, and that the movements performed during training exercises are slow. Therefore, the variation of acceleration  $\Delta \ddot{\mathbf{q}}(t)$  should be small and neglectable. In such case, the target model expressed in Equation (4.34) is reduced to:

$$\begin{cases} \tilde{\mathbf{T}}_h(t) = \mathbf{B}_d \Delta \dot{\mathbf{q}}(t) + \mathbf{K}_d \Delta \mathbf{q}(t) \\ \Delta \mathbf{q}(t) = \mathbf{q}_a(t) - \mathbf{q}_d(t) \end{cases} \quad (4.35)$$

and the admittance function in frequency domain becomes:

$$Y(s) = \frac{\Delta Q(s)}{\tilde{T}_h(s)} = \frac{1}{\mathbf{B}_d s + \mathbf{K}_d} \quad (4.36)$$

One of the results in section 3.5 is that during the test execution, human joint's stiffness and damping vary according to the intention of motion, and that having non-constant admittance model parameters being able to vary accordingly is paramount to obtain good performance. The strategy adopted in this experiment is similar, but it is based on the estimated voluntary human torque: for high values of  $\tilde{T}_h$ , the admittance model parameters should increase to increase training intensity and patient's active participation, while for low values of  $\tilde{T}_h$ , the admittance model parameters should be small to make easier to the user to move the exoskeleton, ensuring training safety and comfort. Intention of motion can be divided in intention to follow and intention to resist the pre-planned trajectories. For a single joint, this is equivalent to:

$$Intention = \begin{cases} \text{positive movement} \rightarrow \text{sign}(\tilde{T}_h(t)) = \text{sign}(\dot{q}_d(t)) \\ \text{negative movement} \rightarrow \text{sign}(\tilde{T}_h(t)) \neq \text{sign}(\dot{q}_d(t)) \end{cases} \quad (4.37)$$

$$B_v = \begin{cases} B_{p0} + \left| \frac{\tilde{T}_h(t)}{T_{id}(t)} \right| \alpha_p, & \text{for positive movement} \\ B_{n0} - \left| \frac{\tilde{T}_h(t)}{T_{id}(t)} \right| \alpha_n, & \text{for negative movement} \end{cases} \quad (4.38)$$

$$K_v = \begin{cases} K_{p0} + \left| \frac{\tilde{T}_h(t)}{T_{id}(t)} \right| \beta_p, & \text{for positive movement} \\ K_{n0} - \left| \frac{\tilde{T}_h(t)}{T_{id}(t)} \right| \beta_n, & \text{for negative movement} \end{cases} \quad (4.39)$$

where  $B_v$  and  $K_v$  are the actively used damping and stiffness values in the target model.  $B_{p0}$  and  $B_{n0}$  are the base damping for positive and negative movements. Parameters  $\alpha_p$  and  $\alpha_n$  are tuned manually to control  $B_v$ . Similar considerations can be made for parameters in the  $K_v$  formula.

Notice that Equation 4.37 is similar to the strategy to control virtual damping proposed in section 3.5. However, in this case, since acceleration contribution is neglected in the target model, it is not possible to consider the sign of the acceleration feedback signal and consider the different signs between the estimated voluntary torque and the planned velocity trajectory.

An important comment must be made on the neglectation of the target inertia matrix. In section 3.5 and section 3.4, it has been shown how the desired inertia influences the stability of the system and how the introduction of an acceleration feedback allows to decrease the constant lower bound in the desired inertia constraint.

In this case, however, the exoskeleton is not designed to compensate its own inertia or to display a particular behavior at the port of interaction. The importance of this article lays on the estimation of the voluntary torque based on dynamic signals, without exploiting EMG signals or other physiological signals, and how to use those signals to create an efficient admittance control for lower-limb rehabilitative exoskeleton.

Figure 4-7 shows the experimental results of tracking under variable admittance conditions. The peaks present in the negative movement regions are due to a decrease in admittance parameters to increase tracking error, in turn to decrease the interaction between the exoskeleton and the human, to protect the patient.

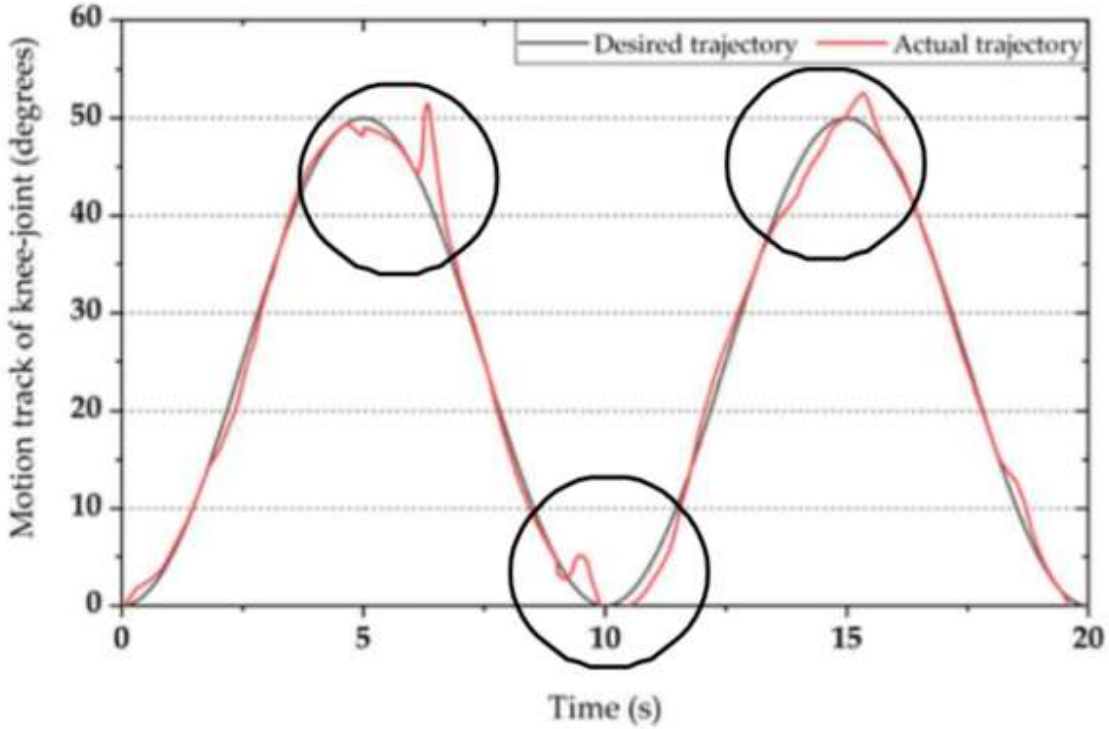


Figure 4-7: Experimental results of tracking under variable admittance conditions. Reprinted from [28].

However, the presented exoskeleton control strategy and the one presented in section 3.5 are not mutually exclusive. In fact, to improve patient's experience, it is possible to merge these two control strategies, in order to minimize the inertial behavior displayed by the machine at low frequencies.

### 4.2.3 Control system based on emulated inertia compensation

In article [21], it is presented a control strategy able to merge the aforementioned ones for a 2-DOF lightweight exoskeleton. The control scheme is reported in Figure 4-8.

The control algorithm is composed of three sections: the target admittance model, the exoskeleton's assistive torque generation based on adaptive frequency oscillator, and the emulated inertia compensation. The input signals are the interaction torques vector  $\tau_i$  and the computed assistive torques vector  $\tau_a$  generated by the inertia compensator. The sum of these two signal forms the input of the virtual admittance, which is used to generate the reference joint angle trajectories vector  $\mathbf{q}_{ref}(t)$ :

$$\mathbf{q}_{ref}(t) = \begin{bmatrix} \int \boldsymbol{\theta}(t) dt \\ \boldsymbol{\theta}(t) \\ \dot{\boldsymbol{\theta}}(t) \end{bmatrix} \quad (4.40)$$

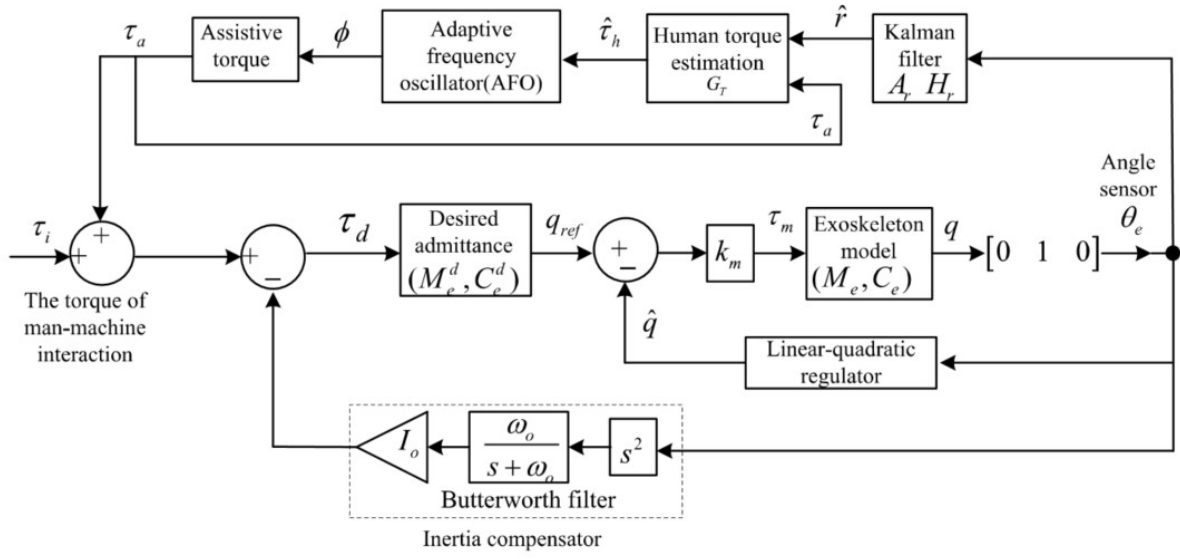


Figure 4-8: Block diagram of the control scheme for lower-limb rehabilitation exoskeleton based on emulated inertia compensation and AFO. Reprinted from [21].

posing  $\theta(t)$  the angle of the exoskeleton leg. The integral of the joint angle is used to ensure zero steady-state tracking error. The reference trajectories are then tracked by using an LQ regulator, and the angular position of the exoskeleton is measured by an encoder.

The admittance model is described as an LTI state-space representation of a third-order state equation, discretized via the Euler method. It is described as follows:

$$\mathbf{q}_{ref}(k) = \mathbf{M}_e^d \mathbf{q}_{ref}(k-1) + \mathbf{C}_e^d \boldsymbol{\tau}_d(k) \quad (4.41)$$

with:

$$\mathbf{M}_e^d = \begin{bmatrix} 1 & T & 0 \\ 0 & 1 & T \\ 0 & -\frac{k_e^d}{I_e^d} T & \left(1 - \frac{b_e^d}{I_e^d} T\right) \end{bmatrix}, \mathbf{C}_e^d = \begin{bmatrix} 0 \\ 0 \\ \frac{1}{I_e^d} T \end{bmatrix}$$

where  $T$  is the sampling period,  $k_e^d$  is the desired stiffness,  $b_e^d$  is the desired damping, and  $I_e^d$  is the desired moment of inertia.

The angle tracking with proportional control is expressed as:

$$\boldsymbol{\tau}_m = k_m (\mathbf{q}_{ref} - \hat{\mathbf{q}}) \quad (4.42)$$

where  $\hat{\mathbf{q}}$  is the state estimate generated by the LQR as it follows:

$$\hat{\mathbf{q}} = f(\mathbf{q}(t), \boldsymbol{\tau}_m(t)) \quad (4.43)$$

being  $\mathbf{q}(t)$  the measured angular position obtained through the encoder.

The estimation of the human voluntary torque is based on the measured angular position, linearized and filter through a Kalman filter, and the assistive torque computed the previous sampling instant. The actual

operative principle lies outside the context of this example. The adaptive frequency oscillator is a structure able to derive the phase  $\phi$  of the net estimated human torque  $\hat{\tau}_h$ , obtained as follows:

$$\begin{aligned}\hat{\tau}_h &= G_T \hat{\tau}_k - \tau_a = \\ &= \begin{bmatrix} k_h + k_e^d & 0 & 0 \\ 0 & b_h + b_e^d & 0 \\ 0 & 0 & I_h + I_e^d \end{bmatrix} \hat{\tau}_k - \tau_a\end{aligned}\quad (4.44)$$

The assistive torque  $\tau_a$  then computed as follows:

$$\tau_a = \tau_{a,0} \cos\phi \quad (4.45)$$

where  $\tau_{a,0}$  is a selected amplitude value.

The inertia compensator has the same structure of the one presented in section 3.5. The angular acceleration is fed back to a Butterworth low-pass filter with a suitable cutoff frequency  $\omega_0$ . Then it is multiplied by the constant negative inertia gain  $I_0$ , used to mask the inertial behavior of the exoskeleton at low frequencies. The transfer function of the inertia compensator is expressed as:

$$H_i = \frac{I_0 \omega_0 s}{s + \omega_0} \quad (4.46)$$

## 4.3 Transparent control applied to exoskeleton devices

I think it is necessary to make a little preamble related to “transparent control” in the context of robotic exoskeletons. Transparent control is a poorly researched argument and if the readers would search it online, they will find only few articles, of which just two will treat directly the problem posed by transparent control for exoskeletons: document [30], that is a European project now concluded with the purpose to develop a lightweight exoskeleton controlled by a state controller, able to ensure the robot’s haptic imperceptibility to the human in normal operating condition, and to provide an assistive torque in case of external perturbations aimed at reducing and losing postural balance, and document about the ABLE exoskeleton presented in section 3.1 [4].

Transparent control is a joint operating mode aimed at rendering the exoskeleton imperceptible to the human, ideally by eliminating, practically by minimizing the interaction forces exchanged between the two coupled systems at the attachment points responsible of haptic sensations while the wearer performs movements in completing a task. Haptic sensations (see Appendix C for more details) are produced by the interacting forces, meaning that the human wearer feels the exoskeleton’s main dynamics, such as the inertia of the exoskeleton, which can hinder natural movements and reduce the range of possible motions. In other words, “transparency in the ability to follow human motions with no delays” [30]. The goal of this exoskeleton control strategy is to create a continuous operating state in which the robot is invisible to the user, avoids hindering user’s movements, and ensures large freedom of movement. When a state transition condition is verified, that means when assistance is needed, for instance, the initial phase of falling is detected, the loss of postural balance is detected, or just even the patient is not performing correctly the rehabilitation exercise, the exoskeleton should abandon gradually the transparent state to enter a more proper cooperative or tutoring state, respectively, helping or imposing to the patient a movement to minimize the transient condition value, and the real-world risk associated to it, to return in transparent state.

This case of cooperative control can be implemented for power augmentation exoskeletons, to leave the freest range of motion to the healthy user, but also in rehabilitation exoskeletons, to let the patient train specific joints or a single joint, expanding in this way the range of possible recovery therapies. Transparent control is adopted also in those applications based on reproducing human motion with minimum delay, such as in haptic and virtual reality (VR) applications.

To eliminate the robotic induced haptic sensations, i.e., tactile sensations, the port of interaction should manifest a low impedance behavior, ideally zero impedance, or equivalently, high admittance behavior, ideally infinite admittance.

The control strategy presented in section 3.5 can be remodeled on the basis posed by ABLE (section 3.1) to make the actuators torques cancel the robot dynamics, zeroing the interaction torques.

Another strategy has been used to control LOPES II in European project “Balance” [30]. The adopted method is based on a non-human model, meaning it is not required to collect physiological signals, nor human muscle models are employed. Conversely, it is based on measuring human motion accelerations, by means of high-performance, low-noise, and low-delay IMUs attached to the human’s limbs or feet and using these signals as references for the robot real-time controller.

Historically, acceleration sensors have been severely prone to noise and scarcely adopted. However, there are four reasons behind the exploiting of IMUs in this project. First, the important jump ahead in IMUs development, which resulted in producing reliable high-performance sensors. Second, the filtering-based

single or double differentiation of velocity or position signal, respectively, amplify analog and quantization noise, add delays in measurements, and limit the bandwidth. Third, it has been proved in sections 3.4 and 3.5 that an additional acceleration feedback is useful in compensating for inertial dynamical effects of the exoskeleton. Fourth, IMUs have low impact on robot design, conversely to force (torque) sensors, and are not time consuming or impractical as EMG-based technology in measuring the desired signals.

The main aspect of the transparent control strategy developed in the following is that uses the second order time-derivative of the interaction force,  $\ddot{f}_i = \frac{d^2}{dt^2}(f_i)$ , as state variable.

In section 3.5, the exoskeleton and the human were coupled by means of a rigid ankle brace, modeled as a rigid coupling connection. Practically, instead, due to the presence of a cuff in plastic or other lightweight and comfortable materials on the robot side, and the muscle and the fat tissue at the human side of the connection, it is more adequate to model the coupling element at least as an elastic attachment, as in [30], or a parallel of spring and damper as shown previously in sections 4.2.1 and 4.2.2.

To avoid some rocks in the journey to present the transparent control, consider the 1-DOF lumped parameter model used many times in the course of this Thesis project. Both human and robot's inertias are simplified in lumped masses,  $m_h$  and  $m_r$ , respectively, the coupling element is purely elastic, modeled with a spring with stiffness  $k_a$ , responsible of the generation of the force of interaction  $f_i$ . The human net muscle force acting on the human inertia is  $f_h$ , while the robot force  $f_r$  is the amount of force at the output of the actuator and transmission drive system.

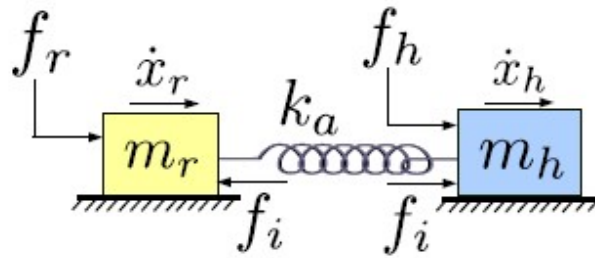


Figure 4-9: Simplified lumped-parameter linear 1-DOF model of the human-exoskeleton coupling, to highlight the main dynamics in the transparent control problem. Reprinted from [30].

The equations of motion of the coupled system in Figure 4-9 are the following (omitting time variable  $t$  for reading simplicity):

$$f_r - f_i = m_r \ddot{x}_r \quad (4.47)$$

$$f_i = k_a(x_r - x_h) \quad (4.48a)$$

$$\ddot{f}_i = k_a(\ddot{x}_r - \ddot{x}_h) \quad (4.48b)$$

$$f_h + f_i = m_h \ddot{x}_h \quad (4.49)$$

The combination of the second order time-derivative of the interference force (4.48b) and (4.47) allows to define the dynamical equation of the interaction force:

$$m_r \ddot{f}_i + k_a f_i = k_a(f_r - m_r \ddot{x}_h) \quad (4.50)$$

In Figure 4-10, it is presented the open-loop block diagram describing the dynamics of the coupled system. The control variable is the robot force,  $f_r$ , the state variable is the interaction force,  $f_i$ , and  $m_r\ddot{x}_h$  represents a hybrid disturbance input dependent on both the robot inertia and the human acceleration.

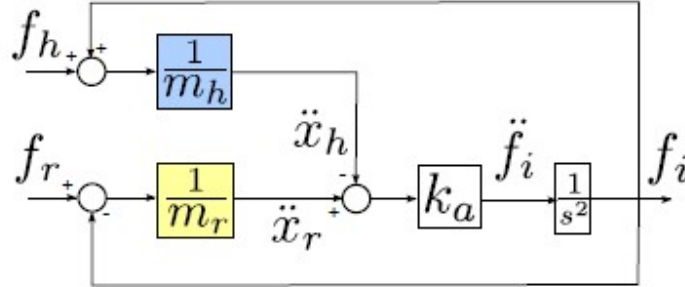


Figure 4-10: Block diagram of the model in Figure 4-9.

Notice that  $f_i$  is naturally fed back into the system.

The objective of transparent control is to ensure that  $f_i$  converges to zero within a small settling time.

The human disturbance input can mar the interaction force control performance and cannot be compensated by a feedback controller. Thus, it is important to introduce a feedforward controller to perform an a-priori compensation for this term. The controller should provide a compensation force:

$$f_{r_{ff}} = m_r \ddot{x}_h \quad (4.51)$$

In Figure 4-10, it is required to know the inverse dynamics of the robot, while the feedforward command requires to know the direct dynamics of the robot. It is also necessary to measure the human acceleration. The addition of this compensation results in the interaction force dynamics becoming human-independent, which improves the versatility of the controller.

Thus, expressing the robot force as  $f_r = f_{r_{ff}} + u = m_r \ddot{x}_h + u$ , and assuming no sensor error, once transposed in frequency domain via Laplace transform, Equation (4.50) becomes:

$$\left( \frac{m_r s^2}{k_a} + 1 \right) F_i(s) = U(s) \quad (4.52)$$

obtaining transfer function:

$$\frac{F_i(s)}{U(s)} = \frac{1}{\frac{m_r}{k_a} s^2 + 1} \quad (4.53)$$

Since there is no damping factor, the roots of the characteristic equation of Equation (4.53) are  $s = \pm \sqrt{-k_a/m_r}$ , and the system response would be purely oscillatory with frequency defined by the attachment's stiffness and the robot's inertia. To bring the interaction force to zero we need a feedback controller that is able to impose a convergent dynamics for the interaction force dynamics.

Such controller cannot be an impedance controller, since it cannot mask the robot inertia, leading to a situation in which the wearer must exert a muscle net force able not only to move their passive dynamics, but also drag the robotic structure's inertia.

It is possible to adopt two strategies to reach a transparent behavior. The first one is fairly pragmatic: employing a feedback controller that measures and regulates the interaction force  $f_i$ . The second one can be understood by taking a closer look to Equation (4.48b): the second order time-derivative of the interaction force is proportional to the difference between the human and robot accelerations. Thus, ensuring that  $\ddot{x}_h - \ddot{x}_r = 0$  will produce  $\ddot{f}_i = 0$ , and by integration, posing zero initial condition, will result  $\dot{f}_i = f_i = 0$ .

The first one is not easy to implement since it relies on force (torque) sensors, which are voluminous and difficult to mount at the port of interaction. In the assumption that there are no sensor's distortions on the interactive force measured signal, it is possible to implement a proportional-derivative feedback controller in addition to the feedforward one:

$$f_r = f_{r_{ff}} + k_p(f_{i_{des}} - f_i) + k_D(\dot{f}_{i_{des}} - \dot{f}_i) \quad (4.54)$$

where  $f_{i_{des}}$  is the desired interaction force, i.e., constant zero, and  $k_p$  and  $k_D$  are the proportional and derivative gain, respectively.

Set  $f_{i_{des}} = 0, \dot{f}_{i_{des}} = 0$ , the roots of the characteristic equation are:

$$s = \frac{-k_a k_D \pm \sqrt{(k_a k_D)^2 - 4m_r k_a (1 + k_p)}}{2m_r} \quad (4.55)$$

The proportional gain  $k_p$  can be designed to produce a critically damped response, while  $k_D$  can be designed to meet the desired settling time.

The acceleration feedback controller needs a second acceleration sensor to measure the robot acceleration  $\ddot{x}_r$ . In general terms, embedding an IMU on an exoskeleton is an easier job than embedding a force sensor. The feedback controller should be of the proportional-integral type, and the human acceleration  $\ddot{x}_h$  should be employed as reference signal:

$$f_r = f_{r_{ff}} + k_p(\ddot{x}_h - \ddot{x}_r) + k_D(\dot{x}_h - \dot{x}_r) \quad (4.56)$$

The roots of the characteristic equation are:

$$s = \frac{-k_l \pm \sqrt{k_l^2 - 4(m_r + k_p)k_a}}{2(m_r + k_p)} \quad (4.57)$$

Gains  $k_p$  and  $k_l$  can be designed to produce the desired convergent dynamics of the interaction force.

Intuitively, the basis of the second strategy is that two systems coupled by an elastic element will not generate any relative acceleration, hence any interaction force dynamics, if they move in the same way. In addition, it can be shown [30] that the phase shift between the acceleration signals affects performance more intensively than the magnitude difference. Hence, it is paramount to ensure the synchronism of the two coupled systems.

The equation of motion of the considered coupled human/robot system in joint space can be described as:

$$\mathbf{M}(\mathbf{q})\ddot{\mathbf{q}} + \mathbf{h}(\mathbf{q}, \dot{\mathbf{q}}) = \mathbf{S}^T \boldsymbol{\tau} + \mathbf{J}_c^T \boldsymbol{\lambda} + \mathbf{J}_a^T \mathbf{f}_i \quad (4.58)$$

where  $\mathbf{q}$  is the vector of joint positions,  $\mathbf{M}(\mathbf{q})$  is the inertia matrix,  $\mathbf{h}(\mathbf{q}, \dot{\mathbf{q}})$  is the Coriolis, centripetal, and gravity forces vector,  $\mathbf{S}^T$  is the robot actuated joint selection matrix,  $\boldsymbol{\tau}$  is the robot actuator torque command vector,  $\mathbf{J}_c^T$  is the transpose of the Jacobian matrix of linearly independent constraint,  $\boldsymbol{\lambda}$  is the linearly independent constraint forces vector,  $\mathbf{J}_a^T$  is the Jacobian matrix of the attachment point  $\mathbf{x}_r$ , and  $\mathbf{f}_i$

is the interaction forces vector.

The robot actuated joint selection matrix  $\mathbf{S}^T$  allows to choose which joints will be actuated and which joints will be left passive. Differently to what explained in section 3.3, in this case it is considered also the vector of force constraints  $\boldsymbol{\lambda}$  in addition to the contact point forces vector  $\mathbf{f}_i$ , to consider eventual constraint imposed by the environment (not the human).

The interaction forces vector is expressed in Cartesian coordinates:

$$\mathbf{f}_i = k_{att}(\mathbf{x}_r - \mathbf{x}_h) \quad (4.59)$$

As already mentioned, probably the reader already expects this part, it is important to investigate the stability and performance limits of the transparent controller. The analysis will be focused on the low-frequency range, since major of human movements and human/robot coupled movements happen in the low-frequency range.

Expand the model depicted in Figure 4-9 by considering also the actuator and the transmission dynamics (Figure 4-11), characterized by stiffness  $k_t$ , actuator mass  $m_a$ , and dissipative effect  $b_r$ , and the human limb's impedance, characterized by variable stiffness  $k_h$  and variable damping  $b_h$ . The block diagram for a generic actuator acting on a wearable robot (blue) coupled to a human limb (red) is reported in Figure 4-12. Notice as the interaction force  $f_i$  couples the systems dynamics in series through an internal feedback connection.

The transfer function  $F_r(s)/\dot{X}_a(s)$  has a numerator of order 4 and a denominator of order 5. Considering an additional second order dynamics with gain 1 for the actuator velocity, representing the transfer function between the actuator's output velocity,  $\dot{X}_a(s)$ , and the actuator's input voltage or current,  $U_a(s)$ , the denominator of the total transfer function  $F_r(s)/U_a(s)$  has order seven.

Figure 4-13 shows the frequency response of the open-loop transfer function  $F_r(s)/U_a(s)$  for an independent robot, not attached to the human, and a wearable robot. At low frequencies, frequencies of interest for human movements, due to the resonance/antiresonance pair introduced by the coupling element, there is a severe phase drop for the wearable robot, causing an increase in sensitivity of the closed-loop system at low frequency, threatening the coupled system instability. The integrator action present in the coupled system is produced by the variable human stiffness  $k_h$ , resulting in a linear increase of the robot force  $f_r$  when the robot removes the human from its reference position. The resonance at high frequencies is due to the transmission dynamics for both cases, due primarily to the transmission stiffness  $k_t$  and the robot mass  $m_r$ . Fortunately, that frequency range is far above the bandwidth of interest.

To achieve fast convergence time and good closed-loop force tracking performance, it is important to compensate for the natural velocity feedback present in force dynamics. A successful strategy used in high-performance torque-controlled robot that helps in increasing the bandwidth of the controlled is to measure and continuously provide through a feedforward branch an extra velocity term through the actuator,  $\dot{x}_{ex} = \dot{x}_r$ , such that the robotic force dynamics becomes:

$$\dot{f}_r = k_t((\dot{x}_a + \dot{x}_{ex}) - \dot{x}_r) = k_t\dot{x}_a \quad (4.60)$$

being  $\dot{x}_a$  the actuator's output velocity.

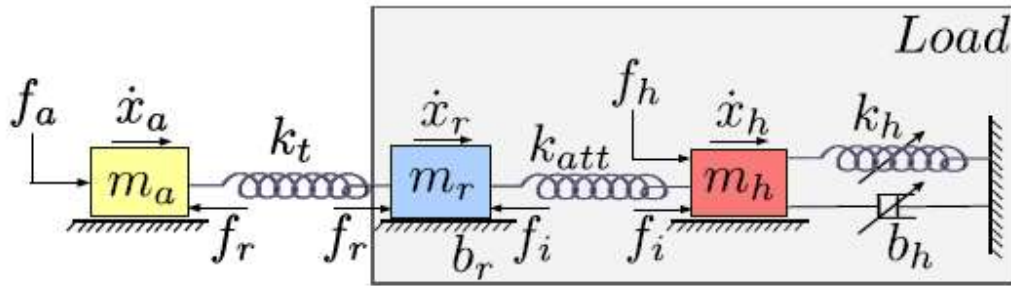


Figure 4-11: Expanded schematic of the simplified model in Figure 4-9, introducing the motor and transmission dynamics (haptic components). The human limb's dynamics is modeled as a variable impedance. Reprinted from [30].

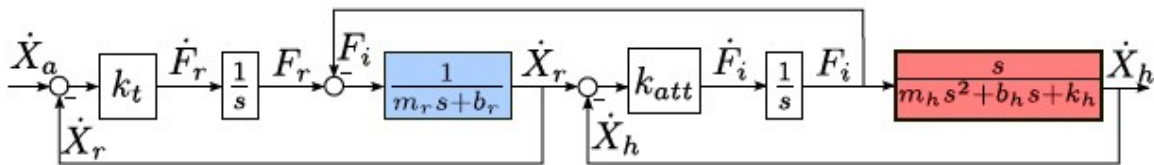


Figure 4-12: Block diagram describing the model presented in Figure 4-11 in Laplace domain. The considered input is the actuator velocity, the considered output the human limb velocity. Reprinted from [30].

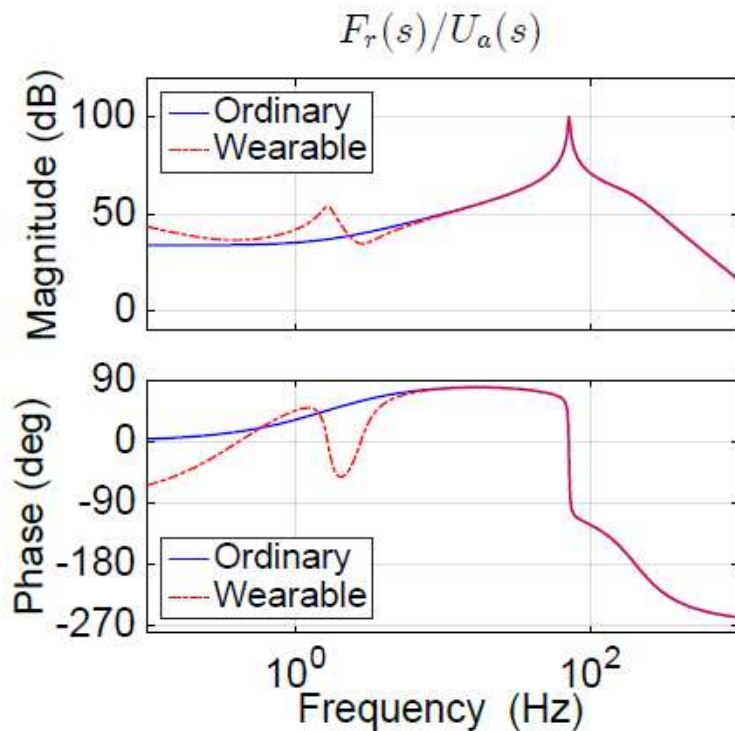


Figure 4-13: Comparison between the plant frequency response of an ordinary bipedal robot and an exoskeleton. Reprinted from [30].

To analyze the effects of the new feedforward compensation strategy on coupled systems, which tend to become unstable at low frequencies when subjected to external disturbances, it is useful to perform a sensitivity analysis comparing stand-alone feedback controller and the controller with the additional feedforward velocity compensation.

The sensitivity transfer function is the closed-loop transfer function mapping the external disturbances  $D(s)$  to the robot force  $F_r(s)$ , and the force reference  $F_{r_{ref}}(s)$  to the tracking error  $e(s) = F_{r_{ref}}(s) - F_r(s)$ :

$$S(s) = \frac{1}{1 + L(s)} = \frac{F_r(s)}{D(s)} = \frac{e(s)}{F_{r_{ref}}(s)} \quad (4.61)$$

being  $L(s) = C(s)(F_r(s)/U_a(s))$  the loop gain, with  $C(s)$  being the controller's transfer function. The ideal sensitivity function  $S(s)$  should be low at the frequencies of interest, indicating a good disturbance rejection capability and low tracking error, while it should high at higher frequencies to attenuate sensor noise.

The peak of the sensitivity function  $S(s)$  is a reliable indicator of relative stability: larger the peak, the closer to instability.

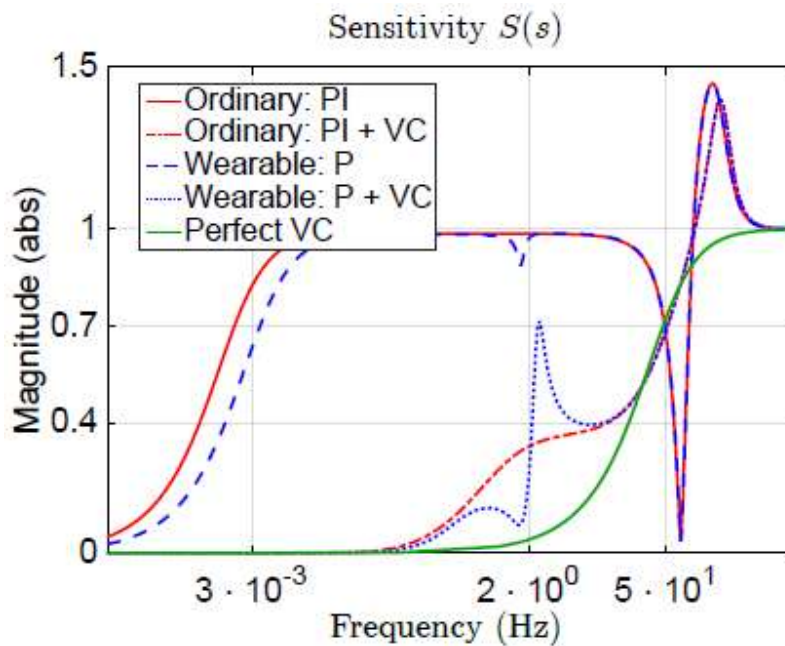


Figure 4-14: Magnitude comparison of the sensitivity function for an ordinary bipedal robot and an exoskeleton under different control conditions. Reprinted from [30]

Figure 4-14 shows that, for the used values of robot and human' dynamical characteristics and for the actuator dynamics, the velocity compensator increase the bandwidth of about 4 orders of magnitude, and in the case of the coupled system,  $S(s)$  has a dent around the human/robot attachment natural frequency, due to the resonance/antiresonance pairs introduced by the attachment, meaning the system is less robust against disturbances and system variations in that neighborhood. It has been showed in other tests [30], that the more rigid the attachment is, i.e., higher  $k_{att}$ , the higher the sensitivity gets in that neighborhood.

To solve this problem, it is possible to implement a notch filter aimed at minimizing the attachment stiffness effect at that frequency. Use complex conjugate zeros to attract the lightly damped frequency poles. Compensating for the dent at the attachment frequency pushes the sensitivity peak around the actuator frequency, at high frequencies where the robot does not operate, hence, out the range of frequencies of interest. This effect is unavoidable and is called waterbed effect, since similar to the surface of a waterbed, when something pushes on a side, the other side will form a hill due to the change in volume displacement.

A second filter is applied to the feedforward path only to minimize the effects of the actuator's dynamics. It has as natural frequency twice the natural frequency of the actuator,  $\omega_a$ , and complex zeros around  $\omega_a$ . The obtained sensitivity attenuation in the middle frequencies will not degrade the sensitivity peak (Figure 4-15).

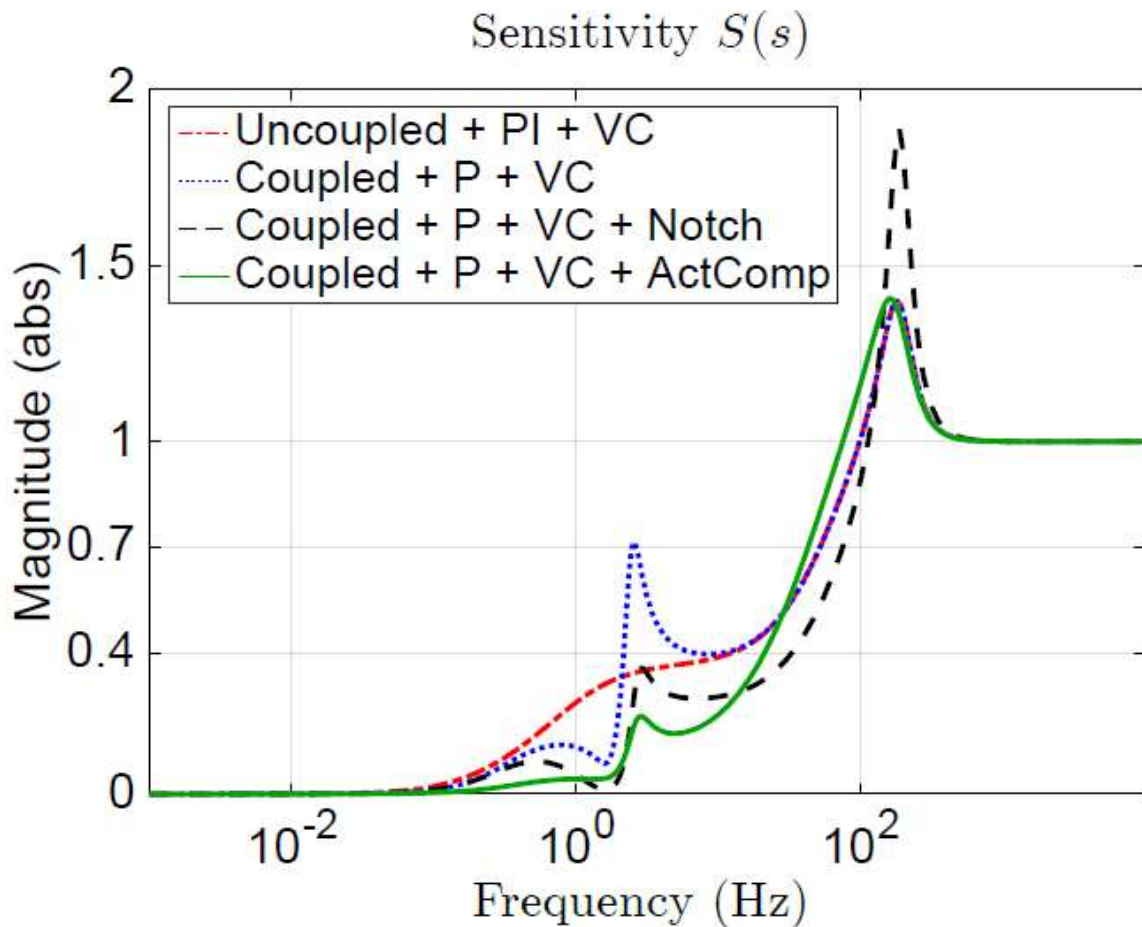


Figure 4-15: Plot of the magnitude of the sensitivity function for an ordinary bipedal robot and an exoskeleton, considering the proposed corrections. Reprinted from [30].

In conclusion, to ensure transparency the exoskeleton must be able to follow human motions, human accelerations without delays: the accelerations of the robot and the human may not be equal in intensity but must be in phase. To achieve this result, it is paramount to reduce the apparent inertia of the robot, i.e., the inertia felt by the user. From a hardware point of view, it is important to design lightweight robot links, although this implies a tradeoff between power and weight: lower the weight, the lower the admissible maximum torque values. From a software point of view, it is important to design an interaction controller able to reduce the robot inertia at the port of interaction and that is able to generate torque command to mimic the human action. To achieve this, it is paramount to have the most accurate model of the robot, since the more accurate, the better the human acceleration tracking, and to have low delays in measuring and filtering the robot and human' accelerations.

## 4.4 Mixed control: tutoring-coordination-cooperation

Mixed control is an exoskeleton control strategy in which the user has a certain degree of control authority over the coupled exoskeleton/human system, therefore the wearer will be to control one or more postural tasks through some joints left passive by the exoskeleton, while the robot will perform the remaining and complementary tasks. According to the amount of user's control authority in the coupled exoskeleton/human system, it is possible to verify three different mixed control conditions: tutoring, cooperation, and coordination.

Tutoring identifies the mixed control condition in which the robot has full control over the task, without necessity of wearer intervention, basically imposing the pre-generated motion trajectories to the entire human-exoskeleton systems. This strategy can be adopted by power augmentation exoskeletons when the human muscle is not able to generate torque at all. These devices are targeted to help people suffering from severe motion disorders or limb paralysis.

Cooperation identifies the mixed control condition in which the wearer has partial control authority over the tasks by controlling one or more joints, left passive by the robot controller. The tasks are performed partially by the human and the exoskeleton. The control purpose is to obtain partial compliance to human motion without degrading its performance.

Coordination identifies the mixed control condition in which the wearer has almost full control authority over the tasks to be performed by controlling several joints of the coupled system. The control purpose is to ensure transparency to avoid motion hindering, and to performing other tasks, generally left to the exoskeleton's control, and to be ready to intervene when dangerous situations arise.

The aforementioned control strategies and the possibility to switch from to another is particularly appealing to exoskeleton designer, especially in the rehabilitation field. In fact, leaving to the physiotherapist the responsibility to set the level of transparency according to the patient's recovery level [31], or being able to set a different control strategy when assistance is needed, will be the first approach to a desired level of flexibility long searched in this engineering sector and for daily-life exoskeleton companion devices. However, due to hardware design, unavoidable cost increase, and software limitations related to such level of flexibility, many researchers [29] are yet not convinced the research has reached solidly such results.

In [31], Professors Menga and Ghirardi have presented a first control strategy able to leave the level of transparency  $\beta \in [0; 1]$  of exoskeleton presented in section 4.1 as degree-of-freedom suitably tuned by the physiotherapist, according to the patient's progresses in the rehabilitation therapy. In case of:

- $\beta = 0$  the exoskeleton's controller is in tutoring mode, the exoskeleton imposes the movement to the user, hence, they will perceive the exoskeleton as stiff.
- $0 < \beta < 1$  the exoskeleton's controller is in cooperation mode;
- $\beta = 1$  the exoskeleton's controller is in coordination mode, the exoskeleton is in transparent operating mode, completely compliant to the user's motion.

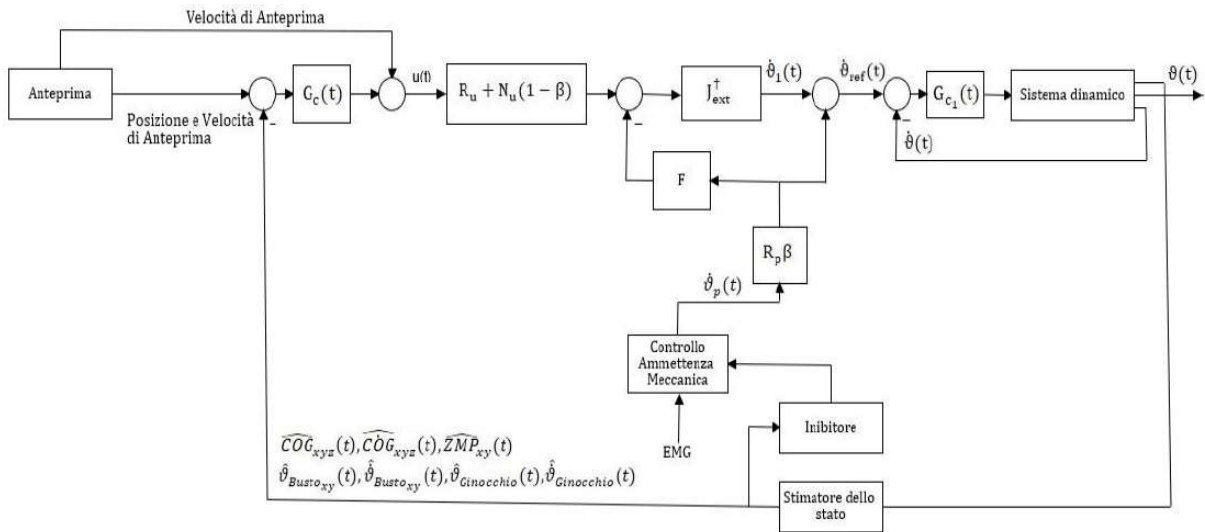


Figure 4-16: Upgraded block diagram of the control scheme presented in Figure 4-2 that allows tunable level of joint transparency.

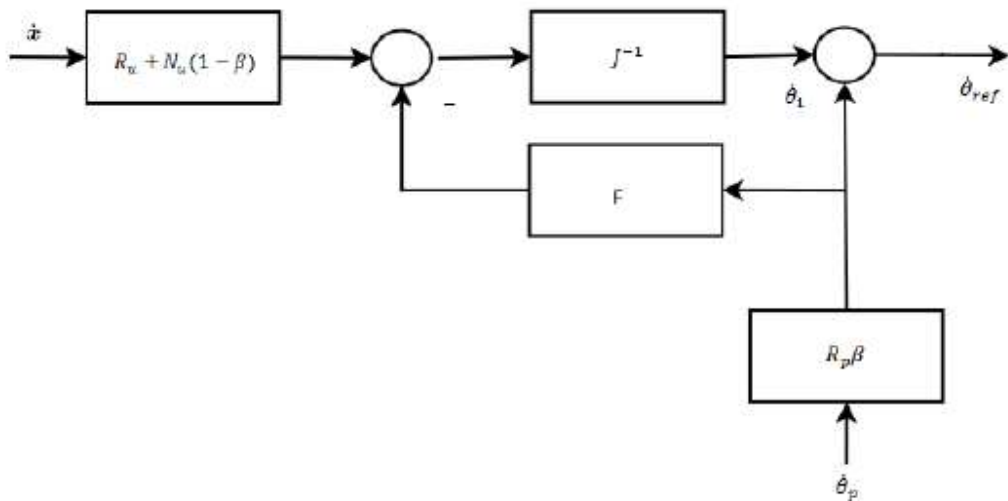


Figure 4-17: Detail of the branch responsible for a tunable level of joint transparency

Figure 4-16 shows the upgraded and expanded control scheme to achieve mixed control through the blocks presented in Figure 4-17.

The inputs to the mixed control block are:

- $u(t)$ : the command vector to identify univocally the posture and the movement of the coupled system.

$$u(t) = \begin{bmatrix} u_{COG_i} \\ u_{COG_x} \\ u_{trunk_j} \end{bmatrix}; \quad i = x, y; \quad j = x, y \quad (4.62)$$

- $\dot{\theta}_p(t)$ : joint velocities vector consequently to the user's torque.

$$\dot{\theta}_p(t) = \begin{bmatrix} \dot{\theta}_{ankle_{p_i}} \\ \dot{\theta}_{knee_{p_i}} \\ \dot{\theta}_{hip_{p_i}} \end{bmatrix}; \quad i = x, y; \quad (4.63)$$

The output of the mixed control block is  $\dot{\theta}_{ref}$ , i.e., the reference joint velocities vector:

$$\dot{\theta}_{ref}(t) = \begin{bmatrix} \dot{\theta}_{ref_{ankle_i}} \\ \dot{\theta}_{ref_{knee_i}} \\ \dot{\theta}_{ref_{hip_i}} \end{bmatrix}; \quad i = x, y; \quad (4.64)$$

$R_u$  is the 3-by-3 diagonal matrix used to select which tasks are performed exclusively by the automatic postural cycle. In case of selected task, on the correspondent position on the diagonal there will be a 1, otherwise 0.

$N_u$  is the nullspace of  $R_u$ , which indicates which tasks are left to the user to be controlled.

$$N_u = I - R_u \quad (4.65)$$

Such tasks can be partially or fully controlled by the patient through the joints selected in the range of 3-by-3 diagonal matrix  $R_p$ .  $N_p$  is the nullspace of  $R_p$ , indicating which tasks are not controlled by the patient. It is defined as  $N_u$ , with  $R_p$  instead of  $R_u$ .

The general expression for the references of the speed control of the actuators is, then, given by:

$$\dot{\theta}_{ref}(t) = J^{-1}u_p(t) + \beta R_p \dot{\theta}_p(t) \quad (4.66)$$

$$u_p = (R_u + N_u(1 - \beta))u - \beta FR_p \dot{\theta}_p \quad (4.67)$$

with  $F = R_u J$ , and condition

$$range(N_u) \subset range(JR_p) \quad (4.68)$$

In the limit case represented by user's full authority control over the coupled system, it follows:

$$N_u = R_p = I \quad (4.69)$$

$$\beta = 1 \quad (4.70)$$

# Chapter 5

## Conclusions

This Thesis project presented some control strategies applied to lower-limb rehabilitation active robotic exoskeleton. It proceeded by presenting the context of rehabilitation exoskeleton and the main exponents in the field, then provided the necessary theoretical background required to completely understand the exoskeleton control problem, and finally provided some control strategies to monitor and recover postural balance based on EMG, motion, and force signals, and to provide patient compliance without having to rely on human-based model. It also focused on a poorly researched aspect, namely transparent control, whose potential, instead, would be of paramount importance for commercial aspects and to present the robotic exoskeletons as daily-life companions and helpers.

However, exoskeleton control design is still in its infancy, due to the hardware and software design complexities, that make difficult to be able to design a product able to satisfy flexibility, user safety, performance, and ergonomics.

The secondary objective of this Thesis is to be a useful guide to every engineering student that approaches for the first time the vast world of exoskeletons, providing simple but precise theoretical background and some useful well-analyzed application examples.

The third objective was to satisfy a personal interest, curiosity, and to test myself, diving in the biomedic/assistive field of Robotics, which is an application environment that has been more or less neglected during the Course of Mechatronic Engineering, focusing mainly on Robotics for industrial purposes.

## Future works

Future projects consist of simulating a state controller able to ensure transparent operative mode as normal operative mode but being able to provide more or less aggressive intervention in case of detected risks, such as risk of falling.

In addition, it should be investigated the application of machine learning and artificial intelligence algorithms to estimate the characteristics of the dynamics of both the human and the exoskeleton, and to be able to manipulate in real-time the values of the target admittance parameter in order to obtain the optimal values to ensure the mission of the robot.

# Appendix

## Appendix A: Fundamentals of bipedal locomotion control

### A1. Support Polygon

The support polygon is a 2D or 3D convex polygon defined by the foot/feet-ground contact points. As hinted by the Figure A-1, in single-stance, when the biped robot structure is supported by one single leg, and only one foot is in contact with the ground, the support polygon corresponds to the area of the foot sole in touch with the floor. In double-stance, when the biped robot structure's weight is borne by both legs, both the feet are in contact with the terrain, the support polygon corresponds to the area of the feet soles and the area between them.

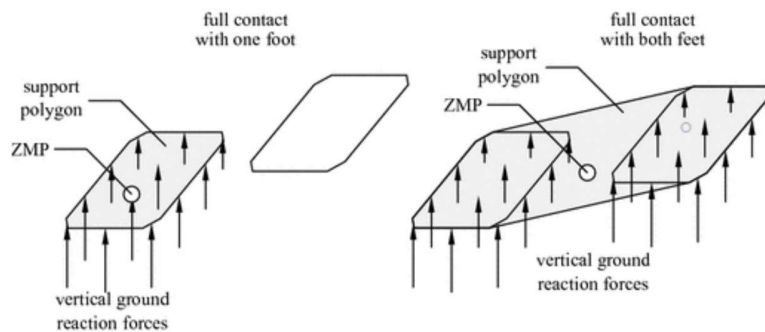


Figure A-1: Support polygon in single stance (on the left) and double stance (on the right)

### A2. Center of Pressure

As the load pressure exerted by the foot on the ground has the same sign, the distributed force can be reduced to a single resultant ground force reaction, whose acting point must be contained within the support polygon edge. The acting point is termed Center of Pressure (CoP).

### A3. Zero-Moment Point (ZMP): theory and stability criterion

The research about biped locomotion finds its roots in Yugoslavian professor Vukobratovic and Juricic' pioneering work [32]. The proposed method for gait synthesis (called semi-inverse method) based on ZMP was the fundamental boost for the development of gait planning and control for stable biped artificial work, despite of the limitation that the motion can be synthesized only for as many joints as the zero-moment conditions can be preset. [33].

Biped walking can be decomposed into two different phases, periodically alternating, characterized by different constraints and, consequently, by different stability conditions: the double-stance support phase and the single-stance support phase. The statically *stable* double-support phase is the phase of the gait during which the weight of the whole mechanism is supported simultaneously on both feet in contact with the ground or reacting surface, creating in that way a closed kinematic chain robot's mechanism-ground.

The foot-ground contact can be considered as an additional passive joint. The statically *unstable* single-support phase is the phase of the gait during which only one leg bears the weight of the entire structure, only one foot is in contact with the ground while the other is in air to perform a step, moving from the rear to front position. Having a “flying” foot let the robot’s structure and the ground create an open kinematic chain.

A robotic leg resembles a human leg. It presents three segments (or links), the thigh, the tibia or shin, and the foot. These three links are connected by three joints, the hip joint, the knee joint, and the ankle joint. In theoretical literature, for detailed analysis and simulation purposes, the hip and the ankle joints are generally 3-DOF spherical joints, while the knee joint is simply a 1-DOF rotoidal joint. In more practical applications, it is possible to reduce the redundancy of the leg’s mechanisms maintaining a good degree of model accuracy. The simplest mechanism is composed by three 1-DOF rotoidal joints.

The foot structure can be further decomposed into three main functional structures, the heel, the sole, and the toes. The heel is the first part of the foot that enters in contact with the ground during a step, while the toes are the last. When the foot is leaving the ground, the toes cannot provide enough support to the entire structure, thus, postural equilibrium is based on the position of the ZMP within a double-stance support polygon, whose dimensions depend on the acceleration of the center of mass and the ability to predict the position of the future landing foothold.

The foot itself can be controlled only indirectly, by commanding a suitable dynamic of the mechanism above it. Therefore, the overall indicator of the mechanism behavior must reside in the point of the sole where the resultant of all the forces can be applied. This specific point was termed Zero-(tilting) Moment Point (or, shortly, ZMP).

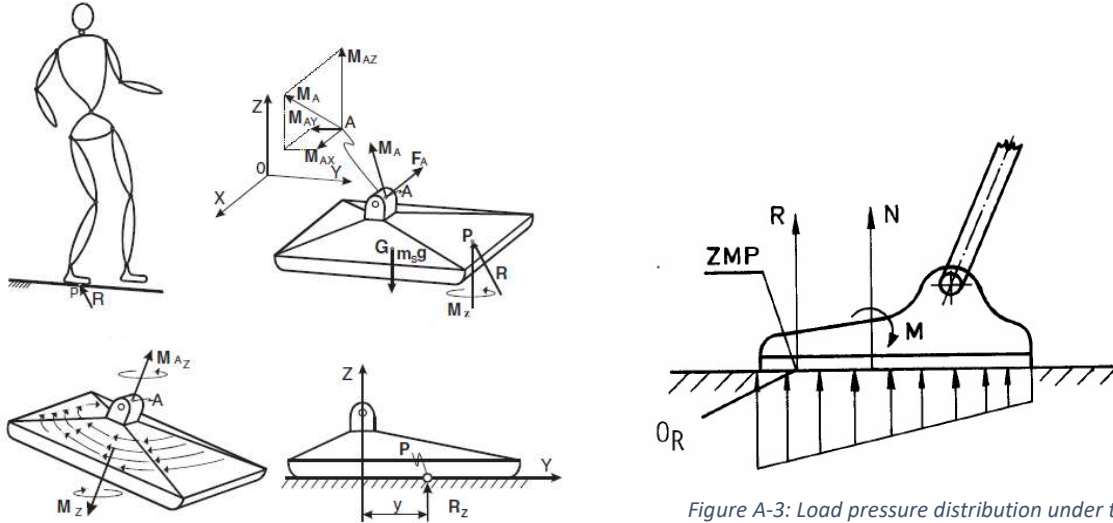


Figure A-3: Load pressure distribution under the supporting foot.

Reprinted from [33].

### A3.1. The ZMP Notion

Let the author point out the most important task demanded to a legged robot during gait is to keep postural balance, which can be achieved by ensuring that the whole foot's sole's area, not only the edge, is in contact with the reacting surface, from now on simply called the ground.

To start the analysis, consider a two-legged mechanism in single-stance, with the whole foot touching a horizontal flat surface (the "floor" or "ground") without slippery. For simplification purposes, replace the entire multichain above the ankle joint with a resulting force  $\mathbf{F}_A$  and momentum  $\mathbf{M}_A$  vectors, and place the reference frame  $O_{xyz}$  at the ground level.

Let bring our attention to the reaction force and moment generated by the floor. The load pressure under the foot has the same sign, therefore it is possible to reduce it into a resulting ground reaction acting at the Center of Pressure (CoP), marked as point  $P$ , within the boundary of the foot sole. Notice carefully that this is force that keeps the entire structure in equilibrium. The ground reaction can be modeled as a three-component force vector  $\mathbf{R} = [R_x, R_y, R_z]^T$  and momentum vector  $\mathbf{M} = [M_x, M_y, M_z]^T$ .

At rest, assuming no slippery, the foot and the ground exchange static friction forces at contact points, such as acting point  $P$ , and the floor will exert a normal reaction which is vertical along the  $z$ -axis, due to the unilateral nature of the contact. Therefore, the ground reaction force components can be rewritten as:

$$\mathbf{R} = \begin{bmatrix} R_x \\ R_y \\ R_z \end{bmatrix} = \begin{bmatrix} F_{fr_x} \\ F_{fr_y} \\ N \end{bmatrix} \quad (A1)$$

where the author indicated the friction forces acting on the horizontal plane as  $F_{fr_x}, F_{fr_y}$  and the reaction normal to the surface as  $N$ .

At rest, assuming no slippery, the foot cannot rotate along the  $x$ - and the  $y$ -axes, therefore the horizontal components of ground reaction moment  $\mathbf{M}$  are zero. Due to their nature, the vertical component of the reaction momentum,  $M_z$ , corresponds to the sum of the momenta given by the friction forces with respect to the origin of the reference system.

Let focus on the "foot system". The static equilibrium equations for the supporting foot are:

$$\mathbf{R} + \mathbf{F}_A + m\mathbf{g} = \mathbf{0} \quad (A2)$$

$$\overline{\mathbf{OP}} \times \mathbf{R} + \overline{\mathbf{OG}} \times m\mathbf{g} + \mathbf{M}_A + M_z + \overline{\mathbf{OA}} \times \mathbf{F}_A = \mathbf{0} \quad (A3)$$

Considering Equation (A2), on the horizontal plane  $xy$ , the components of the reaction force ( $\mathbf{R}$ ) <sup>$xy$</sup> , i.e., the friction forces, must compensate the horizontal components of the resultant applied to the ankle joint ( $\mathbf{F}_A$ ) <sup>$xy$</sup> . Projecting on the  $z$ -axis, the vertical component of the reaction force  $R_z$  must balance the entire system force acting along the  $z$ -axis and the weight of the foot. It is possible to notice that it is the unavoidable feedback with the ground that allows the whole mechanism to keep postural balance.

Considering Equation (A3), the momenta components acting on the  $z$ -axis are the momenta of the friction forces, grouped in  $M_z$ , the horizontal components of  $\mathbf{F}_A$ , and  $\mathbf{M}_{A_z}$ .

Projecting on the horizontal plane, it follows:

$$(\overline{OP} \times \mathbf{R})^H + (\overline{OG} \times m\mathbf{g})^H + (\mathbf{M}_A)^H + (\overline{OA} \times \mathbf{F}_A)^H = \mathbf{0} \quad (\text{A4})$$

The main players are the foot's weight  $m\mathbf{g}$ , the horizontal components  $\mathbf{M}_A$ , the momentum of  $\mathbf{F}_A$ , and the momentum of the reaction forces  $\mathbf{R}$ .  $\overline{OP}$ ,  $\overline{OG}$ ,  $\overline{OA}$  are the radius vectors with respect of the origin of the reference system to the acting points  $P$ ,  $G$ , and  $A$ .

The semi-inverse method proposed by Vukobratović and Juricić consists of plug in the forces acting on the system in Equations (A2) and (A4) and derive, respectively, the intensity and the acting point  $P$ 's planar coordinates of the ground reaction force  $\mathbf{R}$ . It is trivial to observe that the vertical location of  $P$  is at the ground level, so  $(\overline{OP})^z = 0$ .

Let me make some further observations. Since the foot weight is constant, varying the intensity of  $(\mathbf{M}_A)^H$ , the coordinates of  $P$  must vary accordingly to verify (A4). There is an implicit constraint of the acting point  $P$ 's coordinates which is better to be highlighted: the contact point the reaction force is acting on must belong to the foot sole, i.e., cannot exceed the food edge boundary, otherwise the ground reaction force would not be applied to the system. Therefore, for increasing values of  $(\mathbf{M}_A)^H$  intensities, the acting point  $P$  moves towards the foot edge, resulting in a shrinking of the support polygon, and the mechanism enters in an unstable equilibrium state. If  $(\mathbf{M}_A)^H$  intensities are even higher, Equation (A4) is no more respected, and the momenta's intensities' disparity generates the so-called tilting or overturning moments  $M_x$  and  $M_y$ , i.e., the horizontal components of the ground reaction moment  $\mathbf{M}$ , which cause the mechanism to rotate about the foot edge and overturn, knocking down the mechanism.

In conclusion, the necessary and sufficient condition to guarantee dynamically stable locomotion is the coincidence of the Center of Pressure (CoP) with the Zero-Moment Point, i.e., the point within the foot sole, or extending to the double-stance case, within the support polygon, at which the resulting ground reaction is applied (CoP) must ensure that the tilting momenta along horizontal planar axes are null (hence the name "Zero-Moment Point"):

$$\begin{aligned} M_x &= 0 \\ M_y &= 0 \end{aligned} \quad (\text{A5})$$

Professors Vukobratović and Juricić provided two interpretations of the Zero-Moment Point in [33].

**ZMP interpretation 1:** The ZMP is defined as that point on the ground at which the net moment of the inertial forces and the gravity forces has no component along the horizontal axes.

**ZMP interpretation 2:** P is the point that  $M_x = 0$  and  $M_y = 0$ ,  $M_x, M_y$  represent the moments around x- and y-axis generated by reaction force  $F_r$  and reaction torque  $T_r$ , respectively. The point P is defined as Zero-Moment Point (ZMP). When ZMP exists within the domain of the support surface, the contact between the ground and the support leg is stable:

$$p_{ZMP} = (x_{ZMP}, y_{ZMP}, 0) \in S,$$

where  $p_{ZMP}$  denotes the location of the ZMP, and  $S$  denotes the domain of the support surface.

The condition presented explicitly in “interpretation 2” implies that no rotation around the edges of the foot occurs. It is interesting to notice that considering the momenta equilibrium equation with respect to the Center of Pressure  $P$  and projecting along the z-axis, the ground reaction moment (the ground friction moment) is equal to:

$$M_z = M_{fr} = -(\mathbf{M}_A)^z - (\overline{\mathbf{OA}} \times \mathbf{F}_A)^z \quad (\text{A6})$$

which is typically non-null. Hence, it is possible, although highly improbable, to have rotational slippage of the foot on the ground surface during gait. If one wants to prevent this condition,  $M_z$  must be null too. To do this, the mechanism must perform additional movements, such as trunk movement along the vertical axis, to ensure that  $(\mathbf{M}_A)^z + (\overline{\mathbf{OA}} \times \mathbf{F}_A)^z = \mathbf{0}$  at the ankle joint.

### A3.2 Fictitious ZMP

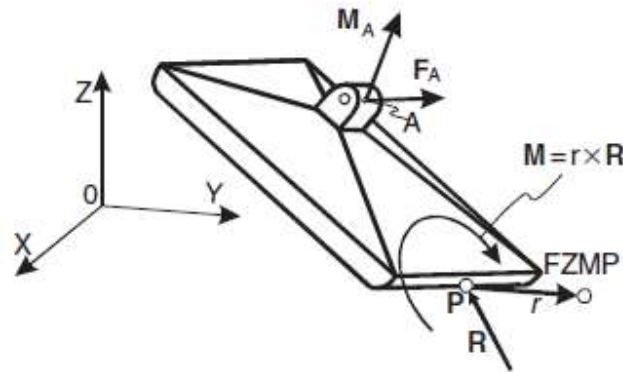


Figure A-4: Representation of the fictitious ZMP.

If the coordinates of the ZMP are not contained within the support polygon, since it is still the point for which Equation (A5) is still valid, it is termed as “fictitious” ZMP (FZMP) or, as suggested by Goswami in [34] Foot Rotator Indicator (FRI).

As stated above, the location of the ZMP varies with changes in the mechanism's dynamics (i.e.,  $F_A$  and  $M_A$ ). By approaching the edge of the support polygon, either in single- or double-stance phase, the support polygon shrinks to a narrow strip, and the mechanism enters unstable equilibrium conditions. Therefore, if there are not additional external momenta, the system is in equilibrium, resembling a ballerina on the foot tips. If additional momenta start to act on the system, whose intensity is related to the distance of the FZMP with respect to the support polygon edge, the mechanism overturns, resulting in a knockdown.

The FZMP has been used in one of the first postural balance control strategy as a transition condition from normal state to "emergency" state. The operating function of that strategy was based on the human spontaneous balance recovery strategy, i.e., by altering the moment of inertia of the body, performing fast and large movements with the upper body, while the adjustments at the lower limbs aimed at increasing the support polygon extension, increasing the step length, so that the FZMP will be contained again within the support polygon. In this case, the FZMP was termed "emergency" ZMP.

The ZMP balance strategy has paved the way for other postural balance recovery strategies, such as Goswami's Foot Rotator Indicator [34] or the Capture Pivot point presented in [30].

#### A4. Gait model: 3D-Linear Inverted Pendulum Model

In absence of detailed data about robot dynamics, the simplest yet suitably accurate model to represent bipedal locomotion is the so-called Three-Dimensional Linearized Inverted Pendulum Mode (3-D LIPM) and it is based on the ZMP stability criterion. The 3D-LIPM is a linear dynamic mass-concentrated model which approximate the passive ground contact joint to a spherical joint, the robot leg to a massless rod, and the biped's center of mass as a point mass attached to the rod. The walking is approximated as follows. Once the step has been performed, the mass oscillates forward, rotating around the spherical joint. Reached the arbitrary limit of the rotation, dependent on the Center of Pressure and the ZMP locations, the spherical joint is moved forward to let the cycle repeats.

One of the first complete analysis, simulation, and experimentation was conducted by Japanese professor Kajita Shuuji in [19-20].

The 3D-LIPM consists in a point mass  $m$  and a massless rod of length  $r$ .

The position of the point mass is identified by  $p = [x, y, z]$ ,  $\theta_p$  identifies the angle of the rod and the  $x$ -axis,  $\theta_r$  identifies the angle of the rod and the  $y$ -axis.

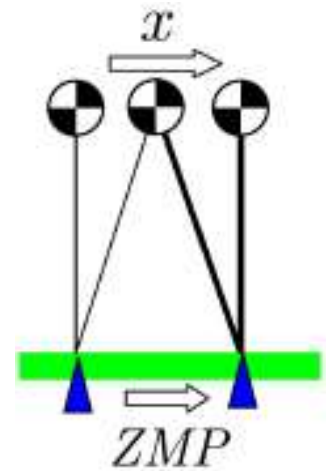


Figure A-5: Simplified walkin.  
Reprinted from [20]

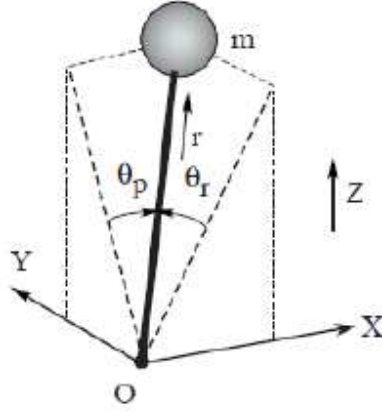


Figure A-6: Inverted pendulum. Reprinted from [19]

The kinematic equations of the inverted pendulum allows to specify uniquely the position of the point mass  $p = [x, y, z]^T$  by a set of state variables  $q = [\theta_r, \theta_p, r]^T$ :

$$\begin{aligned} x &= r \sin \theta_p \\ y &= -r \sin \theta_r \\ z &= r \sqrt{1 - \sin^2 \theta_p - \sin^2 \theta_r} = rD \end{aligned} \quad (A7)$$

The equation of motion of the 3D inverted pendulum at the Cartesian level is given as follows:

$$m \begin{bmatrix} \ddot{x} \\ \ddot{y} \\ \ddot{z} \end{bmatrix} = J^{-T} \begin{bmatrix} \tau_r \\ \tau_p \\ f \end{bmatrix} + \begin{bmatrix} 0 \\ 0 \\ -mg \end{bmatrix} \quad (A8)$$

where  $[\tau_r, \tau_p, f]^T$  are respectively the actuator torque and force associated with the state variables  $[\theta_r, \theta_p, f]^T$ , and:

$$J = \frac{\partial p}{\partial q} = \begin{bmatrix} 0 & rc_p & -s_p \\ -rc_r & 0 & -s_r \\ -\frac{rc_r s_r}{D} & -\frac{rc_p s_p}{D} & D \end{bmatrix} \rightarrow J^T = \begin{bmatrix} 0 & -rc_r & -\frac{rc_r s_r}{D} \\ rc_p & 0 & -\frac{rc_p s_p}{D} \\ -s_p & -s_r & D \end{bmatrix} \quad (A9)$$

where  $c_i = \cos \theta_i$  and  $s_i = \sin \theta_i$ ,  $i = r, p$ .

To avoid the computation of the inverse of the transpose of the Jacobian matrix, multiply by  $J^T$  from the left both sides:

$$m J^T \begin{bmatrix} \ddot{x} \\ \ddot{y} \\ \ddot{z} \end{bmatrix} = \begin{bmatrix} \tau_r \\ \tau_p \\ f \end{bmatrix} - mg \begin{bmatrix} -\frac{rc_r s_r}{D} \\ -\frac{rc_p s_p}{D} \\ D \end{bmatrix}$$

Consider now the equation in the x-direction, we obtain:

$$m \left( -rc_r \ddot{y} - \frac{rc_r s_r}{D} \ddot{z} \right) = \tau_r + mg \frac{rc_r s_r}{D}$$

multiply both sides by  $D/c_r$ :

$$m(-rD\ddot{y} - rs_r\ddot{z}) = \frac{D}{c_r}\tau_r + mgrs_r$$

and remembering the kinematic equations, we obtain a good-looking equation describing the dynamics along the y-axis:

$$m(-z\ddot{y} + y\ddot{z}) = \frac{D}{c_r}\tau_r - mgy \quad (\text{A10})$$

By applying a similar procedure for the second row of (A8) as well, we get the equations for the dynamics along the x-axis:

$$m(z\ddot{x} - x\ddot{z}) = \frac{D}{c_p}\tau_p + mgx \quad (\text{A11})$$

3D-LIPM is based on constraining the motion of the point mass on an arbitrary decided plane. The constraint plane is represented with given normal vector  $[k_x, k_y, -1]^T$  and z intersection  $z_c$  as:

$$z = k_x x + k_y y + z_c \quad (\text{A12})$$

Notice that for rugged terrains, the normal vector should match the slope of the ground, and the z intersection  $z_c$  should be the expected average distance between the system's center of mass (CoM) and the ground.

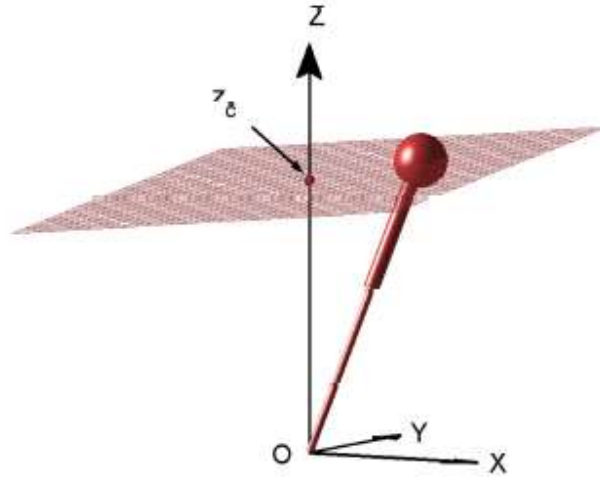


Figure A-7: 3D Pendulum in planar motion constraint. Reprinted from [20]

By substituting (A12) in the previous (A10) and (A11), it follows:

$$\begin{aligned}\ddot{y} &= \frac{g}{z_c} y - \frac{k_x}{z_c} (x\ddot{y} - \ddot{x}y) - \frac{1}{mz_c} u_r \\ \ddot{x} &= \frac{g}{z_c} x + k_y (x\ddot{y} - \ddot{x}y) + \frac{1}{mz_c} u_p\end{aligned}\quad (\text{A13})$$

posed  $u_r, u_p$  as virtual inputs to compensate input nonlinearity:  $\tau_r = \frac{c_r}{D} u_r$  and  $\tau_p = \frac{c_p}{D} u_p$ .

If the constraint plane is horizontal, i.e.,  $k_x = k_y = 0$ , the dynamics under constraint control is given by:

$$\begin{aligned}\ddot{y} &= \frac{g}{z_c} y - \frac{1}{mz_c} u_r \\ \ddot{x} &= \frac{g}{z_c} x + \frac{1}{mz_c} u_p\end{aligned}\quad (\text{A14})$$

where  $m$  is the mass of the pendulum,  $g$  is the gravity acceleration,  $u_r, u_p$  are the torques around  $x$ -axis and  $y$ -axis respectively, and  $z_c$  is the intersection of the arbitrary horizontal plane with the  $z$ -axis. Since the CoM is constrained to move on this horizontal plane,  $z_c$  represents the height of the CoM with respect to the ground.

For small oscillations around the  $x$ -axis and the  $y$ -axis, the formulae (A14) can be further simplified:

$$\begin{aligned}\ddot{y} &= \frac{g}{z_c} y - \frac{1}{mz_c} \tau_r \\ \ddot{x} &= \frac{g}{z_c} x + \frac{1}{mz_c} \tau_p\end{aligned}\quad (\text{A15})$$

In case of an inclined plane (sloped constraint), i.e.,  $k_x, k_y \neq 0$ , it is possible to obtain the same dynamics by imposing an additional constraint:

$$u_r x + u_p y = 0 \quad (\text{A16})$$

for the input torques.

Equations (num Eqn) and (num Eqn) are linear differential equations. The only parameter which governs those dynamics is  $z_c$ , the  $z$  intersection of the plane, while the slope of the plane never affects the horizontal motion.

For the 3D-LIPM with the horizontal constraint, it is possible to compute the Zero-Moment Point (ZMP) as follows:

$$\begin{aligned}p_{ZMP_x} &= -\frac{u_p}{mg} \\ p_{ZMP_y} &= \frac{u_r}{mg}\end{aligned}\quad (\text{A17})$$

where  $(p_{ZM_x}, p_{ZM_y})$  are the coordinates of the ZMP on the floor. By substituting these two equations into the 3D-LIPM model (A14) we obtain:

$$\begin{aligned}\dot{y} &= \frac{g}{z_c}(y - p_{ZMP_y}) \\ \dot{x} &= \frac{g}{z_c}(x - p_{ZMP_x})\end{aligned}\tag{A18}$$

#### A4.1. Cart-Table model-based postural equilibrium control

To control the postural balance of a biped robot, i.e., to control the ZMP position, consider the following equations:

$$\begin{aligned}p_{ZMP_y} &= y - \frac{z_c}{g}\ddot{y} \\ p_{ZMP_x} &= x - \frac{z_c}{g}\ddot{x}\end{aligned}\tag{A19}$$

These equations are the inverse of ( ) and allows to compute the location of the ZMP on the horizontal plane. Further highlighting on the fact that the position of the ZMP depends on the coordinates of the motion constrained CoM:  $(x, y, z_c)$ , the projection on the horizontal plane of the ZMP and the height with respect to the ground.

Each of those equations can be modeled directly with a cart-table model. This model presents a cart of mass  $m$  on a pedestal table of negligible mass, which is free to move along one direction (we need two carts to simulate a planar movement on both  $x$  and  $y$  axes).

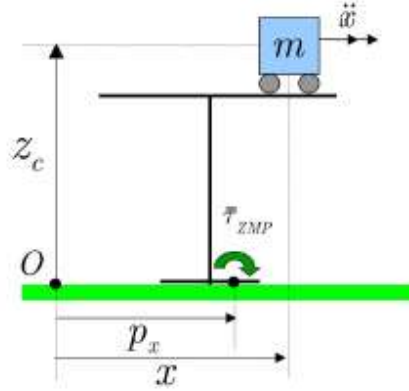


Figure A-8: Cart-Table model, suitably modified to consider ZMP. Reprinted from [20].

As shown in Figure A-8, the foot of the table is too short to let the cart positioning on the table's edge, although, if the cart accelerates with a proper rate, the table can keep upright for a certain time interval.

This being the case, the ZMP exists within the table's foot area. Since the moment around the ZMP must be zero, we have:

$$\tau_{ZMP} = mg(x - p_x) - m\ddot{x}z_c = 0\tag{A20}$$

Given the cart motion as the trajectory of the center of mass of the robot, we can easily compute the resulted ZMP using the ZMP Equations (A18).

Walking pattern generation represents the inverse problem of the aforementioned cart-table model problem, i.e., given the measurements of the time-evolution of the ZMP position or determined the ZMP trajectory by the desired footholds and step period, generate the trajectory of the center of mass (or the trajectory of the cart). This can be achieved in many ways, such as considering the ZMP as a servo control problem, or by preview control, an optimal control strategy based on future predictions of the ZMP positions proposed by Katayama et al. [35].

## Appendix B: The Routh-Hurwitz criterion

The Routh-Hurwitz stability criterion presents one sufficient and one necessary stability condition [36].

The necessary condition requires that all the coefficients of the characteristic polynomial should be positive, hence, for the Cartesian rule, all the roots of the characteristic equation have negative real parts. If the necessary condition is not satisfied, the control system is unstable.

The sufficient condition depends on the form of the sign of the elements in the first column in the Routh array. The Routh array is formed as follows.

- 0) Consider the following characteristic equation of order  $n$ :

$$a_0s^n + a_1s^{n-1} + \dots + a_{n-1}s + a_ns^0 = 0 \quad (B1)$$

- 1) Write all the  $n + 1$   $s^k, k = n, n - 1, \dots, 1, 0$  elements in this order as the column indication of the Routh table.
- 2) Place the coefficients  $a_0, a_1, \dots, a_n$  in the first two rows of the Routh array. In the first row, put all the coefficients with even indices. In the second row, all the coefficients with odd indices.
- 3) The elements in the remaining rows must be computed as follows:

$$-\frac{p_{i-1,1} p_{i-2,j+1} - p_{i-1,j+1} p_{i-2,1}}{p_{i-1,1}} \quad (B2)$$

where, posing that the element to compute is in position  $(i, j)$ , the matrix  $M$  is the  $2$ -by- $(j + 1)$  matrix formed by the elements in rows  $(i - 2)$  and  $(i - 1)$ , and columns from  $1$  to  $j + 1$ , while  $p_{i-1,1}$  is the first element of the row above the one the element to compute is situated.

The sufficient condition requires that all the elements of the first column of the Routh array have the same sign. In fact, every sign change corresponds to a root of the characteristic equation with positive real part, hence, lying in the right half plane (RHP), for which the system is unstable.

To promote understanding, in the following part of Appendix B there is the step-by-step procedure to apply the Routh-Hurwitz criterion, considering as characteristic polynomial the one presented in Equation (B1):

$$a_0s^n + a_1s^{n-1} + \dots + a_{n-1}s + a_ns^0 = 0 \quad (B1)$$

The first step is to verify that all the coefficients are positive. In order to proceed with the procedure, suppose that the necessary condition is verified.

The second step is to build the column indicator of the Routh array:

$s^n$						
$s^{n-1}$						
$s^{n-2}$						
$s^{n-3}$						
$\vdots$						
$s^1$						
$s^0$						

The third step consists in filling the first two rows with the coefficients  $a_k, k = 0, \dots, n$ :

$s^n$	$a_0$	$a_2$	$a_4$	$a_6$	$\dots$	$\dots$
$s^{n-1}$	$a_1$	$a_3$	$a_5$	$a_7$	$\dots$	$\dots$
$s^{n-2}$						
$s^{n-3}$						
$\vdots$						
$s^1$						
$s^0$						

The fourth step consists in filling the remaining rows computing each element as illustrated in Equation (B2):

$s^n$	$a_0$	$a_2$	$a_4$	$a_6$	$\dots$	$\dots$
$s^{n-1}$	$a_1$	$a_3$	$a_5$	$a_7$	$\dots$	$\dots$
$s^{n-2}$	$b_1 = \frac{a_1 a_2 - a_3 a_0}{a_1}$	$b_2 = \frac{a_1 a_4 - a_5 a_0}{a_1}$	$b_3 = \frac{a_1 a_6 - a_7 a_0}{a_1}$	$\dots$	$\dots$	$\dots$
$s^{n-3}$	$c_1 = \frac{b_1 a_3 - b_2 a_1}{b_1}$	$c_2 = \frac{b_1 a_5 - b_3 a_1}{b_1}$	$\vdots$			
$\vdots$	$\vdots$	$\vdots$	$\vdots$			
$s^1$	$\vdots$	$\vdots$				
$s^0$	$a_n$					

Finally, take note of the number of sign changes in the first column (highlighted in yellow). If there are not, the system is stable. Conversely, there is at least one characteristic polynomial's root in the RHP, thus, the system is unstable.

## Appendix C: Haptics

The word “haptics” derived from the Greek term “haptesthai” that means “of or relating to the sense of touch” [37]. Haptics refers to the science of manual sensing and manipulation through touch. The first allows to explore and extract information from the environment, the second to modify the environment.

Haptic technologies started drawing attention for two main reasons. First, it has been proven that haptic operative modes reduce the perceived musculoskeletal loading in terms of pain and discomfort in all those applications relying on man-machine interaction. The second reason is related to the potentiality and characteristic of the human sense of touch. The skin is an interface able to differentiate four modalities of sensations: touch (including pressure), cold, heat, and pain. Touch is twenty times faster than vision, allowing to perceive different stimulus every 5 ms. Touch is highly sensitive to vibration up to 1 kHz, with sensitivity peak around 250 Hz. To give an idea of the sensory potential of the human skin, the skin receptors in the human palm can sense displacements down to  $0.2 \mu\text{m}$  in length. In addition, differently from the other feedback communication systems employed in devices for man-machine interaction, based on vision or audition, touch allows a bidirectional flow of energy, resulting in both sensing and acting on the environment.

Human haptic perception may be defined as the process of interpreting touch information to identify and recognize objects. It is based on tactile perception through the skin receptors, i.e., the ability to extract cutaneous information about the superficial characteristics of an object (the geometrical distribution, texture, slippage, roughness, temperature, etc.) by contact, and kinesthetic perception through the muscle and tendon receptors, which allows acquire knowledge about the dynamical properties of an object, also called kinesthetic information, such as its weight and inertia, forces and torques from the environment.

Haptic devices for man-machine interaction can be subdivided into two subsystems: the haptic interface and the virtual environment.

The haptic interface is the real system used to communicate with the human user’s nervous system exchanging information bidirectionally, i.e., generally, the haptic interface measures contact forces or receives kinematic inputs provided by the user and returns haptic feedback in the form of force exchange, pressure, or vibration, according to the computed reaction in the virtual scene.

Haptic interfaces can be divided into two categories: force feedback devices and tactile devices. Force feedback devices display kinesthetic stimuli (force and/or torque) perceived by the user as resistive force, friction, roughness. These devices present three to six DOFs and behave similarly to small robots mechanically interacting with the users. The end-effector consists of a tool-type probe, called proxy, which is grasped and moved by the user to move the virtual correlative, called avatar, in the (virtual) haptic scene. Whenever the avatar collided with virtual objects in the scene, a force/torque is returned to the human as a feedback through the proxy’s dynamics.

Tactile devices display virtual object’s properties provided as cutaneous sensations perceived by the human skin. To do so, these devices are constituted by arrays of actuators uniformly distributed in direct contact with the human skin.

It is not unusual for haptic device designers to combine the two types of devices to provide a haptic feedback/sensation felt more natural by the user.

The virtual environment that corresponds to the second subsystem of a haptic device is referred as haptic rendering and collects the algorithms and software to simulate the physical properties of touched objects in the scene, such as texture, stiffness, and weight, and to compute interaction forces or torques, displayed in output by the haptic interface. It is responsible of functions such as collision detection and force computation algorithms.

The haptic rendering relies on the ability to find the point(s) of contact to detect collisions and compute the related collision forces. The solution is the "locality", i.e., the algorithm focuses only on the bounding volume of the avatar and the virtual objects' volume that is within that range. Collision happens when the avatar's boundary surface penetrates or is penetrated by a virtual object's boundary. Interaction force computation depends on the indentation depth, i.e., the distance of volume overlapping, the property attributed to the virtual objects, and the kinematic information measured by the haptic interface. This reference command is provided to the haptic interface hardware, to be displayed to the human.

# Bibliography

- [1] Molteni, F.; Gasperini, G.; Cannaviello, G.; Guanzioli, E.; “Exoskeleton and End-Effector Robots for Upper and Lower Limbs Rehabilitation: Narrative Review”. *Innovations Influencing Physical Medicine and Rehabilitation*, 2018, <https://doi.org/10.1016/j.pmrj.2018.06.005>
- [2] Wang, T.; Zhang, B.; Liu, C.; Liu, T.; Han, Y.; Wang, S.; Ferreira, J.P.; Dong, W.; Zhang, X.; “A Review on the Rehabilitation Exoskeletons for the Lower Limbs of the Elderly and the Disabled.” *Electronics* 2022, 11, 388. <https://doi.org/10.3390/electronics11030388>
- [3] Yang, X.; She, H.; Lu, H.; Fukuda, T.; Shen, Y.; “State of the Art: Bipedal Robots for Lower Limb Rehabilitation.”. *Appl. Sci.* 2017, 7, 1182; <https://doi.org/10.3390/app7111182>
- [4] Bastide, S.; Vignais, N.; Geffard, F.; Berret, B.; “Interacting with a ‘transparent’ upper-limb exoskeleton: a human motor control approach”, 2018 IEEE/RSJ International Conference on Intelligent Robots and Systems (IROS), Oct 2018, Madrid, France. pp. 4661-4666. <https://hal.archives-ouvertes.fr/hal-02183873>
- [5] Garrec, P.; Friconeau, J. P.; Measson, Y.; Perrot, Y.; “Able, an innovative transparent exoskeleton for the upper-limb”, in *Proc. IEEE/RSJ Int. Conf. Intelligent Robots and Systems*, pp. 1483-1488, 2008. 978-1-4244-2058-2/08/\$25.00
- [6] Hogan, N.; "Impedance Control: An Approach to Manipulation: Part I—Theory" *1984 American Control Conference*, 1984, pp. 304-313, doi: 10.23919/ACC.1984.4788393
- [7] Hogan, N.; Buerger, S. P.; “Impedance and Interaction Control”, 2018, in “*Robotics and Automation Handbook*”, Kurfess T.H., pp. 376-399, ISBN 0-8493-1804-1
- [8] Colgate, E.; “The control of dynamically interacting systems”, 1988, <https://dspace.mit.edu/handle/1721.1/14380>
- [9] Hogan, N.; “On the stability of manipulators performing contact tasks”. *IEEE J. Robotics and Automation*, 1988, 4:677-686.
- [10] Keemink, A.Q.; van der Kooij, H.; Stienen, A.H.; “Admittance control for physical human–robot interaction”. *The International Journal of Robotics Research*. 2018;37(11):1421-1444. doi:10.1177/0278364918768950
- [11] Alessandro De Luca, “Robotics 2 - Impedance Control”. 2020. URL: [https://www.youtube.com/watch?v=IolG5V\\_skv8](https://www.youtube.com/watch?v=IolG5V_skv8)
- [12] Hogan, N.; “Impedance Control: An Approach to Manipulation: Part II—Implementation.” *Journal of Dynamic Systems Measurement and Control-Transactions of The Asme* 107 (1985): 8-16.

- [13] De Luca, Alessandro; slide “Impedance Control”, [http://www.diag.uniroma1.it/deluca/rob2\\_en/15\\_ImpedanceControl.pdf](http://www.diag.uniroma1.it/deluca/rob2_en/15_ImpedanceControl.pdf)
- [14] Aguirre-Ollinger, G.; Colgate, J. E.; Peshkin, M.; Goswami, A.; “A 1-DOF assistive exoskeleton with virtual negative damping: Effects on the kinematic response of the lower limbs”. *IEEE/RSJ International, 2007*. doi: 10.1109/IROS.2007.4399147
- [15] Aguirre-Ollinger, G.; Colgate, J. E.; Peshkin, M.; Goswami, A.; “Active-Impedance Control of a Lower-Limb Assistive Exoskeleton”. *IEEE International, 2007*. doi: 10.1109/ICORR.2007.4428426
- [16] Aguirre-Ollinger, G.; Colgate, J. E.; Peshkin, M.; Goswami, A.; “Design of an active one-degree-of-freedom lower-limb exoskeleton with inertia compensation”. 2011. *The International Journal of Robotics Research, 30(4): 486-499*. doi: 10.1177/0278364910385730
- [17] Aguirre-Ollinger, G.; Colgate, J. E.; Peshkin, M.; Goswami, A.; “A one-degree-of-freedom assistive exoskeleton with inertia compensation: The effects on the agility of leg swing motion”. 2011. *Proceedings of the Institution of Mechanical Engineers Part H Journal of Engineering in Medicine 225(3):228-45*. doi: 10.1243/09544119JEIM854
- [18] Durandau, G., Farina, D., Asín-Prieto, G. et al. “Voluntary control of wearable robotic exoskeletons by patients with paresis via neuromechanical modeling”. *J NeuroEngineering Rehabil* 16, 91 (2019). <https://doi.org/10.1186/s12984-019-0559-z>
- [19] Kajita, S.; Kanehiro, F.; Kaneko, K.; Yokoi, K.; Hirukawa, H.; “The 3D Linear Inverted Pendulum Mode: A simple modeling for a biped walking pattern generation”, in *Proc. IEEE/RSJ Int. Conf. Intelligent Robots and Systems*, [https://www.cs.cmu.edu/~hgeyer/Teaching/R16-899B/Papers/KajitaEA01IEEE\\_ICIRS.pdf](https://www.cs.cmu.edu/~hgeyer/Teaching/R16-899B/Papers/KajitaEA01IEEE_ICIRS.pdf)
- [20] Kajita, S.; Kanehiro, F.; Kaneko, K.; Fujiwara, K.; Harada, K.; Yokoi, K.; Hirukawa, H.; “Biped walking pattern generation by using preview control of zero-moment point”, in *Proc. IEEE/RA 2:1620-1626 vol.2, 2003*, doi: 10.1109/ROBOT.2003.1241826
- [21] Han, Y.; Zhu, S.; Zhou, Y.; Gao, H.; “An admittance controller based on assistive torque estimation for a rehabilitation leg exoskeleton”. *Intelligent Service Robotics 12(3):1-11*, 2019. doi: 10.1007/s11370-019-00289-4
- [22] Menga, G.; Ghirardi, M.; “Modeling, Simulation, and Control of the Walking of Biped Robotic Devices – Part I: Modeling and Simulation Using Autolev”. *Inventions, 2016, 1, 6*. <https://doi.org/10.3390/inventions1010006>
- [23] Menga, G.; Ghirardi, M.; “Modeling, Simulation, and Control of the Walking of Biped Robotic Devices – Part II: Rectilinear Walking”. *Inventions, 2016, 1, 7*. <https://doi.org/10.3390/inventions1010007>
- [24] Menga, G.; Ghirardi, M.; “Modeling, Simulation, and Control of the Walking of Biped Robotic Devices – Part III: Turning while walking”. *Inventions, 2016, 1, 8*. <https://doi.org/10.3390/inventions1010008>
- [25] Menga, G.; Geng, J.; “Lower Limb Exoskeleton Haptic Device for Rehabilitation or Walking, with Improved Postural Equilibrium Control, Man-Machine Interface”. *Robotics* 2020, 7, 28.

- [26] Menga, G.; Ghirardi, M.; “Lower Limb Exoskeleton for Rehabilitation with Improved Postural Equilibrium”. *Robotics* 2018, 7, 28. <https://doi.org/10.3390/robotics7020028>
- [27] Menga, G.; Ghirardi, M.; “Estimation and Closed-Loop Control of COG/ZMP in Biped Devices Blending CoP Measures and Kinematic Information”. *Robotics* 2019, 8, 89. <https://doi.org/10.3390/robotics8040089>
- [28] Tu, Y.; Zhu, A.; Song, J.; Shen, H.; Shen, Z.; Zhang, X.; Cao, G.; “An Adaptive Sliding Mode Variable Admittance Control Method for Lower Limb Rehabilitation Exoskeleton Robot”. *Appl. Sci.* 2020, 10, 2536. <https://doi.org/10.3390/app10072536>
- [29] Liang, C.;Hsiao, T.; "Admittance Control of Powered Exoskeletons Based on Joint Torque Estimation," in *IEEE Access*, vol. 8, pp. 94404-94414, 2020, doi: 10.1109/ACCESS.2020.2995372
- [30] BALANCE project (Balance Augmentation in Locomotion, through Anticipative, Natural and Cooperative control of Exoskeletons), Deliverable 4.2, “Report on ‘Low impedance stable walking on a robot based on human principles’”.
- [31] Menga, G.; Ghirardi, M.; “Control of the Sit-To-Stand Transfer of a Biped Robotic Device for Postural Rehabilitation”. *Robotics* 2019, 8, 91. <https://doi.org/10.3390/robotics8040091>
- [32] Juricic, D.; Vukobratovic, M.; “Mathematical Modeling of a Bipedal Walking System”, *ASME publication* 72-WA/BHF-13, Winter Annual Meeting, New York, Nov. 26-30, 1972
- [33] Vukobratovic, M.; Borovac, B. A.; “Zero-Moment Point – Thirty-Five Years of its Life”, *International Journal of Humanoid Robotics*, 1(01):157-173, 2004, doi: 10.1142/S0219843604000083
- [34] Goswami, A.; “Foot-Rotator Indicator (FRI) point, a new gait planning tool to evaluate postural stability of biped robots”, in Proc. IEEE ICRA, Detroit, 1999, pp. 47-52, <http://www.cs.cmu.edu/~cga/legs/kufflc.pdf>
- [35] Katayama, T., Ohki, T., Inoue, T., Kato, T., “Design of an Optimal Controller for a Discrete Time System Subject to Previewable Demand”, *Int. J. Control*, Vol.41, No.3, pp.677-699, 1985
- [36] Tutorialspoint.com, “Routh-Hurwitz stability criterion”. [https://www.tutorialspoint.com/control\\_systems/control\\_systems\\_stability\\_analysis.htm](https://www.tutorialspoint.com/control_systems/control_systems_stability_analysis.htm)
- [37] El Saddik, A; Orozco, M.; Eid, M.; Cha, J.; “Haptics Technologies: Bringing Touch to Multimedia (1st. ed.)”. 2011. Springer Publishing Company, Incorporated.